2015

NUMERICAL STUDY OF STRUCTURAL RESPONSES OF RIGID AND FLEXIBLE PAVEMENTS UNDER HEAVY VEHICLES' LOADING

Rezwana Kabir
Michigan Technological University, rkabir@mtu.edu

NUMERICAL STUDY OF STRUCTURAL RESPONSES OF RIGID AND FLEXIBLE PAVEMENTS UNDER HEAVY VEHICLES' LOADING

By

Rezwana Kabir

A THESIS

Submitted in partial fulfillment of the requirements for the degree of

MASTER OF SCIENCE

In Civil Engineering

MICHIGAN TECHNOLOGICAL UNIVERSITY

2015

This thesis has been approved in partial fulfillment of the requirements for the Degree of MASTER OF SCIENCE in Civil Engineering.

Department of Civil and Environmental Engineering

Thesis Advisor: *Jacob Hiller*

Committee Member: *William J. Sproule*

Committee Member: *Kuilin Zhang*

Committee Member: *Jiann-Yang Hwang*

Department Chair: *David Hand*

This thesis is lovingly dedicated to our anticipated baby. This thesis also dedicated to my husband, Abdul Motin for his support and encouragement.

TABLE OF CONTENTS

LIST OF FIGURES

LIST OF TABLES

ACKNOWLEDGEMENTS

First of all, I would like to express my deep sense of gratitude, and acknowledge profound indebtedness to my supervisor, Professor Jacob Hiller for his constant guidance, untiring help, invaluable suggestions and unceasing encouragement. He not only supports my academic research but also gives me personal guidance. In addition, I am highly grateful to Professor William J. Sproule, Kuilin Zhang, and Jiann-Yang Hwang for serving on my dissertation committee.

Financial support of this research from the Department of Civil and Environmental Engineering of Michigan Technological University is appreciated. Finally sincere thanks are offered to members of my family and friends for their cooperation and inspiration during the work.

DEFINITIONS

h	Concrete slab thickness	*in*
k	Modulus of subgrade reaction	*psi/in*
N_f	Number of load repetition to failure	kg/m^3
α	Coefficient of thermal expansion	*in/in/deg F*
ΔT	Temperature difference between top and bottom surface of slab	*degree*

LIST OF ABBREVIATIONS

AC –Asphalt Concrete

CTE – Coefficient of Thermal Expansion

FEACONS – Finite Element Analysis of Concrete Slabs

HMA – Hot Mixed Asphalt

JULEA – Jacob Uzan Layered Elastic Analysis

LTE – Load Transfer Efficiency

MDOT – Michigan Department of Transportation

MEPDG – Mechanistic Empirical Pavement Design Guide

PCC – Portland Cement Concrete

ABSTRACT

NUMERICAL STUDY OF STRUCTURAL RESPONSES OF RIGID AND FLEXIBLE PAVEMENTS UNDER HEAVY VIHICLES' LOADING

By

Rezwana Kabir

The highway system serves as the most critical transportation link in the economic development of a nation. In Michigan, about 74% of all the commodities delivered annually are transported by heavy trucks. The Michigan Department of Transportation (MDOT) permits multi-axle (11 axles) heavy truck with gross vehicle weight (GVW) limit of 164,000 lb., unlike many states having GVW limit of 80,000 lb. The effect of these heavy truck loadings on pavements might accelerate the rate of deterioration for flexible and rigid pavement structures. More detailed knowledge of the interaction of trucks with the pavement structure is essential for better management of the highway network.

In this study, pavement responses (stresses, strains and deflections) are evaluated under loading of multi-axles (11 axles) of heavy Michigan trucks including the impacts of different tire configurations and compared these responses with a standard 5-axle semi-trailer. The effects of truck loading, pavement thickness, joint system and material properties, and environmental (thermal) condition on the pavement damage caused by heavy Michigan trucks are evaluated. The major fatigue and faulting damage for rigid pavements as well as fatigue and subgrade rutting for flexible (asphalt) pavements are analyzed. The finite element method (FEM) based program ISLAB2000 has been used to

compute rigid pavement responses (stresses or deflections). For flexible pavement responses (strains), multilayer elastic theory based program JULEA has been used.

Results show that the standard truck has a higher fatigue damage potential under positive temperature gradient (during daytime) across slab. The Michigan trucks provide a greater fatigue damage potential under negative temperature gradient (during nighttime). Moreover, the positive temperature gradient yields a greater bending stress than that of negative temperature gradient and their critical stress locations are in the opposite surfaces. A thicker slab reduces both the fatigue and faulting damage of pavement. The standard truck has higher faulting damage potential. Moreover, the standard truck exhibits higher risk of both asphalt concrete (AC) fatigue and subgrade rutting damage for the flexible pavement when compared with Michigan trucks. As the number of axles increases, the heavy loads are distributed to larger areas and thus produce lower pavement damage.

CHAPTER 1

INTRODUCTION

1.1. Scope of the study

Michigan trucks are crucial component of Michigan's economy since these carry about half of all freight tonnage moving in Michigan (MDOT 2012). Therefore, Michigan truck weight laws allow greater maximum gross vehicle gross vehicle weight (GVW) than the other states to control axle loads instead of gross vehicle weight. Gross vehicle weight includes the weight of truck, cargo, fuel and driver. Because of the high correlation between the pavement stress and vehicle's gross weight, concerns have been raised that possible damage could be resulted from these MI trucks when they are fully loaded.

The maximum gross vehicle weight allowed on a federal-weight-law-truck is 80,000 pounds, with four of its five axles carrying 17,000 pounds each and steering axle carrying 12,000 pounds as recommended by Federal Highway Administration (FHWA). However, Michigan's truck weight law is designed to control axle loads instead of gross vehicle weight. Michigan limits the weight allowed on individual axles, depending upon the spacing between them, with a maximum of eleven axles. The maximum allowable gross vehicle weight on the heaviest Michigan weight law truck is 164,000 pounds,

unlike many states having GVW limit of 80,000 lb., which can only be achieved by use of eleven properly-spaced axles. Most of these axles carry only 13,000 pounds each.

Michigan road regulation permits several multi-axle trucks for which the extent of the distresses on pavement is still unknown. Several researchers have investigated the pavement damage resulting from different axle and truck configurations (Gillespie et al, 1993; Hajek, 1990, 1995; Ilves and Majidzadeh 1991), yet these studies were limited only to single, tandem, and tridem axles. Unlike many states, MDOT conducted a study in 2009 to address this concern. The study has shown that trucks with single and tandem axles affect pavement cracking more than those with multiple axles and conversely, heavier trucks with multiple axles have more effect on damage, than those with single and tandem axles (Chatti et al., 2009). However, the study was limited only to pavement damage resulting from external truck loading without considering the environmental variables and their impacts on damage accumulation. Additionally, the impact of factors such as varied pavement materials on pavement performance was not studied in detail. More detailed knowledge of the interaction of trucks with the pavement structure is essential for better management of the highway transportation network which will facilitate more rational regulation of unique traffic situations such as the 11-axle truck. The effect of these heavy truck loadings on pavements might be an accelerated rate of deterioration for flexible or rigid pavement structures.

In jointed concrete pavements, the mid-slab edge load locations have typically been considered in standard analysis of a concrete pavement designs (Darter et al. 1995, Darter et al. 2001, Poblete et al. 1990, Guo et al. 2002; Westergaard, 1927). Analysis of

the response of jointed concrete pavement under different slab geometries and material properties has been observed in many studies (Brill, 2000; Rufino and Roesler, 2006). However, the presence of temperature and moisture differences between the top and bottom of the PCC slab can cause curvature of the slab known as curling and warping, respectively. While taking these phenomena into consideration, the location of the critical stresses in the concrete slab is not as easily predictable (Hiller, 2007). Upward curling is the result of negative temperature differentials in the PCC slab (the slab surface is cooler than the bottom of the slab as is typical during nighttime conditions) while downward curling occurs due to positive temperature gradient (typical of daytime conditions). Moisture differences also cause slab curvature in the PCC slab which is known as warping. Upward warping occurs while the slab surface is drier than the bottom, which is typically the case (Jeong and Zollinger, 2005; Yu et al., 1998).

In the presence of positive temperature gradients, stresses induced by vehicular loadings results in fatigue damage on the bottom of the slab at the mid-slab edge as the negative curling stresses usually are subtracted from the load stresses at the bottom of the slab during daytime conditions (Jiang and Tayabji 1998). External axle loads at the transverse joint or corner of the PCC slab can significantly affect the magnitude of upward slab curling and resulting bending stress level (Heath et al. 2003; Heath and Roesler, 2000a). A combined effect of load and temperature scenarios is often required to properly estimate all effects on PCC slab bending and stress development, leading to fatigue cracking formation (Ioannides 1984, Thompson and Barenberg 1992). Given the prominence of temperature curling, the need for a way to account for it in design has

been identified (McCracken, 2006; Hiller, 2007; Wang, 2011; Darestani, 2007; William, 2003). Therefore, there is a need to quantify the relative pavement damage resulting from these multiple axle trucks in Michigan.

Vehicular loads are given much more prominence than environmental conditions in the analysis of asphalt pavements since the immediate pavement responses due to load should be closely related to the long-term asphalt pavement performance and distress development (Gillespie et al. 1993; Hajek, 1990, 1995; Ilves and Majidzadeh 1991; Chatti and Lee, 2003; Chatti and Lee, 2004). Vehicle loads are distributed through the pavement structure to the subgrade soil by the use of all layer of the flexible pavement system. Study has been conducted to estimate the pavement responses (e.g. horizontal tensile strains) which could initiate cracking at the bottom of HMA and progress to the pavement surface (Matthews et al. 1993).Similarly, given the prominence of vertical compressive strains at the top of the subgrade for the pavement rutting due to compaction and/or consolidation of the subgrade soil, the need for a way to account for it in design has been identified (Wang, 2005).

Gillespie et al. (1993) provided a comprehensive study related to the effect of heavy trucks on pavement damage which concluded different truck characteristics (truck type, axle load, number of axles, spacing between axles, tire type and contact pressure. In this study, analytical models of pavement responses to the moving, dynamic loads of various truck configurations were developed. Moreover, temperature was found as an important parameter in damageability of both rigid and flexible pavements, albeit by different mechanisms in this study. While developed from empirical observations at the

AASHO Road Test, Load equivalency factor (LEF) values for various axle configurations along with axle weight and spacing have a high correlation with pavement strains and deflections, which justifies the use of mechanistic principles to predict pavement distress formation (Hajek and Agarwal, 1990). Moreover, tire and axle types have significant effect on pavement damage. For instance, one tandem axle has been found to cause less fatigue damage than the two single axles (Sebaaly and Tabatabaee, 1992) due to the effect of load distribution on the pavement surface. Increased truck tire pressure can also influence immediate pavement responses, which is closely related to long-term effects on the pavement (Wang 2005).

1.2. Objectives of the study

The objective of this study is to evaluate the pavement responses under loading of multi-axles (11 axles) heavy Michigan trucks including the impacts of different tire configurations and to compare these responses with a standard 5-axle semi-trailer that is widely utilized across the nation. A series of truck configuration and axle parameters are considered to determine the effect of truck loading on rigid and flexible pavements responses for typical Michigan pavement designs and material properties. Moreover, an environmental effect (temperature gradient) is included to analyze the rigid pavement responses for the purpose of determining the relative magnitude of road damage under thermal conditions that areas of the state may undergo. Therefore, the specific objectives of this study are the following:

i) To determine the pavement responses (stresses, strains and deflections) under loading of different multi-axle heavy trucks.

ii) To compare the pavement responses between the multi-axle heavy trucks and a typical 5-axle semi standard trailer.

iii) To analyze major damage models incorporating the pavement responses. This objective is accomplished by determination of fatigue and faulting damage models for rigid pavements as well as fatigue and subgrade rutting models for flexible (asphalt) pavements.

iv) To determine the conditions (pavement thickness, joint system, materials, environmental conditions, etc.) in which a fully-loaded (164,000 lb.) 11-axle truck could cause significant damage to the pavement in comparison with a fully-loaded (80,000 lb.) standard 5-axle truck for typical Michigan conditions.

v) To make recommendations accordingly for regulation of heavy vehicles in Michigan.

1.3. Outline of the thesis

The structure of this thesis is as follows: Chapter 1 has provided an introduction to the objective of the study. Chapter 2 is a literature review that includes a discussion of previous and current response analysis models in flexible and rigid pavements, distresses and damage models in both cases of flexible and rigid pavements. Chapter 2 also provides information on the truck weight laws for Michigan and other states for

comparison. Chapter 3 presents an analysis of rigid pavement structures for typical Michigan conditions to determine the relative magnitude of road damage associated with various variables (e.g. vehicle configuration, relative offset from the pavement edge line, different loading positions, environmental conditions etc). Chapter 4 is an analysis of flexible pavement response from trucks of known axle loads and axle configurations. Chapter 5 presents conclusions as a result of this study.

CHAPTER 2

LITERATURE REVIEW

2.1. Introduction

The highway system serves as the most critical transportation link in the economic development of a nation. In Michigan, about seventy-four percent of all the commodities delivered annually are transported by trucks on highways (TRIP, 2015). Many transportation agencies have imposed strict load limits on gross vehicle weights (GVW) as well as individual axles weights based on the axle type. The first state in US to adopt a specific axle load limit of 18,000 lb. (80 kN) based on controlling damage from wagon wheels on unpaved roads in 1913 was Pennsylvania. According to ICC (1941), the axle weights limits ranged from 16,000 lb. (71 kN) in Alabama to 25,000 lb. (110 kN) in the District of Columbia which were adopted in most states within 20 years. In 1932, the American Association of State Highway Officials (AASHO) recommended an axle limit of 16,000 lb. (71 kN) for single axles. However, a revised policy was made on load limits of 18,000 lb. (80 kN) for single axles and 32,000 lb. (142 kN) for tandem axles in 1946 (AASHO 1946). These thresholds of these axle levels were considered to not affect the majority of vehicles. Based on the AASHO Road Test conducted in Ottawa, Illinois from 1958-1960, axle load limits were recommended as 18,000 lb. (80kN) for single axles and

34,000 lb. (151 kN) for tandem axles respectively in 1964 and were eventually implemented in 1974.

While overload permits are often awarded based on the GVW, Michigan's truck weight law is designed to control axle loads instead of gross vehicle weight. While most of the states adhere to 80,000 lb. (356 kN) limit as recommended by the Federal Highway Administration (FHWA), the maximum allowable gross vehicle weight on the heaviest Michigan weight law truck is 164,000 lb. (730 kN) for an 11-axles truck in the state of Michigan. However, Michigan limits the weight allowed on individual axles, depending upon the spacing between the axles. Most of these axles carry only 13,000 pounds each of eleven properly-spaced axles. While the GVW is of importance in determining pavement damage, individual axle weights are thought to be more of the motivating force in pavement distress development. According to Secretary of State, the numbers of total registered truck are 79,865 (Table 2.1) (MDOT 2012). Of these trucks, 6385 registered trucks are allowed to carry over 80,000 pounds and 2,649 were registered to carry over 145,000 pounds. Since, majority of trucks allowed on interstate highway are assumed to be of 80,000 pounds, it is estimated that fewer than 5% of all trucks using Michigan roads carry more than 80,000 pounds when fully operated.

For the investigation of effective approaches to determine the effect of Michigan trucks loading on the pavement responses, a detail review of theoretical response models for the pavement based on closed form analytical solutions or numerical approaches is addressed here. For applications of external loads, flexible and rigid pavements respond in a different way as distress formation under the same loading conditions result in

different distress development. Therefore, the flexible and rigid pavement response models are also different. The mode of flexible and rigid pavement responses under the application of loads and their corresponding response models are discussed here.

Table 2.1: Population of trucks by weight in Michigan (MDOT 2012)

Elected GVW	**Number of trucks available in MI**
0 to 24,000 lbs.	38,071
24,001 to 26,000	8,079
26,001 to 28,000	1,812
28,001 to 32,000	4,668
32,001 to 36,000	3,309
36,001 to 42,000	1,756
42,001 to 48,000	2,765
48,001 to 54,000	5,384
54,001 to 60,000	1,278
60,001 to 66,000	1,020
66,001 to 72,000	2,612
72,001 to 80,000	2,756
80,001 to 90,000	924
90,001 to 100,000	778
100,001 to 115,000	710
115,001 to 130,000	737
130,001 to 145,000	587
145,001 to 160,000	2,328
160,001 to 164,000	321
All elected-GVW trucks	79,895

2.2. Types of pavement

There are three general types of pavements in service, which are flexible, rigid and composite pavements. A flexible pavement consists of an asphalt concrete (AC) wearing course, an asphalt binder course underlain by one or more base layers and subbase layers which may or may not be stabilized (Fig. 2.1). A rigid pavement, also known as concrete or Portland cement concrete (PCC) pavement contains one or more concrete layers, finite in length and width, known as concrete slab (Fig. 2.1). This concrete slab rests on a foundation soil, known as subgrade with or without a subbase. Sometimes, there is a de-bonding layer (a base layer) between the concrete slab and subbase to reduce early age cracking, provide subsurface drainage, and uniform support. Engineered transverse and longitudinal joints connect the concrete slabs to each other and with the shoulder, for which slabs can expand or shrink according to temperature gradients. A composite pavement typically consists of an AC layer as surface course and PCC slab as base (Fig. 2.2). It is rarely used as a new constructed pavement, but instead commonly used as a rehabilitated pavement with the overlay providing added structural support and a smoother driving surface initially.

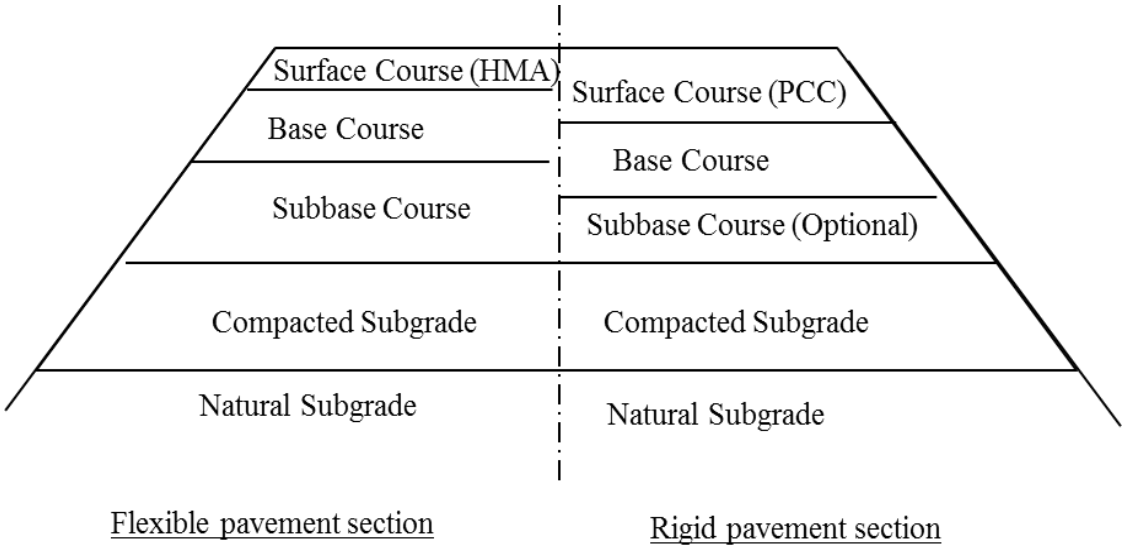

Figure 2.1: Typical sections of a flexible pavement and a rigid pavement.

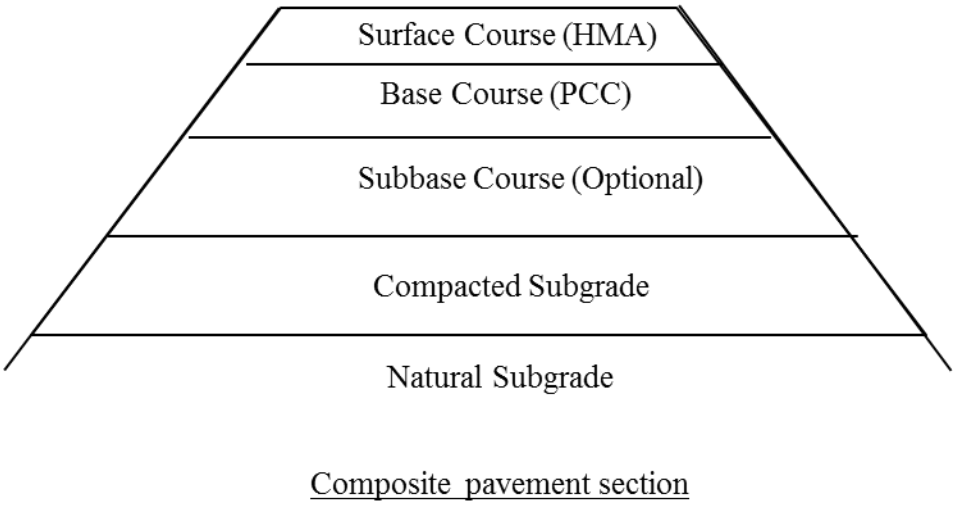

Figure 2.2: Typical sections of a composite pavement.

2.2.1. Failure mechanisms of pavements

The failure mechanism pavement depends on the types of pavement and its material properties, loading and environmental condition. The distress formation in to primary type of pavements: rigid pavement and flexible pavement are discusses here. There are varieties of distresses existing in both flexible and rigid pavements, but not all of them are analyzed in this study. Only the load-related and well-defined mechanistic models for prediction are considered in this study.

2.2.1.1. Rigid pavement distress formation

A major failure in concrete pavement structures is fatigue crack formation and propagation. It is a consequence of stresses due to a repeated traffic loading that may not exceed the flexural strength of concrete pavement, but when repeated applied these stresses can propagate structural cracks though the PCC layer of the pavement. These stresses can be manifested through external loads, temperature gradients, moisture gradients, as well as a combination of the three at any given time (Roesler, 1998).The resulting change of stress due to the repeated load applications, micro-cracks accumulate and propagate in the concrete of a slab, which eventually extends to the surface (or to the bottom), resulting in transverse cracks (i.e. cracks that is perpendicular to the direction of traffic), longitudinal cracks (cracks that is parallel to the direction of traffic), and/or corner breaks (see Fig. 2.3). For the fatigue damage analysis, the stresses or strains at the bottom of the PCC surface layer are commonly used because in most cases, the maximum tensile stresses are predicted at the bottom layer due to traffic loading near the

midway of longitudinal edge of PCC slab. However, this is not always the case when temperature and moisture gradients are involved (Hiller, 2007). A critical response of rigid pavement for top-down cracking is characterized as tensile stress at the top of the slab when a combination of axles of vehicle loads the opposite ends of a slab simultaneously under high negative temperature gradients.

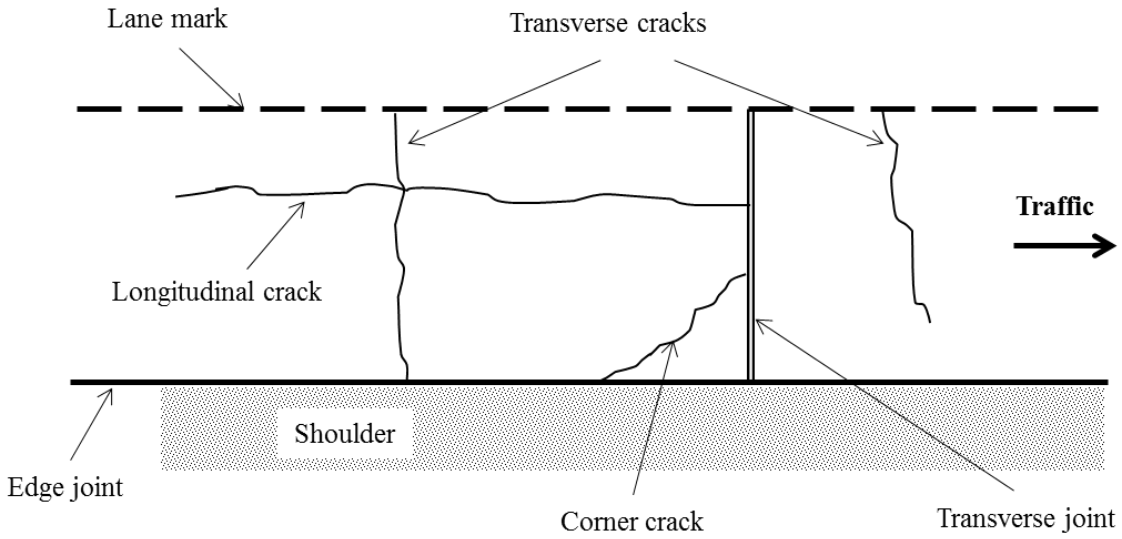

Figure 2.3: Distresses that develop in the rigid pavement under traffic loading.

Transverse joint faulting is another primary distress occurring in concrete pavements. It is measured as the difference in elevation across a transverse joint. With a repeated heavy axle loading and an insufficient load transfer between the adjacent slabs, a joint faulting occurs. Since the faulting damage incorporates the elevation difference between the unloaded and loaded slabs, the pavement deflections at the loaded and unloaded slabs are commonly used for the faulting damage analysis. Many factors could

attribute to the development of faulting including repeated heavy axle loading, insufficient load transfer at a transverse joint, erodible base or subgrade material, and free moisture in the pavement structure.

When excess moisture during the Spring thawing period exists in a pavement structure with an erodible base or underlying fine-grained subgrade materials, repeated heavy loading could cause pumping of excess water along with fine materials from the bottom of the slab through the transverse joint or along the shoulder. This pumping process eventually will result in void below the slab corner when vehicle loading leaves the slab. Pumping is caused by rapid vertical deflection of the leave slab at a transverse joint, which leads to the ejection of water with fine materials.

In addition, some of the fine materials that are not ejected by the pumping process will be deposited under the approach slab corner. This deposition process will eventually cause the elevation rise of the approach slab. The combination of the approach slab elevation rise and lose of the subgrade support of the leave slab can lead to significant faulting at the two adjacent joints, especially for joints without dowel bars. Corner crack can eventually occur because of the significant faulting damage.

An induced tensile stress in the pavement highly dependents on the magnitude and location of traffic load and the configuration of vehicles (Yu et al., 1998; Hiller and Roesler, 2002; Sargand and Abdalla, 2006). In addition, axle type, tire type, vehicle suspension, tire pressure and other factors such as pavement properties and environmental factors can have various damaging effects (Gillespie et al., 1993; Fekrat, 2010; Wang, 2011). Therefore, stresses on the pavement should be computed for many different cases, including traffic loads at different locations on pavements subjected to

environmental factors. Although field tests (McCracken, 2006; Chatti et al., 2009) are capable of making these computations, the analysis is very expensive which requires hundreds of thousands to millions of stress and deflection measurements to compute damage over a region of interest. A 2D (two dimensional) finite element method, which is a robust and widely acceptable numerical technique for stress analysis, is used in this study to reduce the computational time.

A pavement deformation due to a variation of temperature or moisture content across the depth of concrete pavement is referred to as a curling or warping, respectively. Other slab displacements that are due to environmental factors are a permanent built-in negative curling that occurs during the concrete hardening, a permanent warping that occurs due to differential drying shrinkage, and a creeping due to weight of slab (Yu et al., 1998; Yu et al., 2004).

2.2.1.2. Flexible pavement distress formation

The most common failure mode in asphalt pavement is the fatigue cracking which is caused by a horizontal tensile strain at the bottom of hot mixed asphalt (HMA) layer. This distress is also known as alligator cracking or bottom-up cracking. Repeated traffic loads, higher wheel loads, and greater tire pressures cause more bending of the HMA layer, which results in tensile stress and strain to develop cracks at the bottom of the layer. Another major failure mode is rutting, which is a permanent deformation in the pavement along the wheel path. Rutting is due to vertical (compression) strain at the top of each layer in the flexible pavement system. These multiple layers of AC, base, and

subbase materials are designed to protect the subgrade soil from excess shear forces from wheel loads, which can lead to subgrade rutting. For asphalt pavements, environmental effects are accounted for in varied resilient moduli of the layers, which lead to changes in pavement damage resulting from different axle load combined with truck configurations (Gillespie et al, 1993 Hajek, 1990, 1995, Ilves and Majidzadeh 1991, J. M. Sadeghi and M. Fathali 2007).

2.2.1.3. Mechanistic prediction of distresses

The mechanistic methods of pavement structural response models compute stress, strain and deflection in the pavement structure due to traffic loads and/or climatic factors. Numerous mechanistic methods have been developed ranging from Boussinesq's one-layer model to multi-layer elastic theories to finite element models to predict or assess pavement performance that reflect current paving materials and traffic conditions. The effects of varying restraint conditions, temperature gradients, and load magnitudes on the measured critical stresses, strains and deflections can be characterized and help provide a clearer picture of all the parameters affecting pavement distress formation. This mechanistic prediction method accounts for the incremental damage associated with each load applied to the pavement throughout the design life of the structure.

2.3. Flexible pavement response models

2.3.1. Boussinesq Single layer model

One of the first mechanistic models for pavement response prediction was developed by a French mathematician and physicist named Joseph Valentin Boussinesq. In the Boussinesq theory (1885), the pavement responses (stresses, strains and deflections) are determined in a homogenous, isotropic and linear elastic half space soil mass subjected to a static point load. The following assumptions (Venkatramaiah, 2006) are considered for the Boussinesq's equations:

i) The pavement system is an elastic, homogenous, isotropic, and semi-infinite medium.

ii) The soil medium obeys Hooke's law relating stress and strain elastically

iii) The soil of the pavement structures weightless.

iv) The initial stress of soil is zero.

v) There is no change in the volume of soil upon application of load.

vi) There is no shear stress on the top surface of the soil (from acceleration/deceleration of the wheel loads) and the load is vertical point load acting on the surface at a specific location.

vii) The distribution of stresses is symmetrical with respect to z axis.

viii) The continuity of stress is considered to exist in the soil.

Although the Boussinesq's equations were originated for a vertical point load (Fig. 2.1), later these equations were extended for uniformly distributed load (Newmark, 1947; Sanborn and Yoder, 1967).The Boussinesq's equations are very useful tool for providing

a basis for pavement analysis development; however, these equations are seldom used as the main design theory due to their extreme limitations to real-life pavement applications today.

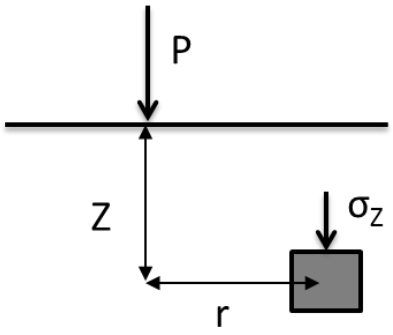

Figure 2.4: Point loading at the surface in a homogeneous, isotropic and elastic media.

2.3.2. Burmister two layer elastic model

Donald Burmister's theory (1943) is considered to be a better model over Boussinesq's theory for the analysis of flexible pavement behavior. Boussinesq's equations were developed assuming that the pavement system as a homogenous mass, but in reality, pavements typically have multiple layers with a stiffer layer on top. The assumptions adopted in Burmister's theory to calculate stresses, strains and displacement for a two-layered flexible pavement system (Fig. 2.2) include:

i) The pavement system consists of two layers. Each layer is homogenous, isotropic and linearly elastic.

ii) Each layer obeys Hooke's law.

iii) The top layer consists of a uniform, finite thickness and infinite dimensions in all horizontal directions, resting on a semi-infinite elastic half-space.

iv) The initial stress and deformation of soil before application of load is zero.

v) The soil is weightless.

vi) For the case of fully bonded layer interfaces, the normal stresses, vertical displacements and radial displacements are same.

vii) For the case of frictionless interface, there is discontinuity of shear stress and radial displacement at each side of the interface.

viii) A circular, distributed uniform load to approximate the effects of tire pressure versus a point load

These improvements lead to a better understanding of how the asphalt layer could be designed since a finite thickness for the top layer was required, unlike the Boussinesq theory. However, the Burmister's equations are seldom used for analytical solutions of pavement analysis, since these equations have been extended to a three-layer system (Burmister, 1945) to obtain a closer approximation of an actual pavement system.

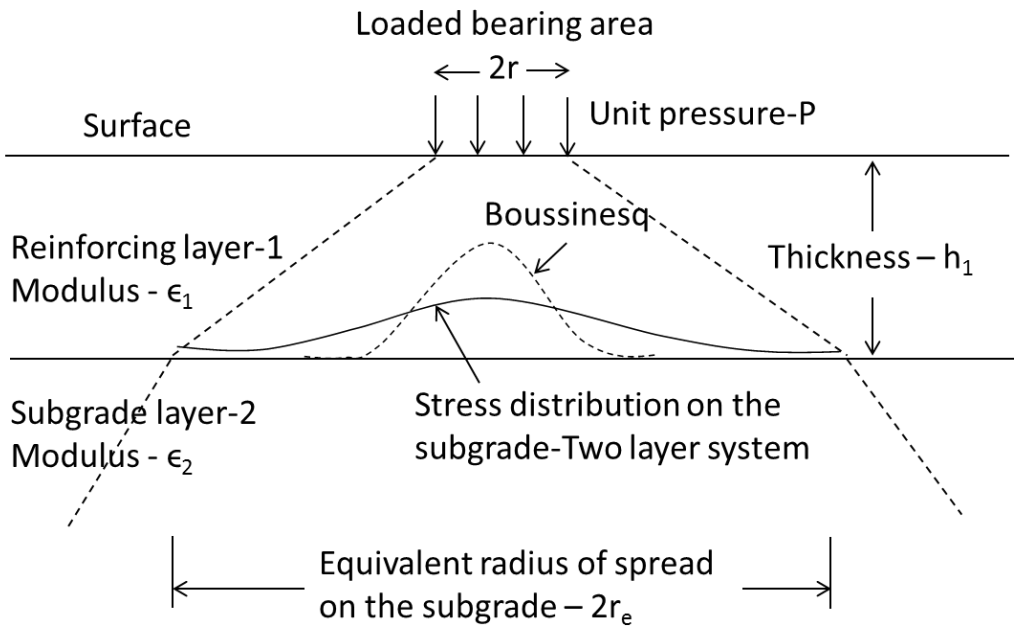

Figure 2.5: Schematic of Burmister's two-layer system.

2.3.3. Multi-layer elastic theory model

Acum and Fox (1951) described a three-layer system for the stresses and displacements based on variables such as the radius of the uniformly loaded circular area, the thickness of the two top layers (to account for the effect of a base layer), and the elastic moduli of the three layers. Jones (1962) extended the Acum and Fox's theory working on the same parameters, but under a wide range. However, the three-layer system of pavement is only considered with a single concentrated force or uniformly distributed load. Schiffman (1962) developed new solutions for the analysis of stresses and deflections which considered tangential loads and non-uniform loads in an N-layer elastic system (Fig. 2.3). The N-layer system allows one to account for the effects of all layers in a typical flexible pavement system under layered elastic theory.

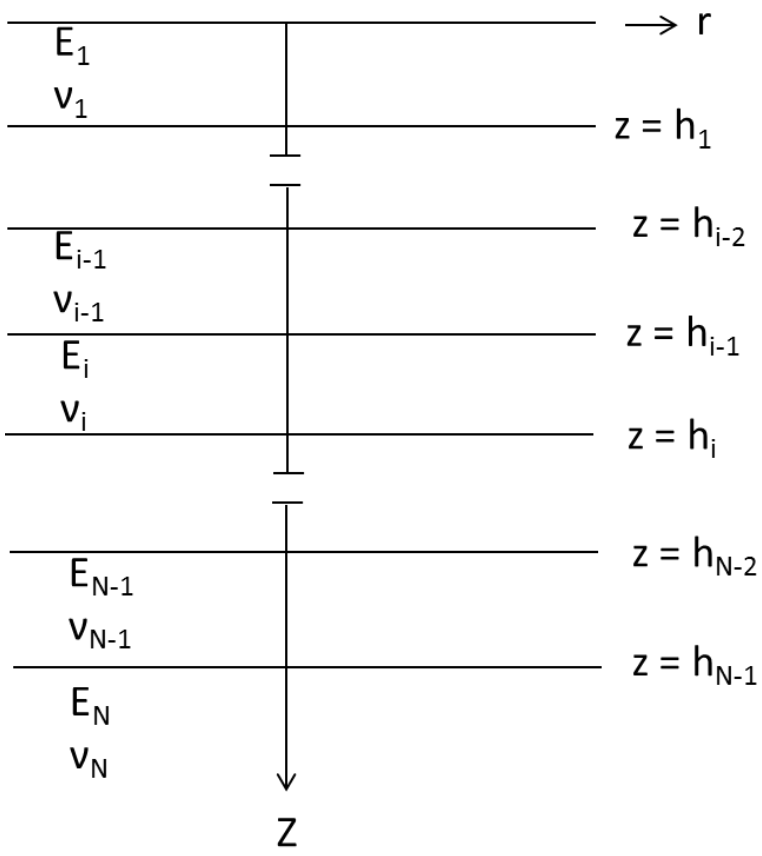

Figure 2.6: Schematic of N-layer elastic system.

However, Schiffman's analytical solutions required quite complex computations and therefore could not be directly applied in engineering practice. Since then, many elastic layered computer programs have been developed based on the multi-layered elastic theory. Some of these programs include CHEVRON, BISAR, ELSYM5, KENLAYER, and WESLEA. In case of multi-layer elastic theory program, the flexible pavement systems are often treated as linearly elastic. Among all these models, WESLEA is a multi-layer linear elastic program developed by the U.S. Army Corps of Engineers Waterways Experiment Station (Van Cauwelaert et al., 1989). This program has the

capability of analyzing more than ten layers with more than ten loads to account for multiple axle loadings. A modified version of WESLEA, referred as Jacob Uzan Layered Elastic Analysis (JULEA), has been integrated into the recent published Mechanistic Empirical Pavement Design Guide (MEPDG) as the major response model for flexible pavements (NCHRP, 2004).

The MEPDG design procedure assumes that the load-strain relationship is linearly proportional (NCHRP, 2004). For the case of a purely linear material behavior, the JULEA multilayer elastic theory program is used for the pavement response model. The basic assumption of linear elastic analysis is that the pavement response (stress or strain) is linearly proportional to the applied load. As the load increases or decreases on the pavement surface, the response at a given point will increase or decrease linearly. In this procedure, the loaded area is assumed to be circular with uniform contact pressure. However, the MEPDG considers only one tire pressure value for the entire load spectrum and the recommended tire inflation pressures for commonly used truck tires fall within a range of 96 psi to 120 psi (Thyagarajan, 2009).

The KENLAYER program can also model the pavement layers as being either linear elastic with a computational time ranging from very short (less than 1 second) to up to 25 seconds for a 9-layer system with 35 stress computation points per layer (NHCRP, 2004). However, JULEA is nearly an order of magnitude more efficient than KENLAYER. A typical flexible pavement design scenario would require on the order of one second or less per analysis to be efficient under a mechanistic design scenario to account for changes in moduli and load configurations. JULEA is capable for the most

complex analysis for a nine-layer pavement system, a total of 315 stress calculation points (9 depths, 35 radial locations per depth), and a dual tandem tire configuration (with automatic superposition of tire loads by the program). JULEA provides an excellent combination of analysis features, theoretical rigor, and computational speed for linear pavement analyses to determine the pavement response for the cases in which all materials in the pavement structure can realistically be treated as linearly elastic. This program requires quick computation times and minimal input parameters which consist of thicknesses and elastic properties of the layers and the tire contact radius and pressure. This is the primary reason for its inclusion as the response prediction algorithm for real-time computation for flexible pavements in the MEPDG.

Several other computation model programs have been developed to model flexible pavement systems. A 3-D finite element program called ILLI-PAVE was developed by Raad and Figueroa (1980) to model the flexible pavement behaviors. Finite element analysis (FEA) counts the non-linearity in the unbound materials more accurately in the flexible pavement system**.** For the non-linear materials, response is not linearly related to the applied load and the material is defined as stress dependent as the materials. However, incorporation of unbound material nonlinearity in the FEA solutions will increase the required execution times for pavement analysis. The Guide for Mechanistic-Empirical Design of new and rehabilitated pavement structures (2004) assumes linear elastic models for flexible pavement layer. Therefore, in this study FEA study has not been used for flexible pavement analysis because of the additional computational time needed for FEA.

2.4. Rigid pavement response models

The multi-layer elastic theory model is not considered appropriate tool for rigid pavement response (stress, strain or deflection) analysis (Ullidtz, 1987). This is primarily due to the discrete slab size effects in rigid pavements. The PCC slab of rigid pavements transfer the traffic load to a wider area with higher structural capacity than flexible pavements because concrete has higher modulus of elasticity than asphalt (WSDOT, 2003). Moreover, due to presence of longitudinal and transverse joints, load transfer mechanism (e.g., dowel bars, aggregate interlocks), and effects of environmental conditions (e.g., temperature curling, moisture warping) on rigid pavements, the analysis becomes more complicated and therefore different tools are required for rigorous analysis.

2.4.1. Westergaard's analytical solution

Harald Malcolm Westergaard developed one of the earliest theories(1926) fora closed-form analytical solution for jointed concrete pavement responses (i.e. stresses, deflections) due to traffic loading and environmental effects (e.g. thermal curling) (Westergaard, 1926a and 1926b). The basic assumption of his model is that no shear interaction in the subgrade (i.e. Winkler foundation condition) occurs. The subgrade is characterized by a single parameter, the modulus of subgrade reaction or the k-value assumed to be constant during shear deformation (Darestani, 2007). The vertical pressure of the subgrade to the concrete slab is a constant which equals to subgrade reaction (k)

times the vertical deflection. The following assumptions were made in Westergaard's original work (Westergaard, 1926a):

i) The concrete slab is assumed to be a homogeneous, isotropic, elastic solid in equilibrium

ii) The classic Kirchhoff medium-thick plate theory is assumed for the concrete slab, i.e. the transverse shear stresses are ignored

iii) The reaction of the subgrade is only vertical and is proportional to the deflection of the slab

iv) The concrete is resting on a set of springs with the spring constant k, independent of the slab deflection

v) The thickness of the slab is uniform

vi) Three loading conditions are considered: interior loading, corner, and edge

vii) The loading pressure is assumed to be distributed uniformly over a circular or semi-circular area with radius a (Fig. 2.4)

viii) The slab is only subjected to one wheel load.

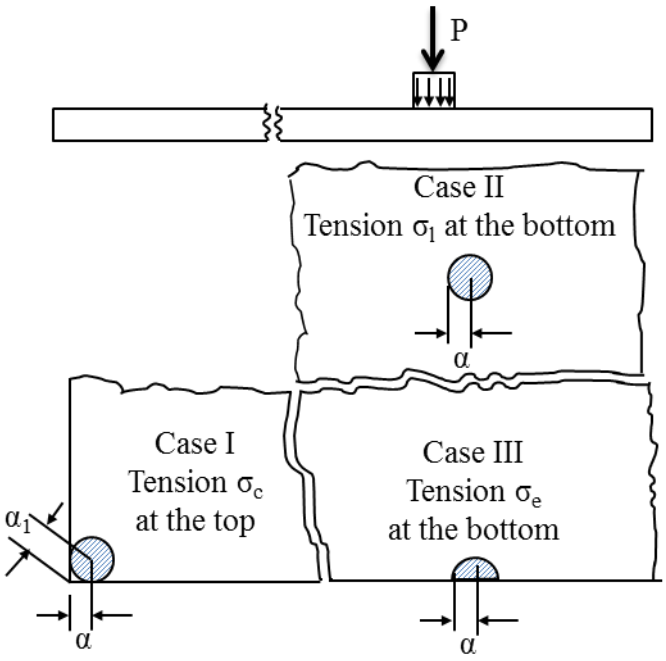

Figure 2.7: Schematic is showing three loading conditions for Westergaard equations.

Though Westergaard's equations were used to calculate the stresses as well as deflections of rigid pavements subjected to load and curling under the theory of three loading locations, these analytical solutions do not represent the actual pavement behaviors because of too many idealized limitations. Moreover, another limitation in this theory is the inability to count multiple wheel loads which is a serious constraint in practical application.

2.4.2. Improved analytical models based on Westergaard's theory

Many improved models have been developed based on Westergaard's theory. Pickett and Ray (1951) developed influence charts based on Westergaard equations which considered the multiple wheel loadings applied to the pavements. Both Winkler (dense liquid) subgrade and the elastic solid subgrade conditions were included in their study. Later, the Newton-Raphson iteration procedure was developed to convert multiple wheel loadings to an equivalent single load which would produce the same bending stress and used this transformed loading in Westergaard's equations (Salsilli et al. 1993) for a single location of the slab. Three axle load configurations were considered: dual, tandem and tridem. Although closed-form analytical solutions have been widely used in the past in pavement analysis and design, the assumptions made to develop those solutions have too many limitations and can dramatically complicate the analysis. These models include graphical influence diagrams based on the work of Westergaard to calculate responses under limited loading conditions without load transferring mechanism.

2.5. Finite element models

The finite element method (FEM) has become a widely used tool for rigid pavement analysis since the early 1970s. FEM overcomes the limitations of analytical solutions in several ways. FEM can calculate pavement responses (i.e. stresses, strains and deflections) or a variety of input parameters (axle position, axle load levels, multiple slabs, curling etc.) and thus is a powerful tool to conduct combined temperature and mechanical loading analysis. With the development of a two dimensional (2-D) linear

elastic finite element model, the concrete slab was modeled with medium-thick plate elements (Wang et al., 1972). These theories are sometimes referred to as 2.5D FEA since the models predict pavement responses in both horizontal directions as well as at the top and bottom of each layer modeled. The classical plate theory based on Kirchhoff hypothesis was incorporated in their study to calculate the response of rigid pavements subjected to wheel loading. In this model, the foundation was modeled as an infinite elastic half space. The stresses and deflections computed with the finite element model were compared with those from Westergaard's equations. The comparison showed that the analytical solutions give lower stresses and deflections in most cases. However, in their model, the load transfer mechanism between slabs was not considered in rigid pavement analysis. Later, in another 2-D FEM, the foundation was modeled as an elastic continuum and the effect of load transfer from adjacent slabs were considered as well (Huang, 1974).

However, a more general 2-D finite element program was developed following the earlier FEM, referred to as ILLI-SLAB (Tabatabaie and Barenberg, 1978 and 1980). This model used medium-thick elements like earlier models and also incorporated the effect of bonded or un-bonded base layers using a second layer of plate elements below the concrete slab. The subgrade was modeled as Winkler foundation in their study. Later implemented finite element programs included such programs as JSLAB (Tayabji and Colley, 1986), FEACONS (Finite Element Analysis of CONcrete Slabs) (Tia et. al., 1987) and others. However, these models can analyze only a single layer slab when a temperature gradient is introduced. Other models i.e. WESLIQUID (Chou, 1981) and

KENSLABS (Huang, 1993) can analyze a two-layer slab system, but only if the temperature gradient is linear and both layers are subjected to the same temperature gradient. This provides a severe limitation as the thermal properties of different layers often lead to different thermal gradients through the depth of a rigid pavement structure. However, the ILLI-SLAB program differs from all other programs in the following ways (Khazanovich, 1994; Khazanovich and Yu, 1998):

i) A wide selection of subgrade models, including Winkler, elastic solid, Pasternak, Kerr-Vlasov and Zhemochkin-Sinitsyn-Shtaerman.
ii) An ability to analyze the effect of the independent actions of two pavement layers.
iii) An ability to analyze the effect of linear and nonlinear temperature distribution throughout the pavement thickness.
iv) An ability to analyze partial-depth cracks using fracture mechanics principles in newer versions of the program.

Although ILLI-SLAB incorporates a number of subgrade models that represent the realistic characterization of a PCC slab, the Winkler model is recommended for the MEPDG due to its simplicity and computational time requirements. A significant analysis of curling of two unbound pavement layers has been implemented in ILLI-SLAB program, whereas curling can cause the upper pavement slab to lift off the underlying pavement or stabilized base. The latest enhancements to ILLI-SLAB include ILSL2, developed at the University of Illinois, and a revised version of ILSL2 namedISLAB2000, developed by ERES Consultants (now ARA). FEM results from the ISLAB2000 version have been integrated into the new Mechanistic-Empirical Pavement

Design Guide as the rigid pavement structural response model (Khazanovich, 1994; Khazanovich and Yu, 1998) through the use of a trained artificial neural network (ANN). ISLAB2000 (ERES, 1999) is a 2-D finite element program for rigid pavements that utilizes medium-thick plate theory and builds upon the development of earlier ILLI-SLAB programs (Tabatabaie and Barenberg, 1978; Ioannides, 1984; Korovesis, 1990; and Khazanovich, 1994). The capabilities of ISLAB2000 are much greater than those of earlier models because it can model several layers of a pavement system which exhibit more accurate analysis. This model has the ability to model multiple important features of pavement system **(**multiple slabs, multiple layers, mismatched joints, multiple loads, temperature curling).

There are several 3-D, nonlinear dynamic finite element models such as ABAQUS (Zaghloul et al., 1994; Uddin et al., 1995; Kuo et al.,1995; Darter et al.,1995; Masad et al.,1996) and EVERFE (Davids,1998) to model the response of jointed plain concrete pavement systems due to wheel loads and environmental effects. However, those 3-D non-linear dynamic models also have limitations. The modeling needed for 3-D analysis requires considerable expertise in engineering mechanics from the user and each analysis demands a large amount of computation time (on the order of 20+ minutes per scenario). Due to these factors, the applications of these programs are usually limited to research purposes.

Hammons (1997) conducted a study considering a single slab resting on the Winkler foundation and loaded by a single load at its interior or at the edge to make a comparison between ABAQUS (3D FEM) and ILLI-SLAB (2.5D FEM). He concluded

that ILLI-SLAB is a reliable tool for a simplified analysis of rigid pavement systems. Moreover, Hammons concluded that the ILLI-SLAB model provides sufficient accuracy for the analysis of pavement systems while ABAQUS modeling is unnecessarily complicated for most practical purposes.

2.6. Flexible pavement distress model

The critical stress or strain values determined for each incremental load, these values are converted to incremental distresses, either in absolute terms (e.g., incremental rut depth) or in terms of a damage index (e.g., fatigue cracking).For flexible pavement designs, the MEPDG divides the structural layers of the design into sublayers. The JULEA program then calculates the critical responses in each sublayer. Due to this use in the MEPDG, the JULEA multilayer elastic computer program was adopted for use in this study to calculate the pavement responses needed for distress predictions. While other distresses are predictedin the MEPDG, the major, load-related distresses analyzed in the design guide for the flexible pavements are: Permanent deformation (or rutting) and Alligator Fatigue Cracking (bottom-up).

2.6.1. Permanent deformation

One of the most important types of load-associated distresses occurring in flexible pavement is permanent deformation. This distress accumulates as a depression or rutting along the wheel path of heavily traveled pavements developing gradually with the number of load repetitions. It is typically the result of consolidation and densification,

and plastic flow of the pavement materials (HMA, aggregate base, and subgrade soils). Rut depth is calculated at the mid depth of each sub-layer of asphalt bonded and un-bonded layers of pavement accumulated at the end of each sub-season in the MPEDG program. The overall permanent deformation for a given season is the sum of permanent deformation for each individual layer or sublayer as the process is repeated for each load level, axle type, sub-season, and incremental analysis period and is mathematically expressed as (NCHRP 2004):

$$\text{RD} = \sum_{i=1}^{nSublayer} \varepsilon_p^i \, h^i \tag{2.1}$$

where RD is rut depth, n-Sublayers is the number of sub-layers, ε_p^i is the total plastic strain in sub-layer i, and h^i is the thickness of sub-layer i.

Huang (1974) adopted two design procedures to limit rutting or plastic vertical deformation. One is vertical compressive strain on top of subgrade and the other is total accumulated permanent deformation on the pavement surface. For rutting model, the approach to calculate the allowable number of axle-load applications to limit rutting related to vertical compressive strain on top of subgrade based on the Asphalt Institute and Shell design methods is shown in Equation below (Huang, 1974)

$$N_d = f_4 \, (\varepsilon_c)^{-f_5} \tag{2.2}$$

where $N_d$is the allowable number of load repetitions and$\varepsilon_c$is the vertical compressive strain on top of subgrade and f_4 , f_5 are the coefficients (used by several agencies)

Table 2.2: Magnitude of coefficients determined by different agencies.

Agency	f_4	f_5
Asphalt Institute	1.365X10-^{9}	4.477
U.K. Transport & Road Research	6.18X10-^{8}	3.95

The procedure to compute rutting or plastic vertical deformation in the MEPDG, in HMA layers is shown in Equation 2.3 below. The calculation uses an accumulation of plastic vertical deformation based on critical plastic vertical strain, specific pavement conditions, and truck loadings.

$$\Delta_{p(HMA)} = \varepsilon_{p(HMA)} h_{HMA} = \beta_{1r} k_z \varepsilon_{r(HMA)} 10^{k_{1r}} n^{k_{2r}\beta_{2r}} T^{k_{3r}\beta_{3r}} \quad (2.3)$$

where

$\Delta_{p(HMA)}$= Accumulated permanent or plastic vertical deformation in the HMA layer/sublayer

$\varepsilon_{p(HMA)}$= Accumulated permanent or plastic axial strain in the HMA layer/sublayer

$\varepsilon_{r(HMA)}$= Resilient or elastic strain calculated at the mid-depth of each HMA sublayer

h_{HMA}= Thickness of the HMA layer/sublayer

n = Number of axle-load repetitions

T = Mix or pavement temperature

k_z= Depth confinement factor

$k_{1,2,3}$= Global field calibration parameters (k1r = -3.35412, k2r = 0.4791, k3r = 1.5606)

$\beta_{1,2,3}$= Local or mixture field calibration constants; for the global calibration, these constants were all set to 1.

$$k_z = (C_1 + C_2 D)0.328196^D \quad (2.4)$$

$$C_1 = -0.1039(H_{HMA})^2 + 2.4868H_{HMA} - 17.342 \quad (2.5)$$

$$C_2 = 0.0172(H_{HMA})^2 - 1.7331H_{HMA} + 27.428 \quad (2.6)$$

where *D* is the depth below the surface and H_{HMA} is the total HMA thickness. Equation (2.7) represents the field-calibrated mathematical equation for rutting in the foundation and all unbound pavement layers.

$$\Delta_{p(soil)} = \beta_{s1} k_{s1} \varepsilon_\vartheta h_{soil} \left(\frac{\varepsilon_0}{\varepsilon_r}\right) e^{-\left(\frac{\rho}{n}\right)^\beta} \quad (2.7)$$

where

$\Delta_{p(soil)}$= Permanent or plastic deformation for the layer/sublayer

n = Number of axle-load applications

ε_0= Intercept determined from laboratory repeated load permanent deformation tests

ε_r= Resilient strain imposed in laboratory test to obtain material properties and ρ

ε_ϑ= Average vertical resilient or elastic strain in the layer/sublayer

h_{soil}= Thickness of the unbound layer/sublayer

k_{s1}= Global calibration coefficients; k_{s1} = 1.673 for granular materials and 1.35 for fine-grained materials

β_{s1}= Local or mixture field calibration constants; for the global calibration, these constants were all set to 1.0.

$$log\beta = -0.61119 - 0.017638(W_c) \quad (2.8)$$

$$\rho = 10^9\left(\frac{C_0}{1-(10^9)^\beta}\right)^{\frac{1}{\beta}} \quad (2.9)$$

$$C_0 = \ln\left(\frac{a_1 M_r^{b_1}}{a_9 M_r^{b_9}}\right) = 0.0075 \quad (2.10)$$

where

W_c= Water content, %

M_r = Resilient modulus of the unbound layer or sublayer

$a_{1,9}$ = Regression constants; a1=0.15 and a9=20.0

$b_{1,9}$ = Regression constants; b1=0.0 and b9=0.0

2.6.2. Alligator cracking (Bottom-up fatigue cracking)

Fatigue cracking is another major load-associated distress in flexible pavement systems. It occurs due to the repeated bending of the HMA layer under traffic. Under repeated load applications, tensile strains and stresses initiate at the bottom of the asphalt layer due to the deflections of the HMA layer and then propagate to the surface. This type of cracking also initiates longitudinal cracks in the wheel path and become interconnected to form a chicken wire/alligator cracking pattern. Bottom-up fatigue cracking is predicted in terms of a damage index and the incremental damage is accumulated for each analysis period using Miner's (Miner 1945) hypothesis as (NCHRP, 2004):

$$D = \sum_{i=1}^{T} \frac{n_i}{N_{f,i}} \quad (2.11)$$

where D is the damage, T is the total analysis period, $n_i$is the actual number of load repetition for period i, $N_{f,i}$ is the number of load repetition allowed under conditions prevailing in i.

For fatigue cracking models, the approach to calculate the allowable number of axle-load applications is needed for the incremental damage index. The allowable number of load repetitions, N_f, based on the Asphalt Institute and Shell design methods is shown in Equation below (used by Illinois Department of Transportation) (Thompson, 1987)

$$N_f = 5X10^{-6}(\varepsilon_t)^{-3} \quad (2.12)$$

where $N_f$is the allowable number of load repetitions to fatigue cracking and ε_t is tensile strain at the bottom of HMA.

Alligator cracks are assumed to initiate at the bottom of HMA layers, while longitudinal cracks are assumed to initiate at the surface of the pavement. For both load related cracking models, the approach to calculate the allowable number of axle-load applications in the MEPDG needed for the incremental damage index is shown using Equation 2.13.

$$N_{f-HMA} = k_{f1}(C)(C_H)\beta_{f1}(\varepsilon_t)^{k_{f2}\beta_{f2}}(E_{HMA})^{k_{f2}\beta_{f3}} \quad (2.13)$$

where

N_{f-HMA}= Allowable number of axle-load applications for a flexible pavement and HMA overlays

ε_t= Tensile strain at critical locations

E_{HMA}= Dynamic modulus of the HMA measured in compression

k_{f1}, k_{f2}, k_{f3}= Global field calibration parameters (k_{f1}=0.007566, k_{f2}=-3.9492, and k_{f3}=-1.281)

β_{f1}, β_{f2}, β_{f3}= Local or mixture specific field calibration constants; for the global calibration effort, these constants were set to 1.0

$$C = 10^M \quad (2.14)$$

$$M = 4.84\left(\frac{V_{be}}{V_a+V_{be}} - 0.69\right) \quad (2.15)$$

where

V_{be}= Effective asphalt content by volume, %,

V_a= Percent air voids in the HMA mixture

C_H= Thickness correction term, dependent on type of cracking

For alligator (bottom-up) cracking:

$$C_H = \frac{1}{0.000398 + \frac{0.003602}{1+e^{(11.02-3.49H_{HMA})}}} \quad (2.16)$$

For longitudinal (top-down) cracking:

$$C_H = \frac{1}{0.01 + \frac{12}{1+e^{(15.676-2.8186H_{HMA})}}} \quad (2.17)$$

where $H_{HMA}$is the total HMA thickness.

2.7. Rigid pavement distress model

Damage analysis can be conducted to determine the relative damage from various types of trucks compared to the damage caused by a standard truck. Faulting and fatigue damage are two primary distresses in jointed plain concrete pavements (JPCP) employed by the Mechanistic-Empirical Pavement Design Guide (MEPDG). For rigid pavements, the finite element analysis program ISLAB2000 is used in this study to compute needed pavement responses. The major distresses analyzed in the design guide for the rigid pavements are: fatigue cracking (bottom-up or top-down transverse cracking) and faulting at the transverse joint.

2.7.1. Fatigue cracking (bottom-up or top-down transverse cracking)

Fatigue cracking of PCC slabs can propagate through bottom-up or top-down mechanism due to traffic loading, curling and warping behaviors, material properties, and construction practices. A critical response of rigid pavement for bottom-up cracking is characterized when the maximum tensile stress location is at the bottom of the slab with axle loading near the midway of longitudinal edge of PCC slab (Heath et al., 2003; Wang, 2011). At this "mid-slab edge" loading condition, curling stress due to negative thermal gradients becomes negligible and positive gradients add to the load stress (Jiang and Tayabji, 1998). In the presence of high negative temperature gradients, the maximum tensile stress occurs on the top of the top slab addressing top-down cracking with axle loading near the transverse joint along longitudinal edge of the slab (Heath et al., 2003; Heath and Roesler, 2000a). Repeated heavy loading of vehicles in the presence of positive or negative temperature gradient eventually result in fatigue damage at critical response locations.

The MEPDG fatigue damage model adapted the following equation to calculate the fatigue damage. The detail descriptions of fatigue damage model using Miner's hypothesis are given as followings (NCHRP 2003):

$$FD = \sum \frac{n_{i,j,k,l,m,n,}}{N_{i,j,k,l,m,n}} \qquad (2.18)$$

where

FD = Total fatigue damage (top-down or bottom-up)

$n_{i,j,k,l,\ldots..}$=Actual number of load applications at condition i, j, k, l, m, n

$N_{i,j,k,l,\ldots..}$= Allowable number of load applications at condition i, j, k, l, m, n

i = Age (accounts for change in PCC modulus of rupture, layer bonding condition, deterioration of should LTE).

j = Axle type (single, tandem, and tridem for bottom-up cracking; short, medium, and long wheelbase for top-down cracking),

k = Load level (incremental load for each axle type),

l = Equivalent temperature difference between top and bottom PCC surfaces.

m = Traffic offset path.

The applied number of load applications (i,j,k,l,m,n) depends on the number of axle types (k) of load level (l) that passed through traffic path (n) under each condition (age, season, and temperature differentials throughout the slab. The allowable number of traffic load repetitions corresponds to the number of the load cycles at which 50 percent chance of fatigue failure is expected (corresponding to 50 percent slab cracking).This is a function of the applied stress and PCC strength (NCHRP 2003). While numerous transfer functions for fatigue have been developed from slab/beam field and laboratory testing, the allowable number of load repetitions is determined by the following fatigue modeling the MEPDG (NCHRP 2003):

$$Log\left(N_{i,j,k,l,m}\right) = C_1 * \left(\frac{M_{Ri}}{\sigma_{i,j,k,l,m}}\right)^{C_2} + 0.4371 \quad (2.19)$$

where

$N_{i,j,k}$ = allowable number of load applications at condition i, j, k, l, m, n

M_{Ri} = PCC modulus of rupture at age i, psi

$\sigma_{i,j,k,...}$ = applied stress at condition i, j, k, l, m, n

C1 = calibration constant = 2.0

C2 = calibration constant = 1.22

In this study, the fatigue damage characterized as allowable number of load repetitions (N_f) of all truck vehicles were estimated and compared with standard 80-kip 5-axle semi-truck.

2.7.2. Faulting at transverse joint

Transverse joint faulting is another primary distress occurring in JPCP. It is defined as the difference in elevation between adjacent joints at a transverse joint. With the presence of moisture in a PCC pavement with underlying fine-grained material, repeated heavy vehicle loadings and poor joint load transfer induces pumping of these fines through the transverse joint or along the shoulder resulting in rapid vertical deflection of the leave slab at a transverse joint (NCHRP, 2003).Pumping commonly is known as the ejection of water with fine materials resulting in voids below the leave slab corner. This leads to a difference in elevation across the joint or crack, or faulting. Severe faulting damage can eventually cause significant amount of corner cracking (Wang, 2011) as the pumping of these fines under the approach slab typically leads to erosion-induced voids under the leave slab. This increases the slab deflections and resulting bending stresses, resulting in a corner crack through fatigue.

The MEPDG faulting damage model adapted an incremental approach to calculate the faulting damage in this study. To calculate the mean transverse joint faulting, an incremental approach is used. For the current month, the faulting from each of the previous months from the start of the pavement life is summed using the equations below (NCHRP, 2003).

$$Fault_m = \sum_{i=1}^{m} \Delta Fault_i \quad (2.20)$$

where $\Delta Fault_i = C_{34} * (Faultmax_{i-1} - Fault_{i-1})^2 * DE_i$, $Fault_m$ represents the mean joint faulting at the end of month m and $\Delta Fault_i$ is the incremental change (monthly) in mean transverse joint faulting during month i.

However, the mean joint faulting at the end of month, m highly depends on the differential energy. The differential energy (DE) is defined as the energy difference in the elastic subgrade deformation under the loaded slab (leave) and the unloaded slab (approach)(NCHRP 2003):

$$DE = \frac{k}{2} (w_l + w_{ul})(w_l - w_{ul}) \quad (2.21)$$

where

DE= differential energy of subgrade deformation

w_l= corner deflection under the loaded slab

w_{ul} = corner deflection under the unloaded slab

k = modulus of subgrade reaction

Faulting damage analysis was also conducted for all truck vehicles and compared with a standard 80-kip five axle semi-trucks in terms of differential energy based on data availability in this study. The term $w_l + w_{ul}$ represents the total sum of corner deflection. Increase of corner deflection represents higher joint faulting. Another term, $w_l - w_{ul}$, represents the difference of corner deflection between the two adjacent slabs. In the case of higher difference of corner deflection also represents higher joint faulting.

CHAPTER 3

DAMAGE ANALYSES IN RIGID PAVEMENTS

3.1. Introduction

The fatigue and faulting damage on the rigid pavement under the loading by standard 5-axles and Michigan 11-axles truck are investigated in this chapter. In order to assess the differences in damage caused by 11-axle and 5-axle trucks on rigid pavements mechanistically, a variety of input parameters which are typical for Michigan concrete pavement sections (axle load levels, complicated wheel configurations/loadings, multiple slabs, temperature curling, etc.) have been considered to conduct a combined temperature and mechanical loading analysis. Finite Element (FE) modeling using ISLAB2000 (ERES 1999) has been conducted for damage analysis to determine the relative damage from various types of truck loading compared to a standard semi-trailer with 5 axles in rigid pavements under different site conditions and design features. Four heavily-loaded, 11-axle Michigan trucks, i.e. MI-13, MI-14, MI-18 and MI-20 (Fig. 3.1), have been selected in this analysis. The standard 5-axle semi-trailer truck (Fig. 3.2) was selected as a control vehicle to assess differences in the rigid pavement response. Among the Michigan trucks, the MI-20 trucks provide more concentrated loads (smaller axle spacing) on the pavement.

(a)

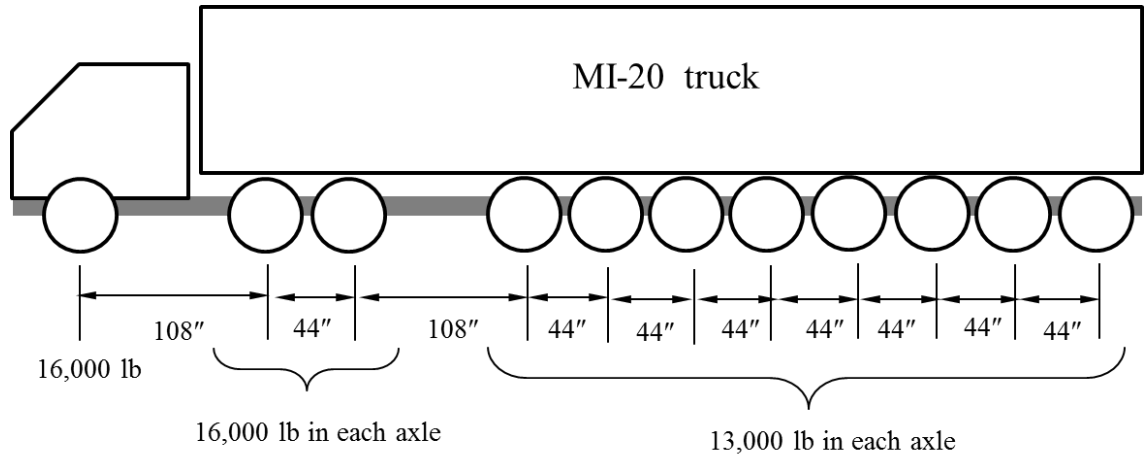
MI-20 truck
108″
44″
108″
44″
44″
44″
44″
44″
44″
44″
16,000 lb
16,000 lb in each axle
13,000 lb in each axle

(b)

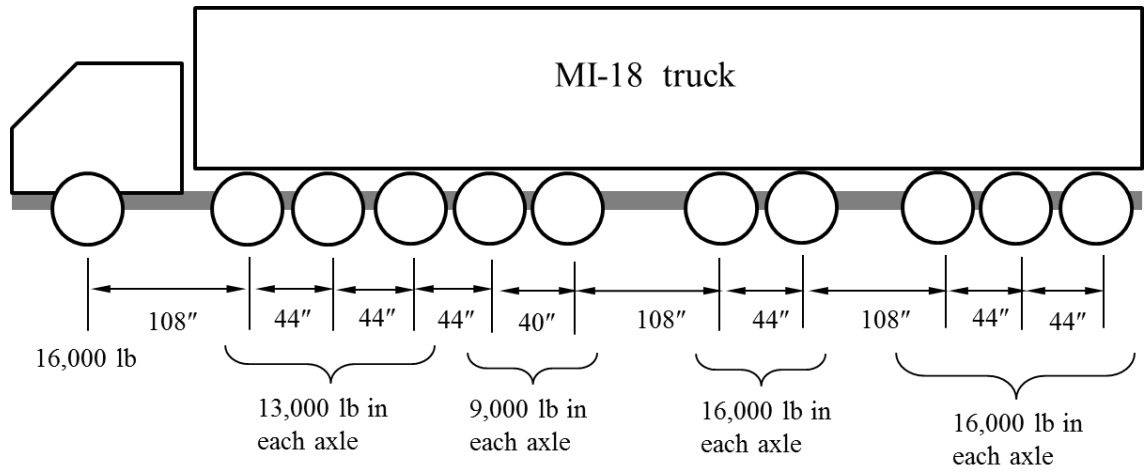
MI-18 truck
108″
44″
44″
44″
40″
108″
44″
108″
44″
44″
16,000 lb
13,000 lb in each axle
9,000 lb in each axle
16,000 lb in each axle
16,000 lb in each axle

(c)

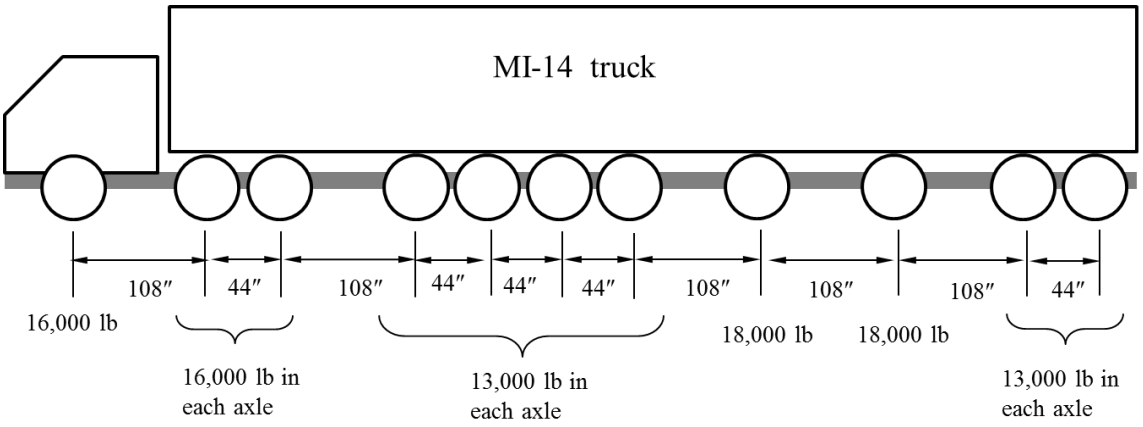

(d)

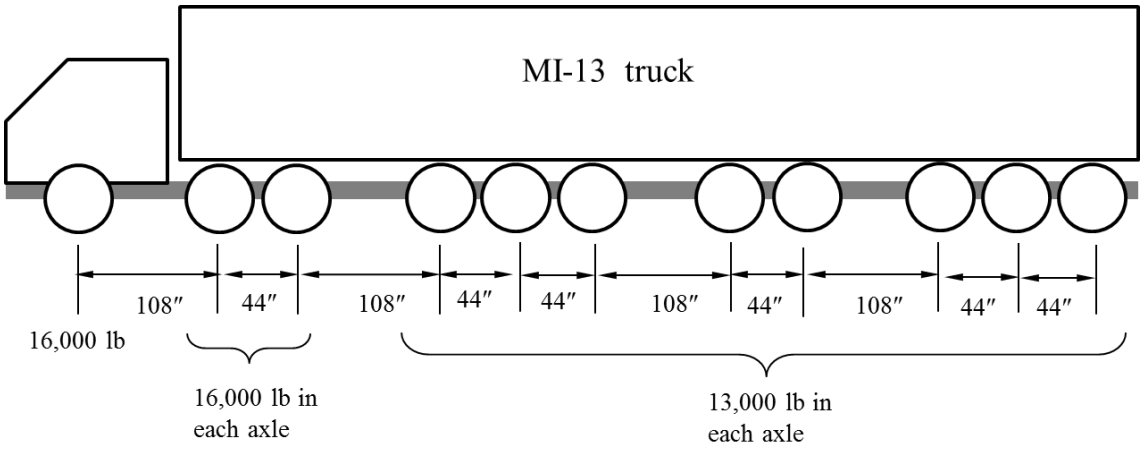

Figure 3.1: Schematics of (a) MI-20, (b) MI-18, (c) MI-14 and (d) MI-13 trucks are showing axle spacing and axle weight.

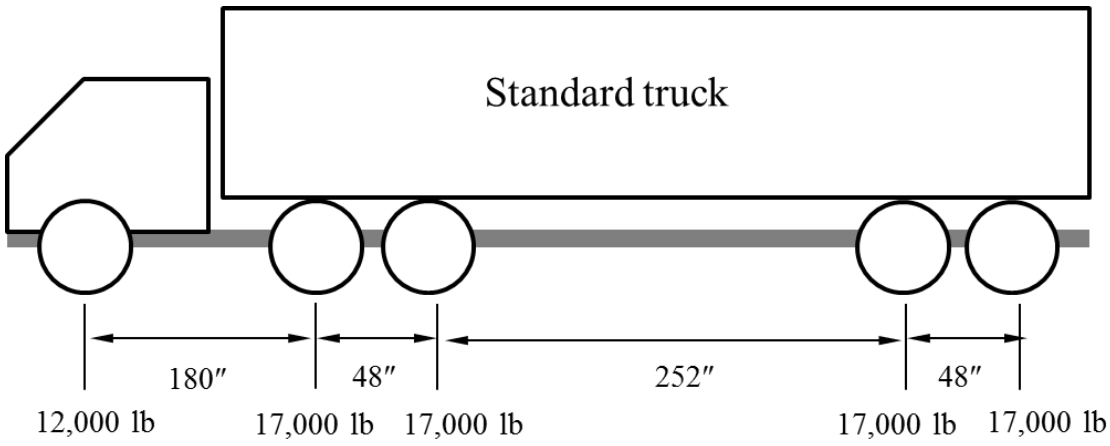

Figure 3.2: Schematic of a standard truck is showing axle spacing and axle weight.

A parametric study was performed by varying different variables in order to identify proper ISLAB2000 inputs for pavement response predictions close to realistic parameters. The variables and their magnitude which comprise the analysis are presented in Table 3.1. The values were selected to represent the range of typical Michigan conditions for jointed plain concrete pavements. The Poisson's ratio, unit weight and elastic modulus of PCC are assumed to be constant which are 0.15, 150 lb. /ft. and $5.0*10^6$ psi, respectively. For the set of variables presented in Table 3.1, about 550 simulations are run for each loading case for each vehicle, which is total of about 22 thousands simulation runs.

Table 3.1: Variables and their magnitude used as input parameter in ISLAB2000.

Input variables	Values
Modulus of subgrade reaction (k)	150, and 250 psi/in
Concrete thickness (h)	8, 10 and 12 inches
Co-efficient of thermal expansion (α)	3E-6, 5E-6, 7E-6 in/in/deg F
Linear equivalent temperature difference (ΔT)	0, -15, -30, +15, and +30°F
Joint spacing	14 feet
Load transverse efficiency at transverse joints	50%, 75%, 90% (load transfer by shear and moment by dowels only)
Load transverse efficiency at longitudinal joints	50%
Slab width and shoulder	12-feet (asphalt shoulder)

For the case of 12-feet slab width (with an asphalt shoulder), the slab edge and lane edge coincide at the same point. Therefore, the referenced load position was modeled at the slab edge and lane edge. The same wander characteristics for the standard lane width and the extended lane width have been shown in several studies (Benekohal et al., 1990; Hiller, 2007). ISLAB2000 could model only static loading condition; the first axle of the vehicle was placed at different positions of the slab and then was moved along the traffic direction at different distances to simulate the dynamic loading condition. The axle loads are stepped across the slab for the analysis of influence line. Depending on the types of truck, the number of loading position varies from 7 to 8. In the case of standard

truck, the steering axle is placed at the right side of the left transverse joint of mid-slab for the starting position and the first axle of first tandem is placed at the left side of right transverse joint of mid-slab for the ending position (Fig. 3.3). For the MI-20, MI-14 and MI-13 trucks, the first axle of first tandem is placed at the right side of left transverse joint of mid-slab for the starting position (Fig. 3.4). The starting position of the MI-18 truck is similar to the standard truck, i.e. the steering axle is placed at the right side of the left transverse joint of mid-slab. The successive positions of axle load for both standard and Michigan trucks are given in Table 3.2.

Six slabs have been used to model the FEA for the case of asphalt shoulder. The mesh size was set to 4 in x 4 in, which is assumed to be a fine mesh to produce accurate results for this analysis (Hiller, 2007). The schematic of mesh generated for the simulation is shown in Fig. 3.5. This mesh setup produces principal tensile stresses collected at 4-inch intervals along both the transverse joint and longitudinal edge (see Fig. 3.5).

(a)

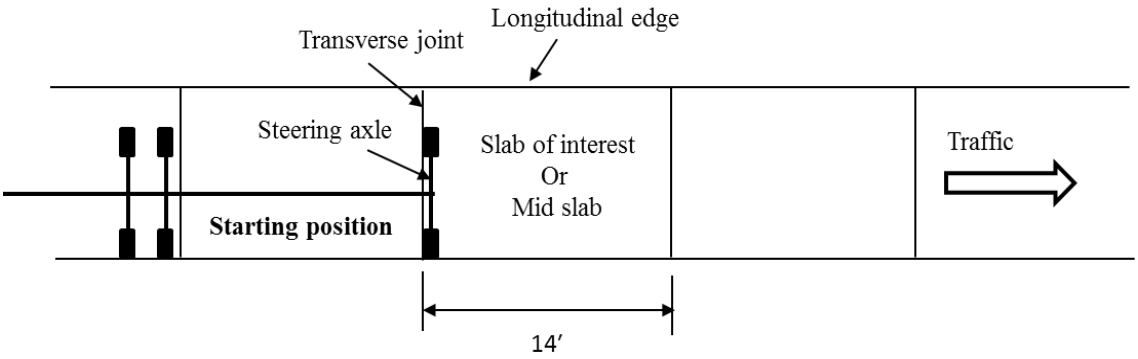

(b)

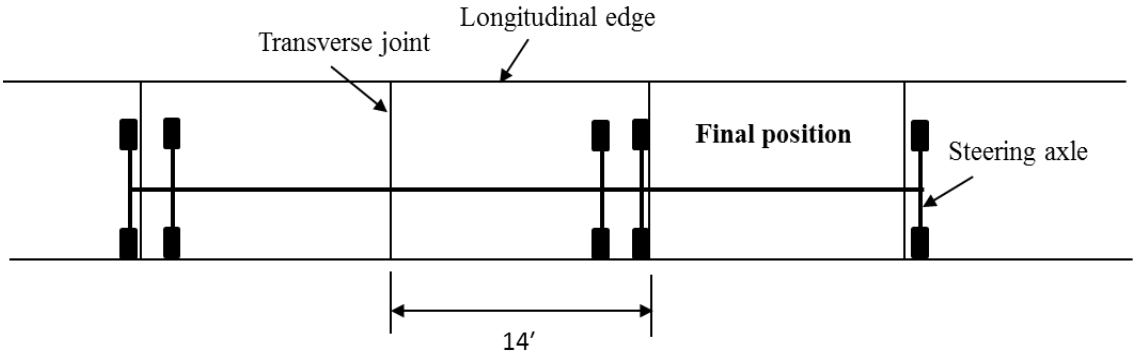

Figure 3.3: Locations of (a) starting and (b) ending positions for the influence line analysis with standard truck as shown in Fig. 3.2. The successive positions of axle load are given in Table 3.2.

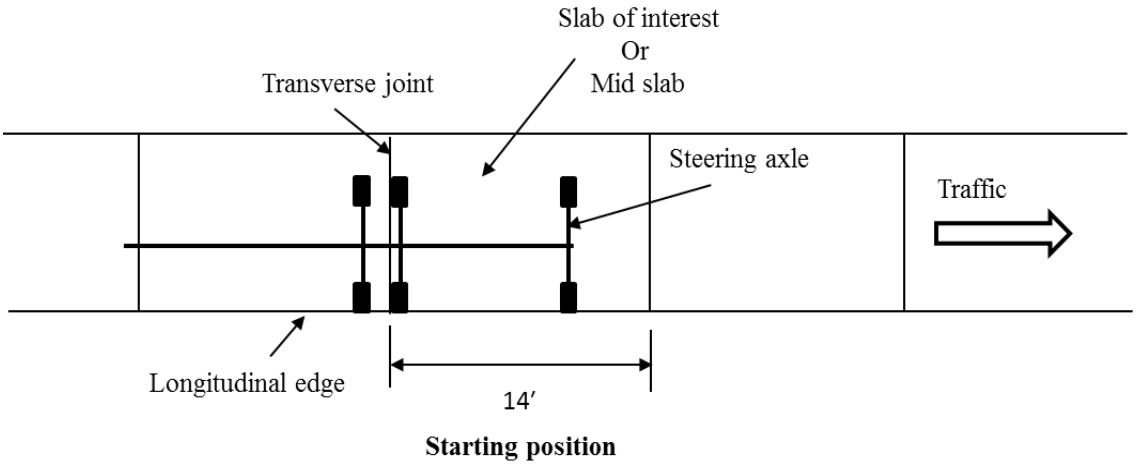

Figure 3.4: Locations of starting positions for the influence line analysis with Michigan trucks (MI-20, MI-14, and MI-13). The first axle of first tandem is placed at the right side of the left transverse joint of the mid slab. The successive and ending positions of the axles loading are given in Table 3.2.

Table 3.2: Offset of steering axle from the left transverse joint of mid-slab for the different axle load positions.

Axle load position number	**Offset of steering axle from the left transverse joint of slab of interest (Mid-slab) (inches)**				
	Standard	**MI-20**	**MI-18**	**MI-14**	**MI-13**
I (starting)	4	112	4	112	112
II	84	156	84	156	156
III	164	192	164	192	192
IV	184	272	200	272	272
V	232	308	236	308	308
VI	264	344	288	344	352
VII	344	396	316	396	388
VIII		424	352	424	

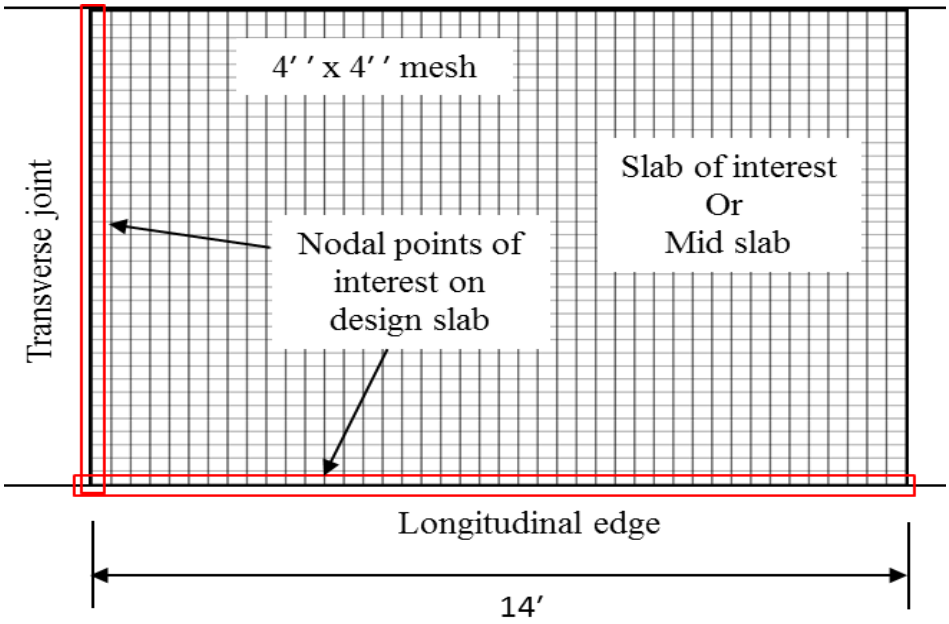

Figure 3.5: A schematic of computational mesh used for simulation in ISLAB. Meshes in the surrounding slabs are similar to the mid-slab which is not shown here.

3.2. Maximum stress analysis

Traditionally, mechanistic-empirical design of rigid pavements has focused on predicting bottom-up transverse fatigue damage at the edge of the slab. However, with the effect of upward curl or negative temperature gradient, a number of locations can potentially exhibit fatigue failure, which accounts for peak tensile stresses being located on the top of the slab. Also load positions on the slab influence the peak tensile stress on the top of slab. Influence line approach is an effective way to show the change of nodal stresses caused by various load positions as the tire passes the slab. Therefore an influence function approach (Byrum and Hansen, 1994; Hiller, 2007) has been adopted to

determine the location and magnitude of the critical stresses for any point of interest along the longitudinal edge and transverse joint of the mid-slab. Finite element analysis from ISLAB2000 program has been used to determine the stresses for all nodes by moving the vehicle at different positions (up to 11 loading positions depending on different vehicle configurations) across the slab and collecting up to 103 individual nodal responses (stress, strain or deflection) depending on the slab geometry.

With the approach of a single axle to the point of interest or mid-point of the slab, the top of the slab goes into tension and curved downward. When the axle load is on the top of the middle portion of the slab, then the top of the slab goes into compression and curved upward. As the tire moves away from the middle portion of the slab, the top of the slab again goes in tension. Then the slab goes back to its zero stress or residual if any temperature or moisture gradient exists. However, the influence line approaches are more complicated since multiple tire loads and axles are considered here simultaneously with the passing of a vehicle rather than only one single load. The maximum stress analyses are conducted on five different types of trucks under different temperature difference (ΔT) between the top and bottom surface of the slab. For the influence line analysis, the maximum stresses versus nodal locations along the longitudinal edge of the mid-slab graph are plotted for all the axle loading positions presented in Table 3.2. The modulus of subgrade reaction was set to 150 psi/in and the concrete slab thickness was considered as 10 inch. The coefficient of thermal expansion was selected as 7E-6 in/in/deg F. The load transfer efficiency for the transverse direction (vertical to traffic direction) was 75%.

3.2.1. Influence line responses for zero temperature difference across slab

Figures 3.6-3.10 exhibit the nodal stresses along the longitudinal edge at the top of mid-slab (slab of interest) for the 0^{o}F temperature differential on a 14-foot slab length with asphalt shoulder respectively for standard, MI-20, MI-18, MI-14 and MI-13 trucks (see Fig. 3.1 and 3.2). The positive and negative signs indicate tension and compression, respectively. The stress condition at the top and bottom of a slab is always assumed to be of equal magnitude but opposite signed; hence only the top slab stress conditions have been shown here.

Figure 3.6 illustrates that, for the case of standard truck, the compressive stress (negative value) at the top of the slab is significantly larger than the tensile stress (positive value). So, the critical tensile stress locations for the pavement structure are typically at the bottom of the slab. It demonstrates that, under no slab temperature difference, the bottom of the slab is crucial in the mechanistic-based pavement design procedure because of the high concentrated tensile stress. On the basis of the comparison of loading positions (Table 3.2) with the axle locations of standard truck (Fig. 3.2), it appears that the 1^{st} axle of tandem of standard truck at left side of right transverse joint of the mid-slab produces the highest pavement stress responses.

Like the standard truck, at the 0F temperature difference, the Michigan trucks also provide higher compressive stress at the top of the slab when compared with tensile stress (Fig. 3.7-3.10). So for the Michigan trucks, the bottom surface of pavement is crucial under the zero temperature gradient between top and bottom surface of pavement. For the MI-20 truck, the 5^{th} axle at the right side of left transverse joint and the 4^{th} axle at left

side of right transverse joint produce the highest stress responses (Fig. 3.7). Figure 3.8 illustrates that the 5th axle of MI-18 truck at the mid-point of mid-slab edge produces the highest pavement stress responses. However, the 6th axle of MI-14 truck at the mid-point of mid-slab edge produces the highest stress on the pavement surface (Fig. 3.9).The MI-13 truck shows that the 2ndaxle of 1sttridem at right side of left transverse joint and the 3rdaxle of 1sttridem at left side of right transverse joint of mid-slab yield the highest stress.

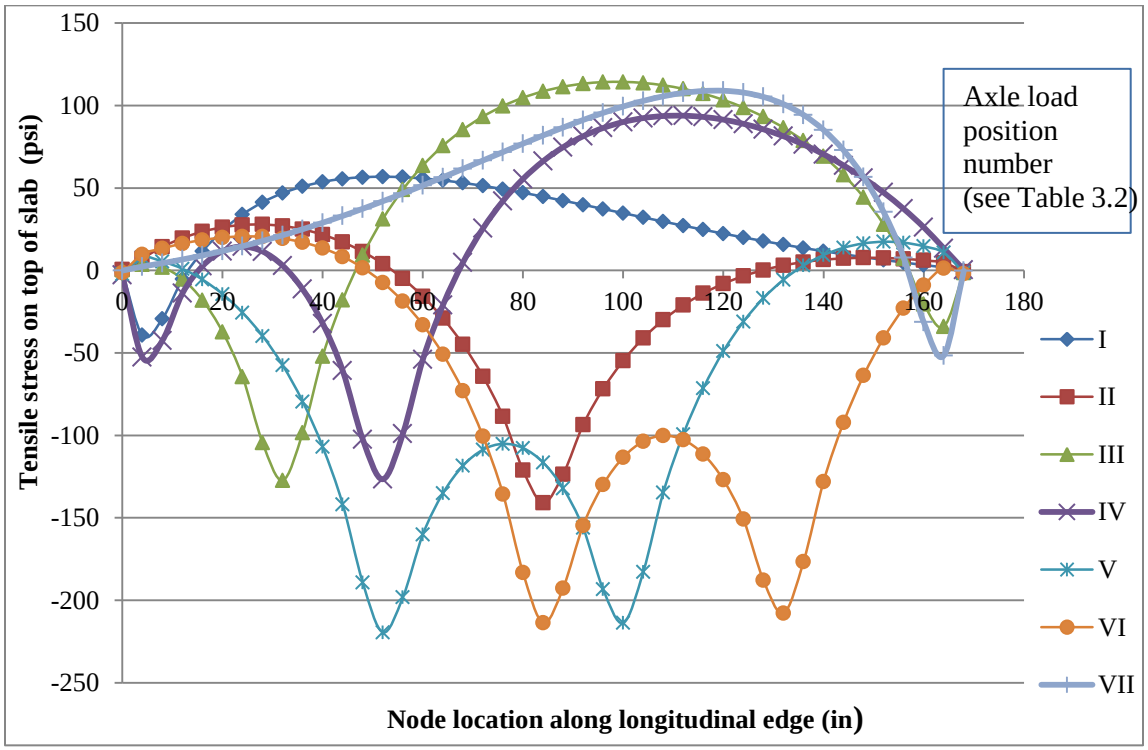

Figure 3.6: Tensile stresses at the top surface of mid-slab along the longitudinal edge with 14-feet joint spacing and asphalt shoulders for the standard truck. Temperature difference between top and bottom of slab (ΔT) is zero.

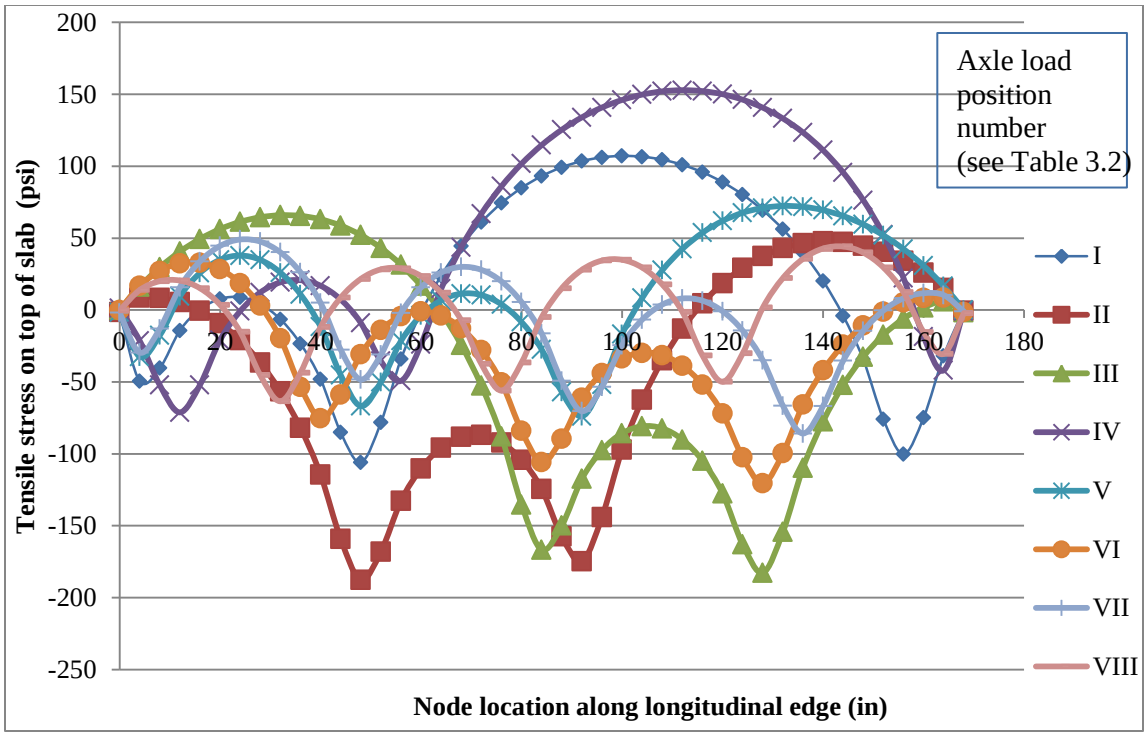

Figure 3.7: Tensile stress at the top surface of mid-slab along the longitudinal edge with 14-feet joint spacing and asphalt shoulders for the MI-20 truck. Temperature difference between top and bottom of slab (ΔT) is zero.

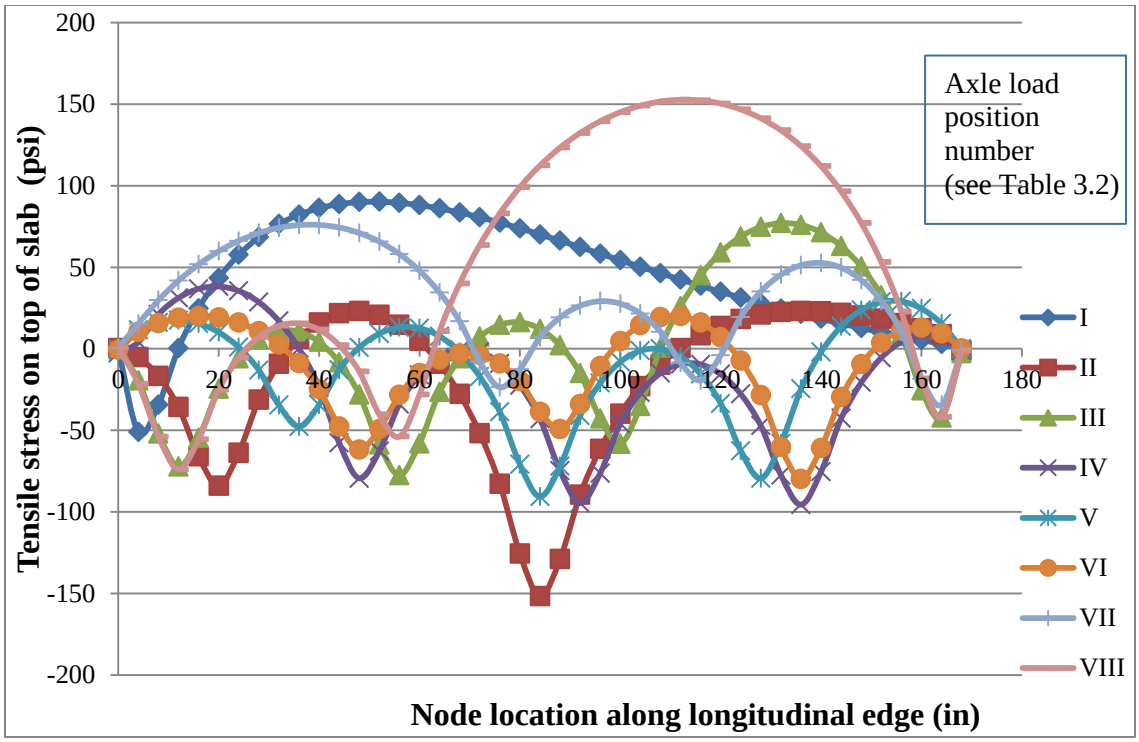

Figure 3.8: Tensile stress at the top surface of mid-slab along the longitudinal edge with 14-feet joint spacing and asphalt shoulders for the MI-18 truck. Temperature difference between top and bottom of slab (ΔT) is zero.

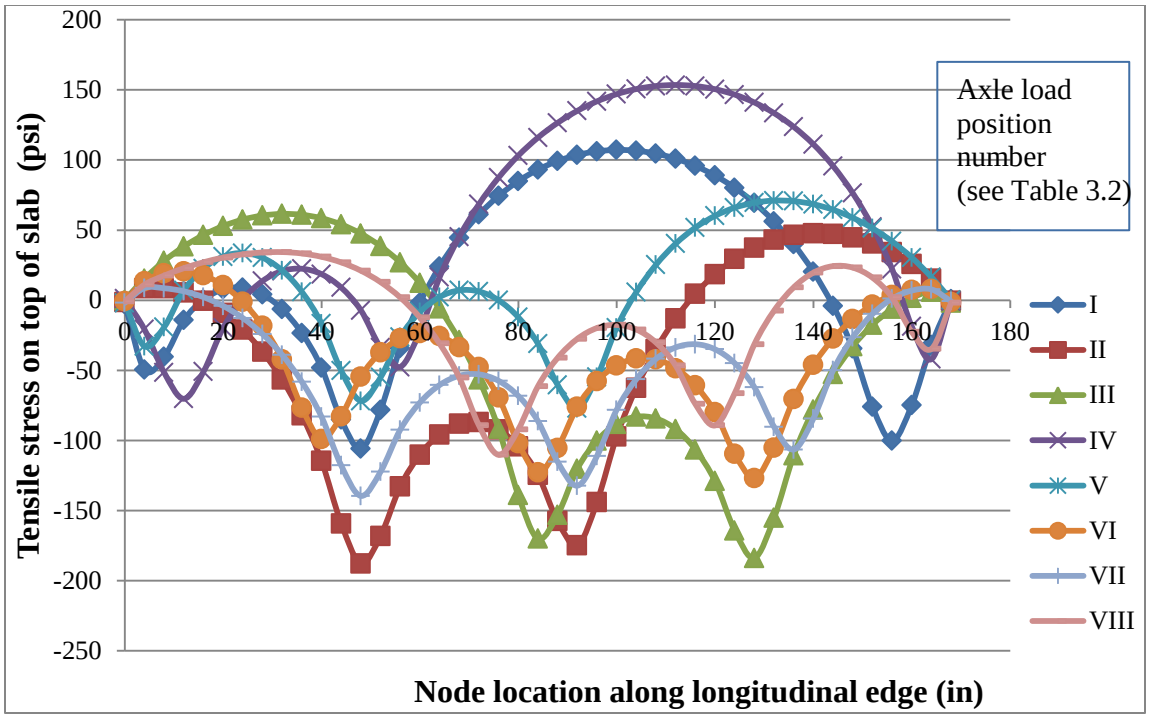

Figure 3.9: Tensile stress at the top surface of mid-slab along the longitudinal edge with 14-feet joint spacing and asphalt shoulders for the MI-14 truck. Temperature difference between top and bottom of slab (ΔT) is zero.

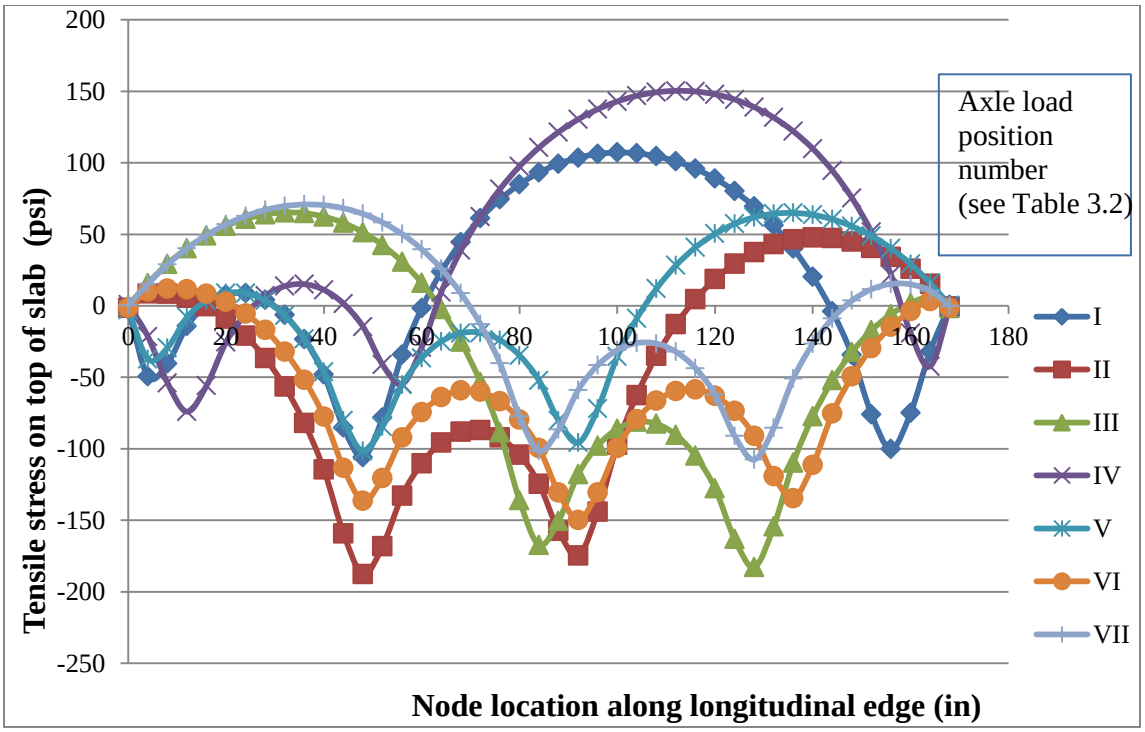

Figure 3.10: Tensile stress at the top surface of mid-slab along the longitudinal edge with 14-feet joint spacing and asphalt shoulders for the Michigan truck MI-13. Temperature difference between top and bottom of slab (ΔT) is zero.

3.2.2. Influence line responses for +30F temperature difference across slab

Stresses induced in the slab under positive linear temperature gradients traditionally lead to bottom-up transverse cracking. On a hot sunny day, while the top of the PCC slab is much warmer than the bottom, the elongation of the top surface is greater than that of the bottom surface, which yields a convex curvature of the slab (Fig. 3.11). For a positive temperature gradient, the middle of the slab provides the least support at slab edges/corners.

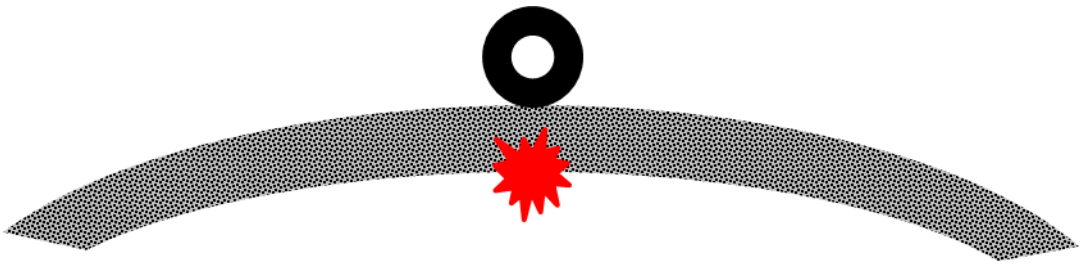

Figure 3.11: Curling of PCC slab due to positive temperature difference with critical traffic loading position resulting in high tensile stress at the bottom of slab.

The tensile stress developed on the top surface of mid-slab under a +30F temperature difference is shown in Figs. 3.12 – 3.16 for the standard and Michigan trucks. For the temperature gradient of +30F, the tensile stress (positive value) develops on the top surface is negligible. The compressive stress (negative value) at the top of mid-slab increases significantly when compared with the zero temperature gradient. For the +30F, the bottom of the mid-slab is crucial for the pavement design because of the high tensile stress at the bottom surface.

For the standard truck, the maximum compressive stress developed at the top of mid-slab appears around the middle of the slab. The MI-20 truck yields slightly less maximum compressive stress at the top surface of mid-slab when compared with the standard truck. The locations of the maximum compressive stress on the mid-slab for both the standard and MI-20 trucks are almost the same. The locations and magnitude of maximum compressive stress for the MI-14 and MI-13 trucks is exactly the same as the MI-20 truck, i.e. the magnitude and location of maximum compressive stress are 342 psi and 92 inches from the left transverse joint of mid-slab, respectively. Among all the trucks, the magnitude of maximum compressive stress for the MI-18 is the lowest which

is about 320 psi. However, the location of maximum compressive stress for the MI-18 truck is exactly at the same location as the standard truck, which is about 84 inches from the left transverse joint of mid-slab.

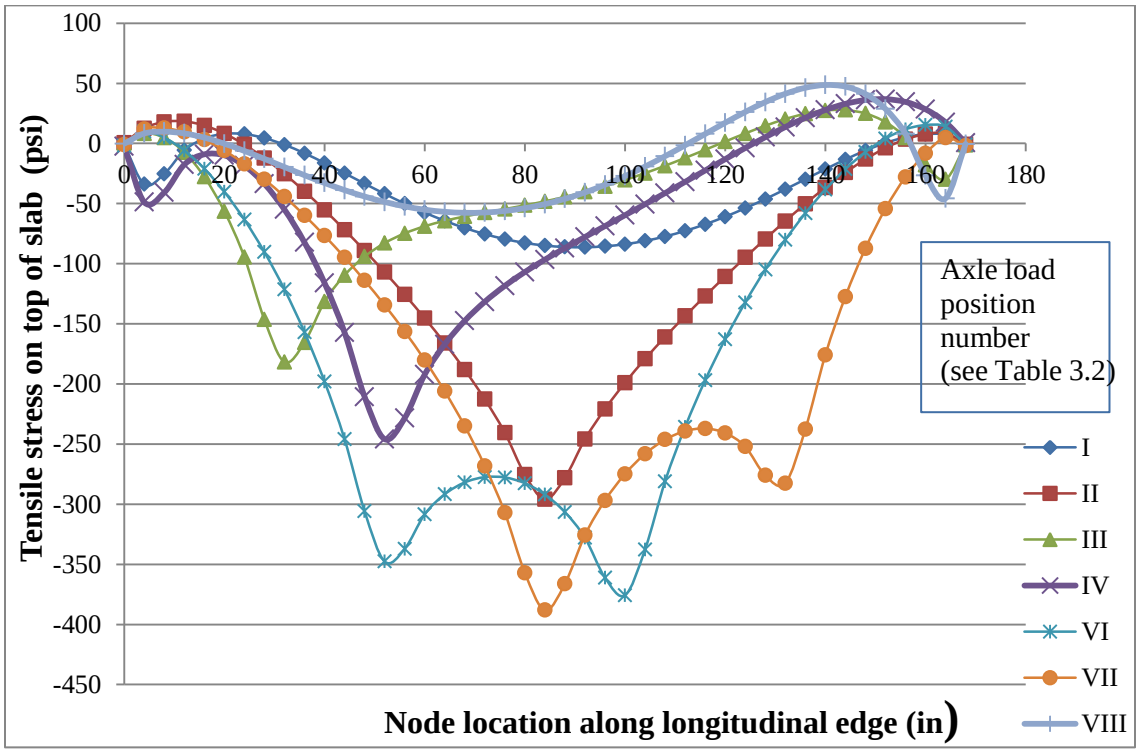

Figure 3.12: Tensile stress at the top surface of mid-slab along the longitudinal edge with 14-feet joint spacing and asphalt shoulders for the standard truck. Temperature difference between top and bottom of slab (ΔT) is +30F.

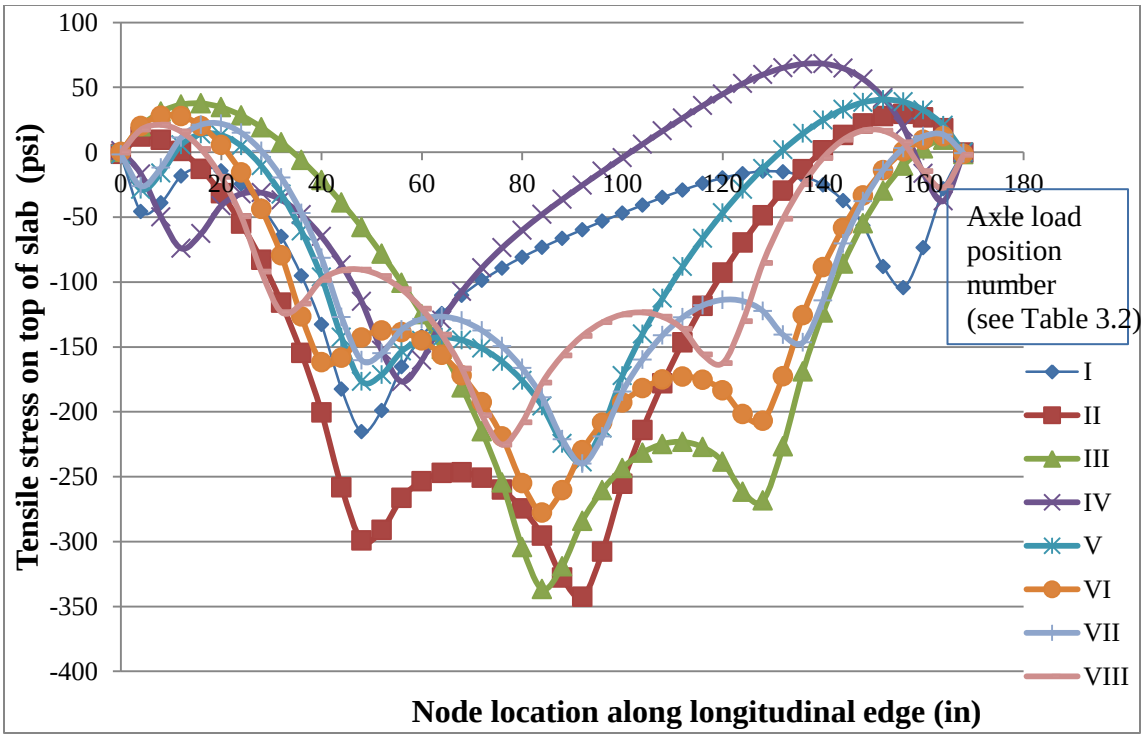

Figure 3.13: Tensile stress at the top surface of mid-slab along the longitudinal edge with 14-feet joint spacing and asphalt shoulders for the MI-20 truck. Temperature difference between top and bottom of slab (ΔT) is +30F.

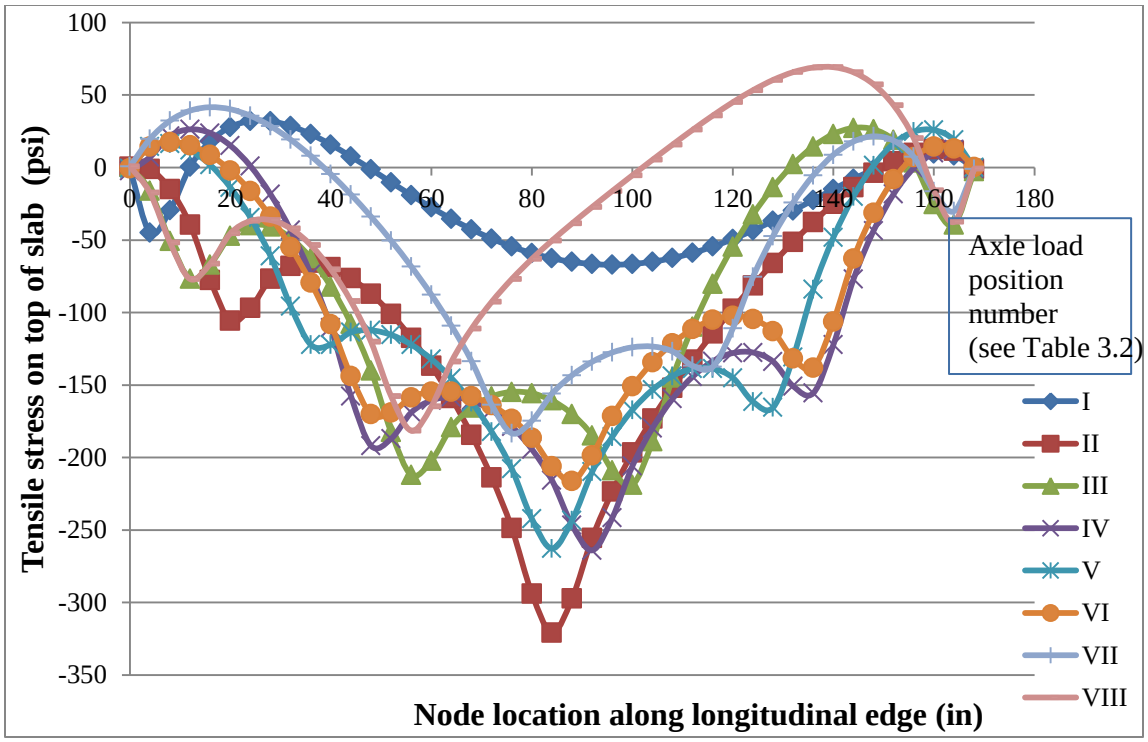

Figure 3.14: Tensile stress at the top surface of mid-slab along the longitudinal edge with 14-feet joint spacing and asphalt shoulders for the MI-18 truck. Temperature difference between top and bottom of slab (ΔT) is +30F.

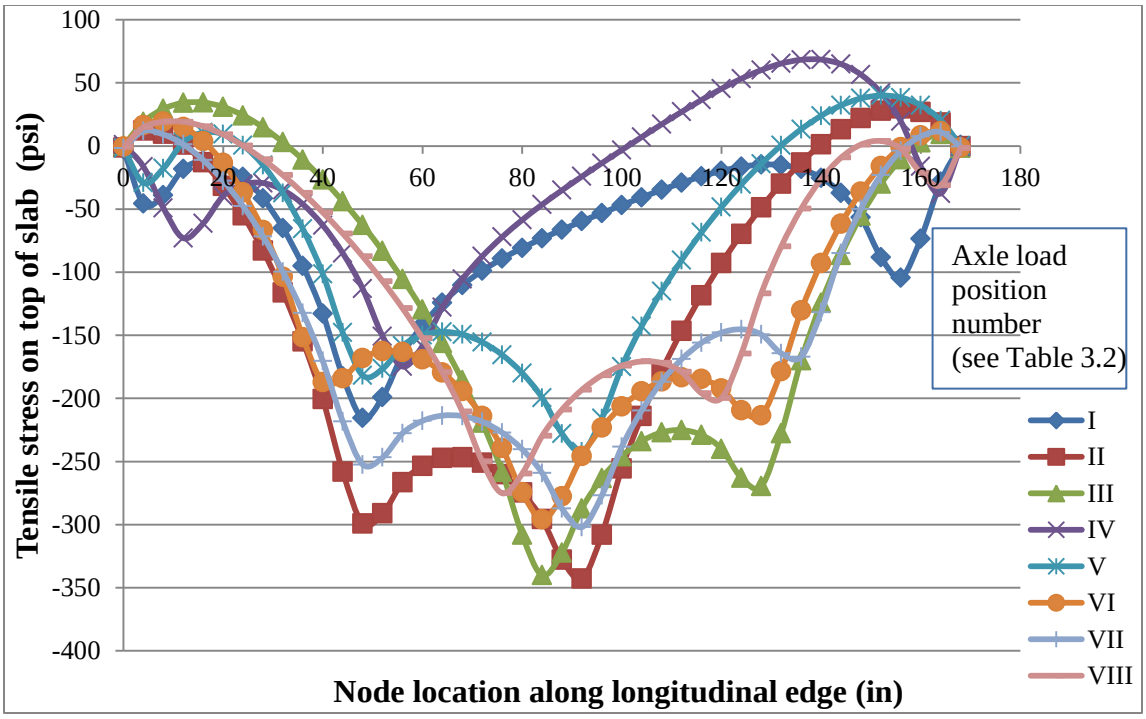

Figure 3.15: Tensile stress at the top surface of mid-slab along the longitudinal edge with 14-feet joint spacing and asphalt shoulders for the MI-14 truck. Temperature difference between top and bottom of slab (ΔT) is +30F.

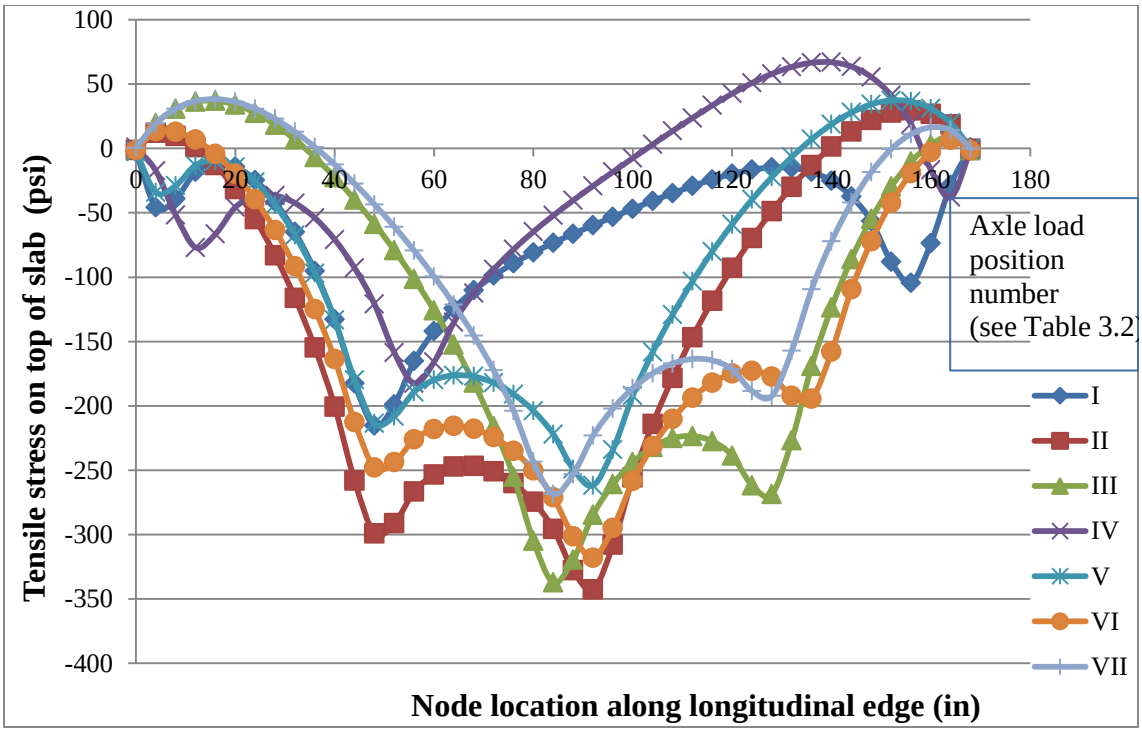

Figure 3.16: Tensile stress at the top surface of mid-slab along the longitudinal edge with 14-feet joint spacing and asphalt shoulders for the MI-13 truck. Temperature difference between top and bottom of slab (ΔT) is +30F.

3.2.3. Influence line responses for -30F temperature difference across slab

The negative temperature gradient develops higher tensile stress at the top surface of a slab than at the bottom surface, which eventually causes top-down fatigue damage (Fig. 3.17). Figure 3.17 shows the deflection of slab for stress at the top of the slab along the wheel path caused by a single load combined with the effect of negative temperature gradient. With the presence negative temperature gradient (which occurs during night time), the top of the slab is always in tension and the bottom is in compression. As a consequence, the slabs are predominantly in a curled upward condition. Because of slab

lift-off due to upward curling, loads that are positioned on unsupported areas can result in large stress increases. The negative temperature gradient results in less subgrade support at slab edges/corners. Therefore, the resulting critical tensile being located on the top of the slab change the critical damage locations from bottom-up to top-down cracking. Due to the factors of irreversible shrinkage in the top of the concrete slab as well as the built-in temperature gradients during the setting of the concrete, a majority of rigid pavements experience a permanent upward curl regardless of the cyclical temperature gradient (positive/negative) (Byrum, 2000). This upward curling of concrete slabs was observed in previous researches for a variety of different climatic regions (Rao et al., 2001; Yu et al., 1998; Yu and Khazanovich, 2001; Poblete et al., 1988).

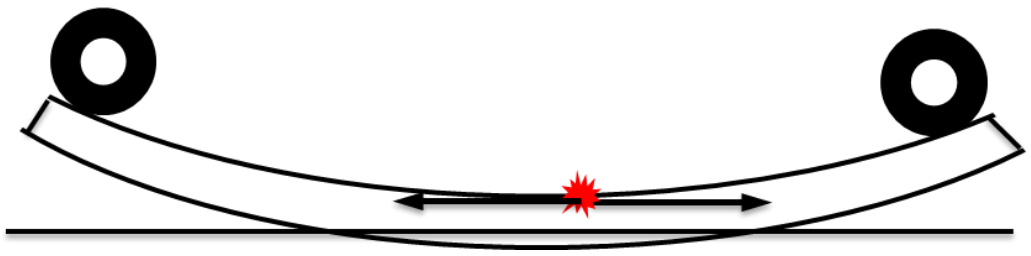

Figure 3.17: Curling of PCC slab due to negative temperature gradients with critical traffic loading positions resulting in high tensile stress at the top of the slab.

Figures 3.18-3-3.22 show tensile stresses at the top surface along the longitudinal edge at the mid-slab for the standard trucks and Michigan trucks (MI-20, MI-18, MI-14 and MI-13 (see Figs. 3.1 and 3.2) under a –30˚F equivalent temperature differential between the top and bottom surfaces of the slab. For all the standard and Michigan trucks, the tensile stress (positive value) is significantly higher than that of compressive stress (negative value). Sounder a negative thermal gradient, the critical tensile stress locations for the pavement structure are typically at the top of the slab. In addition to the higher tensile stress at the top of the slab, the area of the slab under extreme tensile stress is also increased in comparison to the no curling scenarios discussed previously.

The standard truck yields the maximum tensile stress around the middle of mid-slab. The magnitude of maximum tensile stress for the standard truck at the top surface of mid-slab is less than that of Michigan trucks, which is about 270 psi (Fig. 3.18). For all the Michigan trucks (MI-20, MI-18, MI-14, MI-13) the magnitudes and the locations of the maximum tensile stresses are almost the same, which is about 300 psi and 96 inches from the left transverse joint of mid-slab, respectively.

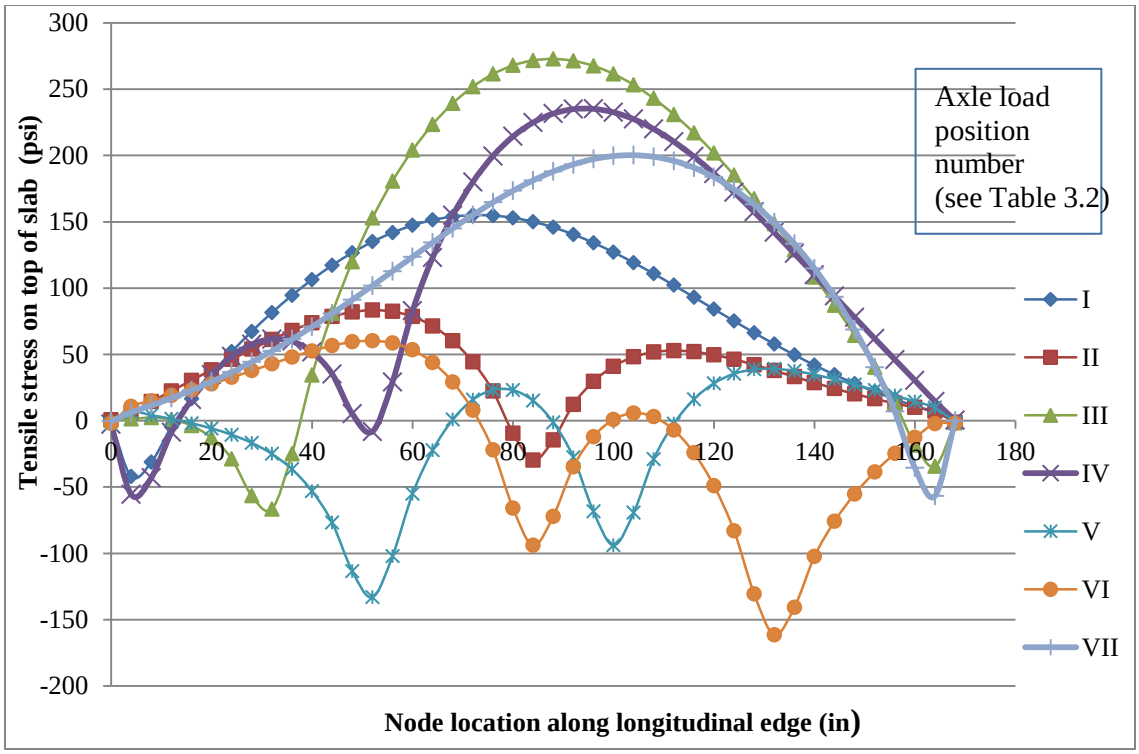

Figure 3.18: Tensile stresses at the top surface of mid-slab along the longitudinal edge with 14-feet joint spacing and asphalt shoulders for the Standard truck. Temperature difference between top and bottom of slab (ΔT) is -30F.

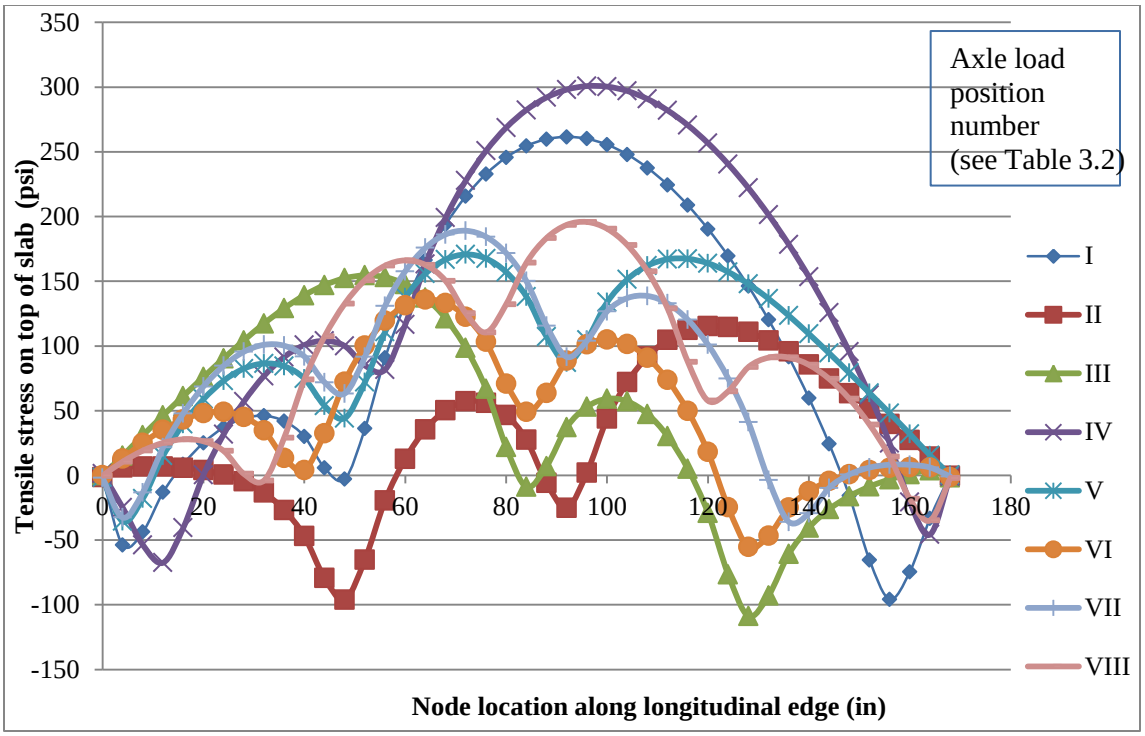

Figure 3.19: Tensile stress at the top surface of mid-slab along the longitudinal edge with 14-feet joint spacing and asphalt shoulders for the MI-20 truck. Temperature difference between top and bottom of slab (ΔT) is -30F.

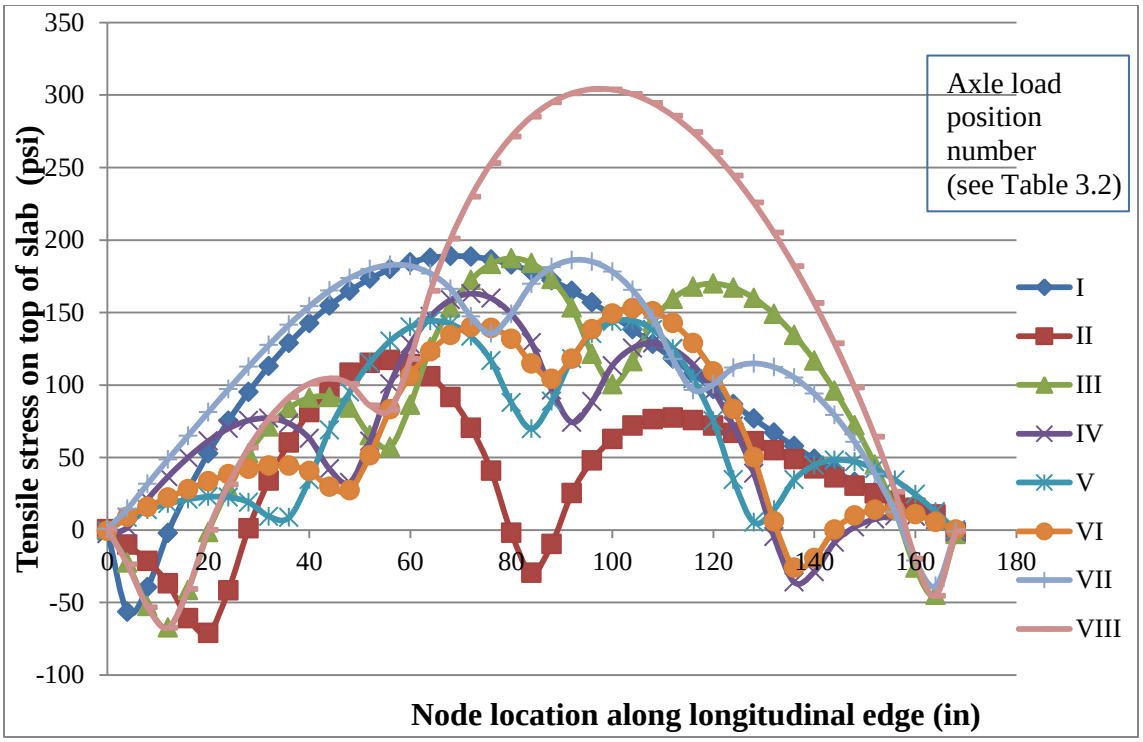

Figure 3.20: Tensile stress at the top surface of mid-slab along the longitudinal edge with 14-feet joint spacing and asphalt shoulders for the MI-18 truck. Temperature difference between top and bottom of slab (ΔT) is -30F.

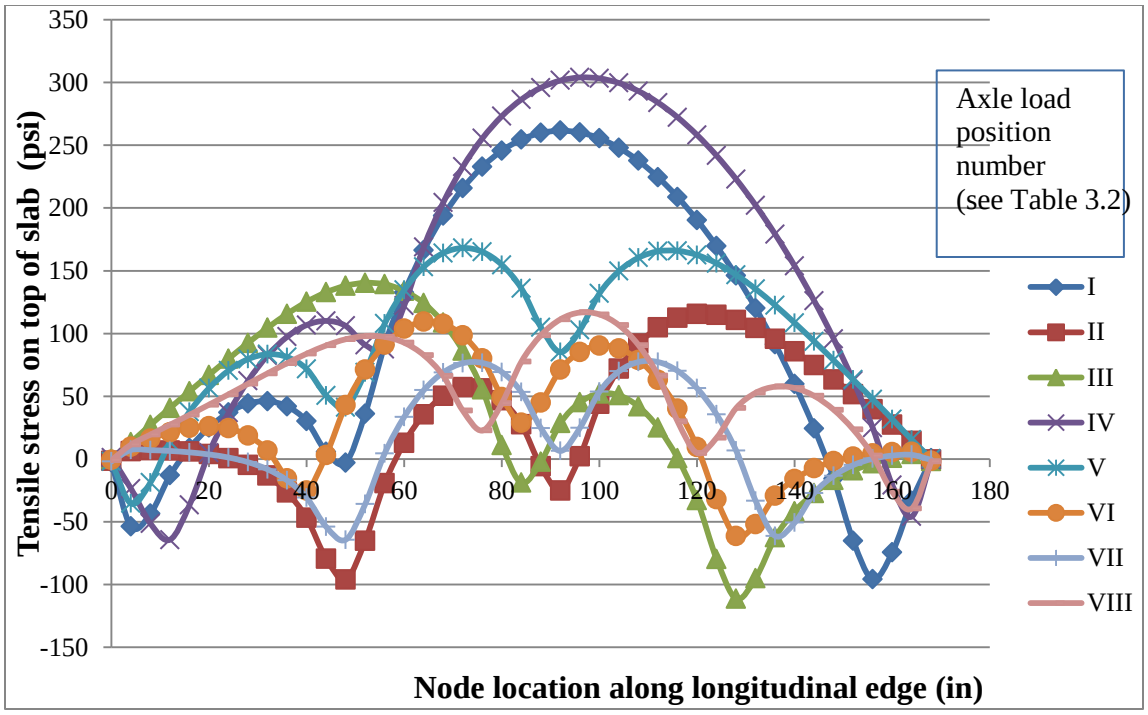

Figure 3.21: Tensile stress at the top surface of mid-slab along the longitudinal edge with 14-feet joint spacing and asphalt shoulders for the MI-14truck. Temperature difference between top and bottom of slab (ΔT) is -30F.

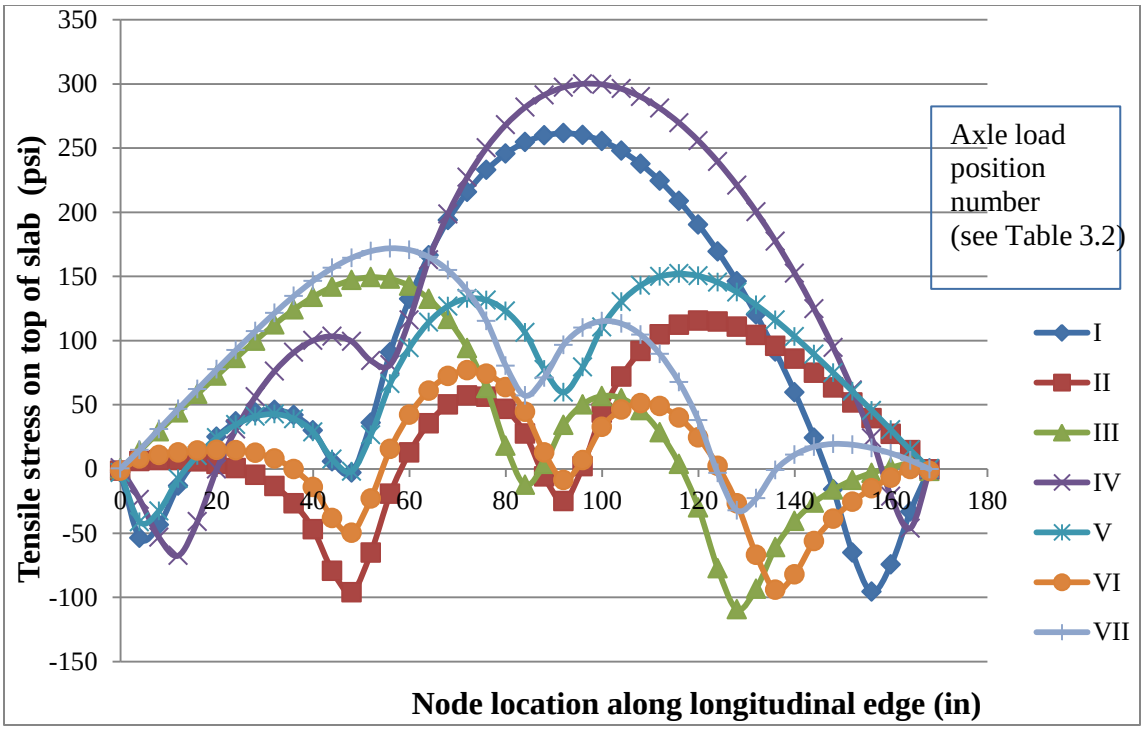

Figure 3.22: Tensile stress at the top surface of mid-slab along the longitudinal edge with 14-feet joint spacing and asphalt shoulders for the MI-13 truck. Temperature difference between top and bottom of slab (ΔT) is -30F.

3.2.4. Effect of temperature gradient on stress responses

The effects of linear temperature difference between the top and bottom surface of pavement on the stresses developed on the slab of interest by the standard and Michigan (MI-20, MI-18, MI-14 and MI-13) trucks are discussed in this section. The loading conditions for which the maximum stress appears for different temperature gradients are considered for this analysis. The temperature gradient varies from -30F to +30F. The magnitude of h, k, LTE and CTE considered for this analysis is 10 in, 150psi/in, 75% and 5E-6 in/in/deg respectively.

Figures 3.23a -3.23e show the effect of temperature difference on the stress developed at the top surface of mid-slab by a standard and Michigan trucks. For all the standard and Michigan trucks, the maximum tensile stress (positive values) on the top surface increases with an increase in the negative temperature difference between the top and bottom surface of slab. The opposite is true for the compressive stress, i.e. the maximum compressive stress (negative values) increases with an increase in the positive temperature difference. The maximum tensile and compressive stress appears for the -30F and +30F temperature gradients, respectively. It indicates that the negative temperature gradient provides a maximum tensile stress on the top surface of slab while the positive temperature gradient yields a maximum tensile stress on the bottom surface of slab.

The location of the maximum tensile stress for the standard trucks appears at the middle of mid-slab for both the +30F and -30F temperature gradients (Fig. 3.23a). For the MI-20 truck, the +30F provides concentrated high compressive stress at two nodal locations, which are about 50 and 90 inches offset from the left transverse joint of mid-slab (Fig. 3.23b). In addition, the -30F yields the maximum tensile stress at the nodal location of 96 inches. For the MI-18 truck with the given loading condition, the maximum compressive stress resulted from +30F temperature difference appears highly concentrated at the nodal position of about 84 inches from the left transverse joint of mid-slab (Fig. 3.23c). The tensile stress developed due to -30F temperature difference is the maximum at the nodal location of 96 inches from the left transverse joint of mid-slab.

Like the MI-20, the MI-14 truck provides the similar results for the different temperature gradients (Fig. 3.23d). Moreover, MI-13 truck yields almost the same magnitude and trend of stresses on the top surface of mid-slab for the different temperature gradients (see Fig. 3.23e), when compared with MI-20 and MI-14 trucks. For the MI-20, MI-14 and MI-13 trucks, the load cases for which the maximum stresses (both tensile and compressive) appeared provides the similar truck load on the mid-slab, i.e. the second axle of tridem for all the MI-20, MI-14 and MI-13 trucks are situated at the right side of the left transverse join. As a consequence, the MI-20, MI-14 ad MI-13 provides the similar results.

For the given loading conditions, a summary of the maximum top and bottom tensile stress for all the standard and Michigan trucks due to negative and positive temperature gradients, respectively is given in Table 3.3. For this set of loading condition, the standard truck provides the largest tensile stress at the bottom of the mid-slab. For all the trucks, the positive +30F temperature gradient yields a greater magnitude of tensile stress when compared with the -30F temperature gradient. It indicates that the +30F temperature gradient has a better potential for pavement damage.

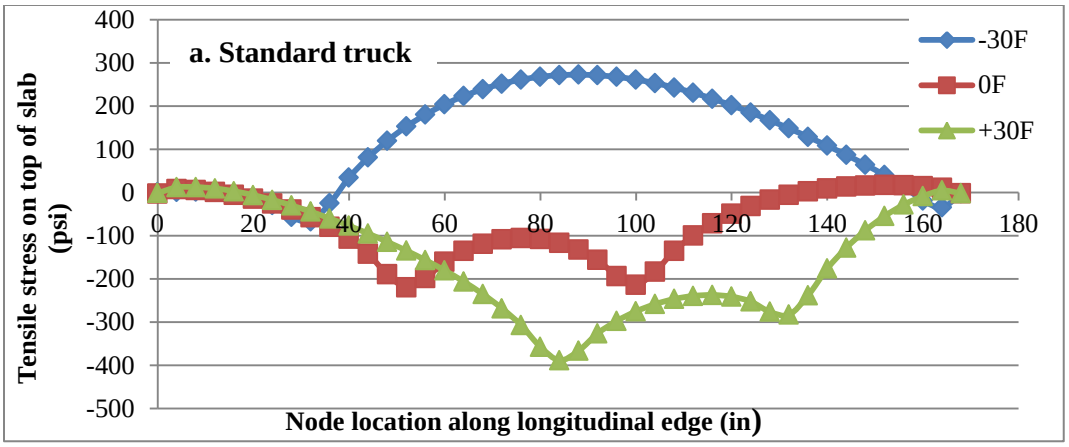
a. Standard truck
Tensile stress on top of slab (psi)
Node location along longitudinal edge (in)
-30F
0F
+30F
400
300
200
100
0
-100
-200
-300
-400
-500
0
20
40
60
80
100
120
140
160
180

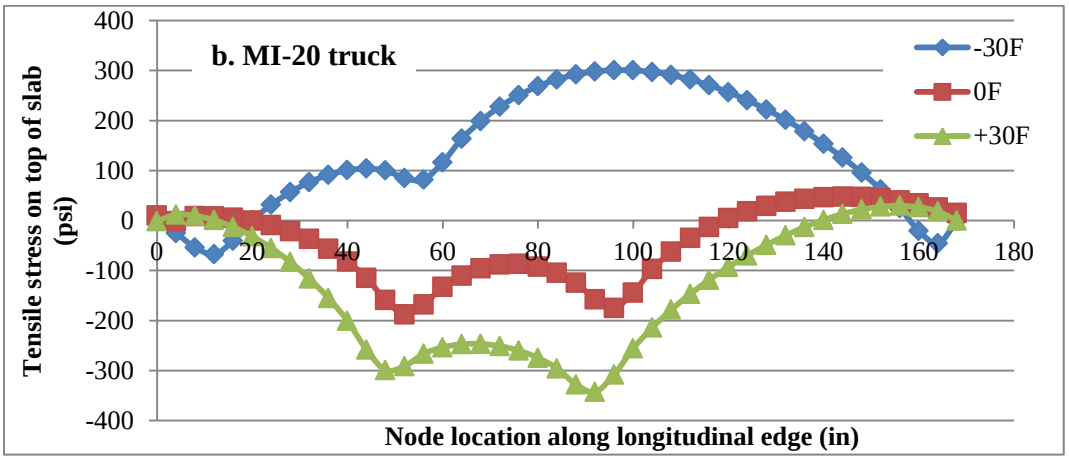
b. MI-20 truck
Tensile stress on top of slab (psi)
Node location along longitudinal edge (in)
-30F
0F
+30F
400
300
200
100
0
-100
-200
-300
-400
0
20
40
60
80
100
120
140
160
180

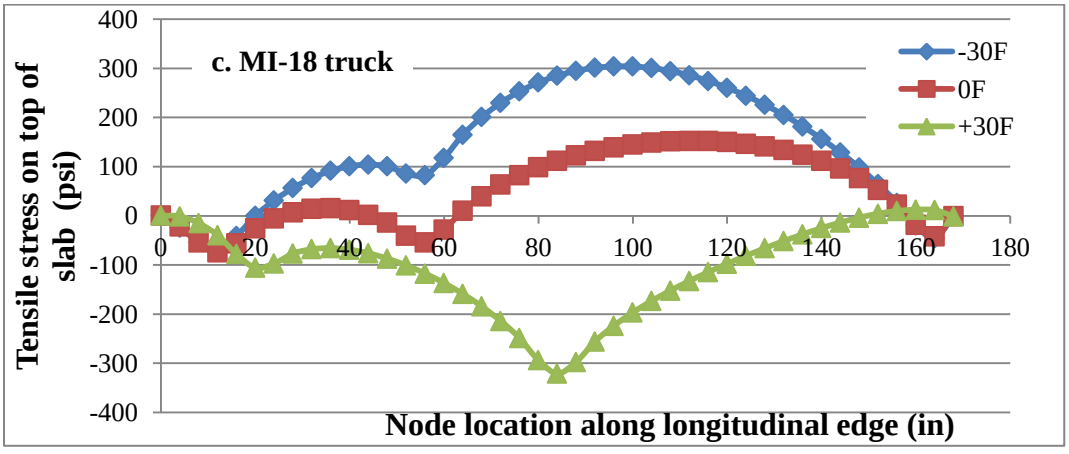
c. MI-18 truck
Tensile stress on top of slab (psi)
Node location along longitudinal edge (in)
-30F
0F
+30F
400
300
200
100
0
-100
-200
-300
-400
0
20
40
60
80
100
120
140
160
180

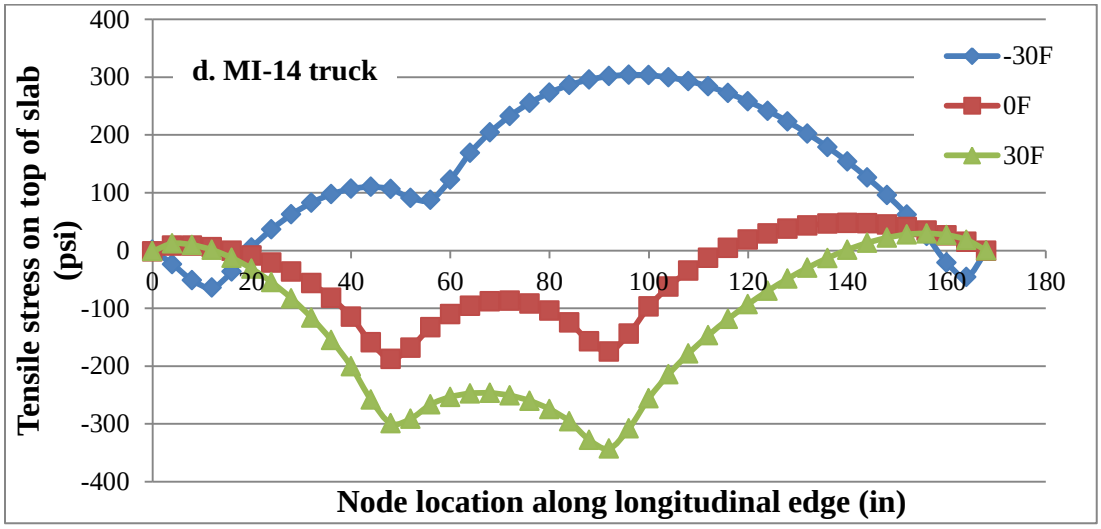

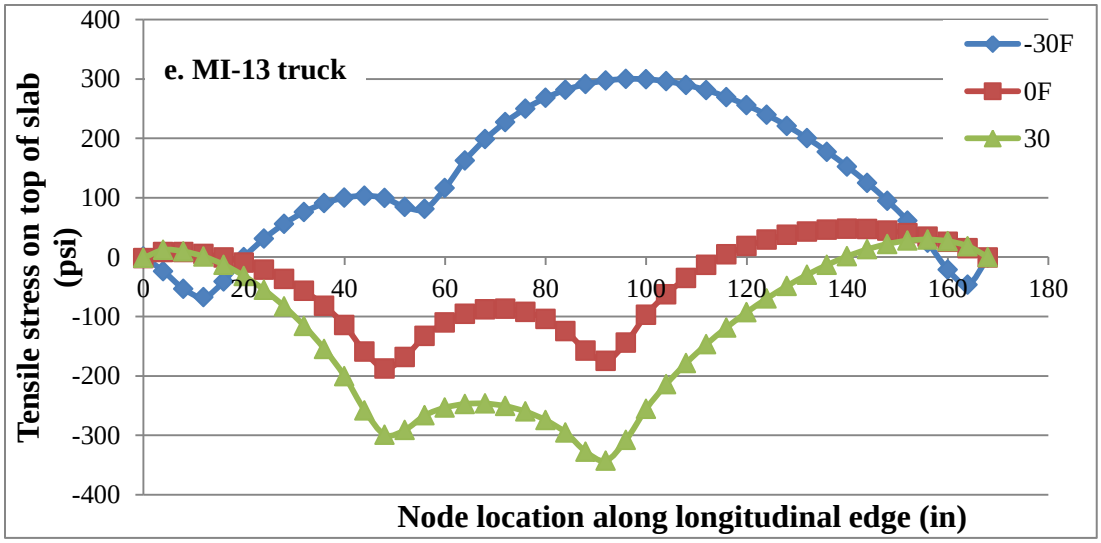

Figure 3.23: Effect of temperature difference on the stress at the top of slab of interest along the longitudinal edge with 14-feet joint spacing and asphalt shoulders for a (a) Standard, (b) MI-20 and (c) MI-14 trucks. (d) MI-14 and (e) MI-13 trucks. The positive and negative signs indicate tension and compression, respectively.

Table 3.3: Maximum top and bottom tensile stresses for the standard and Michigan trucks due to negative and positive temperature gradients, respectively. The magnitude of h, k, LTE and CTE 10 inches, 150 psi/in, 75% and 5E-6 in/in/deg F.

Truck	Maximum top tensile stress (psi) at -30F	Maximum bottom tensile stress (psi) at +30F
Standard	273	388
MI-20	302	343
MI-18	304	321
MI-14	304	328
MI-13	300	343

3.3. Pavement damage prediction

The damage models for fatigue cracking (transverse cracking) and faulting employed by the Mechanistic-Empirical Pavement Design Guide (MEPDG) (ARA 2007) was considered in this study. The MEPDG is recognized as one of comprehensive pavement design procedures using existing mechanistic-empirical technologies. It allows for the total stresses due to load and temperature effect to be correctly predicted.

The critical loading condition and pavement responses were determined for rigid pavements with and without slab curling where slab curling results from temperature difference between top and bottom of slab. The critical rigid pavement response is tensile stress at the bottom of the slab when tandem wheel axles are near the midway of

longitudinal edge or near transverse joint of PCC slab under +30F slab temperature difference condition (see Figs 3.23a-3.23e and Table 3.3). However, in the presence of slab curling behavior, the critical loading location for top-down cracking differs from the bottom cracking. In this cases, it is more likely that transverse joint loading produces the highest pavement stress responses, which further suggests that transverse joints loading deserves greater consideration in concrete pavements.

However, the Michigan trucks have complicated axle configuration (11 axles) with different axle spacing and most likely their gross vehicle weights are significantly greater than standard semi-trucks. The critical loading and response locations were identified in the first step of the damage analysis. In this section, the critical loading locations and the critical damage locations corresponding to joint spacing of 14 feet with asphalt shoulder for those representative vehicles (standard, MI-20, MI-18, MI-14, and MI-13) with and without considering slab curling (ΔT of 0, -15, -30, +15, and +30°F) were investigated.

The determination process of the critical loading condition was performed with all possible combinations of ISLAB2000 input parameters as previously described (see Section 3.1 and Table 3.1) with 7 to 8 loading positions (see Table 3.2) depending on the vehicle configurations respectively for all the vehicles (standard, MI-20, MI-18, MI-14, and MI-13). Here the damage analysis for only a 14-feet (168 inches) slab length with asphalt shoulder has been illustrated.

The maximum bending stress at the top of the slab were extracted from the ISLAB2000 outputs and summarized as shown in Tables 3.4 and 3.5. However, the stresses at the top of the slab will be equal, but opposite sign for the bottom of the slab in every situation. The maximum tensile stress responses at the top and bottom of the slab were compared to determine the critical damage locations for a 14-feet slab with Asphalt shoulder. Two different extreme temperature gradients (-30F and +30F) are considered for the analysis of maximum tensile stress, critical loading condition, and damage location for the Standard and Michigan trucks.

Table 3.4 shows theoretical loading conditions for which a maximum tensile stress appears at the top surface of slab under -30F temperature gradient. All the Michigan trucks yields almost the same magnitude of tensile stress and the standard truck provide much less tensile stress on the top surface of the slab. For all the trucks, under -30F temperature gradient, the critical damage location appears on the top surface of slab. The loading Case-III (see Table 3.2) is the most critical loading scenario for the standard truck (steering axle at left side of right transverse joint). The MI-20, MI-14 and MI-13 provide critical tensile stress for the loading Case-IV (1^{st} axle of tandem at left side of right transverse joint) and the MI-18 yields the highest stress for the loading case of VIII (1^{st} axle of tandem at left side of right transverse joint). The critical tensile stress condition is found for the same values of h, k, LTE and CTE for all the vehicles.

The critical loading condition as well as the location and magnitude of maximum tensile stress at the top surface of slab under the +30F temperature gradient between top and bottom surfaces of slab is shown in Table 3.5. For the +30F temperature gradient, the

standard truck provides the maximum stress, which is about 640 psi. However, the Michigan trucks yields significantly less magnitude of maximum stress, when compared with standard truck. The MI-20, MI-14 and MI-13 show almost the same maximum stress; the MI-18 truck provides much less magnitude of maximum stress when compared with other Michigan trucks. For all the trucks, the maximum stress at the top surface is negative under the +30F temperature gradient. It indicates that the bottom surface of slab is the critical location for all the trucks under the positive temperature gradient. Moreover, the +30F temperature gradient gives much higher magnitude of maximum stress when compared with the -30F. The critical location of damage for the +30F is opposite surface of slab when compared with -30F. In addition, the critical loading case for which the maximum stress appears is different between the +30F and -30F temperature gradient. The loading Case-VI (see Table 3.2) is the most critical loading scenario for the standard truck (1^{st} axle of tandem at mid-point of mid-slab). The MI-20, MI-14 and MI-13 provide critical tensile stress for the loading Case-III (1^{st} axle of tandem at mid-point of mid-slab) and the MI-18 yields the highest stress for the loading case of II (steering axle at mid-point of mid-slab). The other parameters (h, k, LTE and CTE) for the critical tensile stress are found be the same for both the +30F and -30F temperature gradients.

Table 3.4: Maximum stress on the top surface of slab and loading condition of critical damage under -30F temperature difference for the Standard and Michigan trucks in 14-feet slab with asphalt

Truck	Maximum Stress (psi).	Critical damage location	Critical damage condition				
			Loading case (Table 3.2)	h (in)	k (psi/in)	LTE (%)	CTE (in/in/deg F)
Standard	465	Top surface	III	8	150	50	7
MI-20	519	Top surface	IV	8	150	50	7
MI-18	527	Top surface	VIII	8	150	50	7
MI-14	524	Top surface	IV	8	150	50	7
MI-13	523	Top surface	IV	8	150	50	7

Table 3.5: Maximum stress on the top surface of slab and loading condition of critical damage under +30F temperature difference for the Standard and Michigan trucks in 14-feet slab with asphalt

Truck	Maximum Stress (psi).	Critical damage location	Critical damage condition				
			Loading case (Table 3.2)	h (in)	k (psi/in)	LTE (%)	CTE (in/in/deg F)
Standard	639	Bottom surface	VI	8	150	50	7
MI-20	601	Bottom surface	III	8	150	50	7
MI-18	579	Bottom surface	II	8	150	50	7
MI-14	602	Bottom surface	III	8	150	50	7
MI-13	603	Bottom surface	III	8	150	50	7

3.3.1. Fatigue damage analysis

As following the determination of the critical loading and response locations from the previous step, rigid pavement damage predictions for standard and Michigan trucks were performed from critical response results of ISLAB2000 simulations considering all the various parameters related to pavement thickness, joint system and subgrade conditions along with curling condition as described previously (see Section 3.1 and Table 3.1). Both positive and negative linear temperature gradients (ΔT of 0, ±15, and

±30F) for all loading case scenarios were used in this section to predict MEPDG pavement damage model. Fatigue damage equations of MEPDG for rigid pavements described in Section 2.6.1 (see Eq. 2.19) were utilized in pavement damage predictions.

Under a positive temperature gradient, different truck axle loadings along the longitudinal edge of the slab, midway between the transverse joints, bottom-top tensile bending stress is critical, as shown in Fig. 3.24. This stress increases greatly when there is a high positive temperature gradient through the slab. However, for different axle loading near the transverse joint, the top-down tensile stress is crucial for the fatigue damage under negative thermal curling condition as shown in Fig. 3.24.

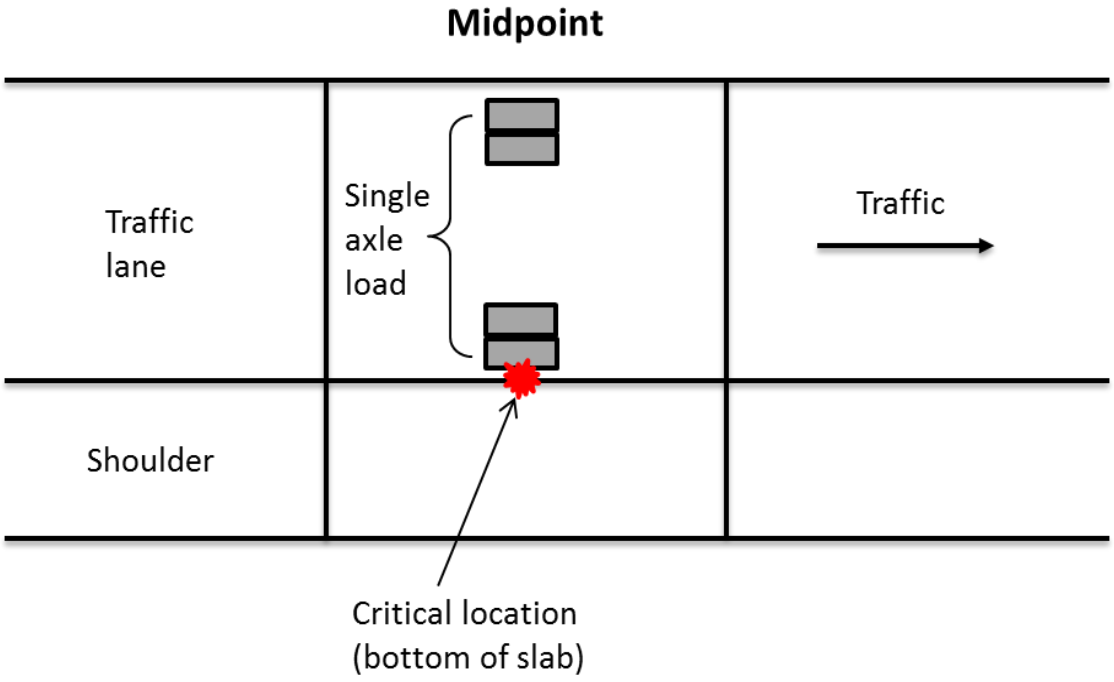

Figure 3.24: Critical load and structural response location for JPCP bottom-up transverse cracking.

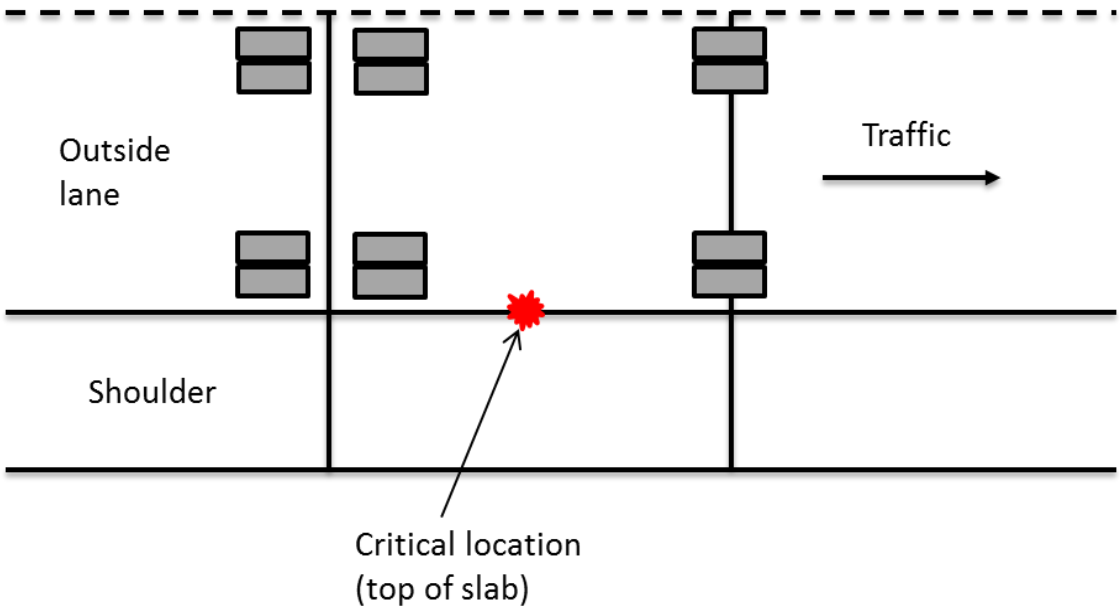

Figure 3.25: Critical load and structural response location for JPCP top-down transverse cracking.

In this section, the bending stress at both top and bottom of the slab is selected to calculate the number of the load repetitions to failure in terms of N_f in fatigue damage analysis. The ratio of maximum stress to the flexural strength or modulus of rupture (MR) of the concrete, also known as stress ratio, was required to compute N_f. It is speculated that if the stress ratio is less than 0.4(some say 0.5) no fatigue damage occurs regardless the number of the load repetitions. On the other hand, fatigue damage is expected to occur in the PCC slab if the stress ratio is over 0.4.In this study, the critical stress ratio is considered to be 0.4. The modulus of rupture is calculated as $E = 33\rho^{3/2}(MR/9.5)$(NCHRP), where $\rho = 150\ lb/ft$is the unit weight and E =5.0*10^6psiis the elastic modulus. For the concrete slab, the modulus of rupture is calculated 780 psi.

The number of load repetitions (N_f) is plotted against stress ratio for all factorial runs of ISLAB2000 for each vehicle for the critical loading cases (see Table 3.4 and 3.5). The maximum tensile stress at the top and bottom of the slab were picked for the damage analysis, in terms of number of loading repetitions to failure N_f. The effect of the slab thickness, temperature gradients and load transverse efficiency in transverse direction to the pavement performance are also investigated here.

Graphs presented in Fig. 3.26 and 3.27 show graphical representations of stress ratio (σ/MR) and number of load repetitions to failure (N_f) correlation for the standard and Michigan trucks where fatigue damage is quantified as a percentage of total design cases that provide σ/MR of 0.4 or greater. Figures 3.26 and 3.27 show the fatigue damage quantity for the +30F and -30F temperature differences, respectively. For the +30F temperature difference, the standard truck shows the maximum pavement damage potential when compared with the Michigan trucks. For the standard truck, more than 33% of design cases provides stress ratio of 0.4 and more, whereas it is it is less than 27% for the Michigan trucks (Fig. 3.26).

For the -30F temperature gradient, in comparison with the standard truck, the Michigan trucks provide a higher percentile of stress ratios that have magnitude of 0.4 or greater (Fig. 3.27). The damage percentage for the standard truck under the negative temperature gradient is about 21%, which was more than 33% for the positive temperature gradient. However, the Michigan trucks give the almost same percentage of damage potential for both the positive and negative temperature gradients, which is about 27%. This result indicates that all the trucks have fatigue damage potential in some extent

depending on the interaction of the factors including material properties and slab curling behavior. Therefore damage analyses results are plotted in separated figures to investigate the effect the slab thickness, temperature gradients and load transverse efficiency in transverse direction to the pavement performance, which are presented in Figs. 3.28-330.

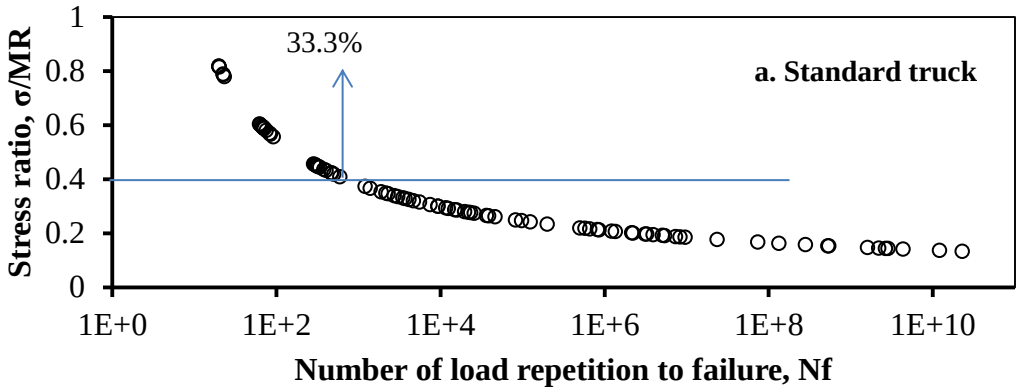
33.3%
a. Standard truck
Stress ratio, σ/MR
1
0.8
0.6
0.4
0.2
0
1E+0
1E+2
1E+4
1E+6
1E+8
1E+10
Number of load repetition to failure, Nf

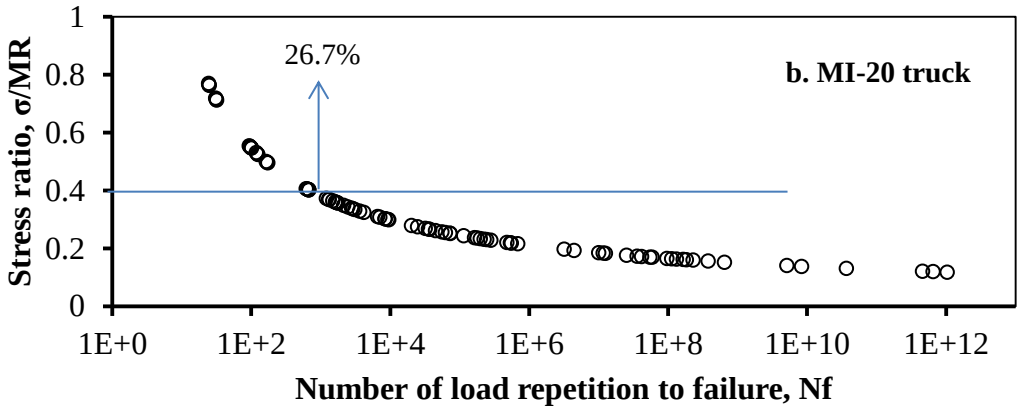
26.7%
b. MI-20 truck
Stress ratio, σ/MR
1
0.8
0.6
0.4
0.2
0
1E+0
1E+2
1E+4
1E+6
1E+8
1E+10
1E+12
Number of load repetition to failure, Nf

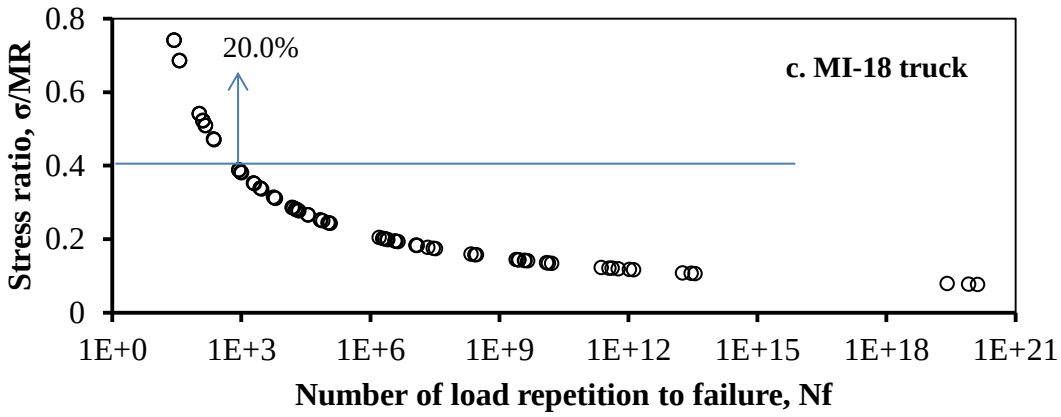
20.0%
c. MI-18 truck
Stress ratio, σ/MR
0.8
0.6
0.4
0.2
0
1E+0
1E+3
1E+6
1E+9
1E+12
1E+15
1E+18
1E+21
Number of load repetition to failure, Nf

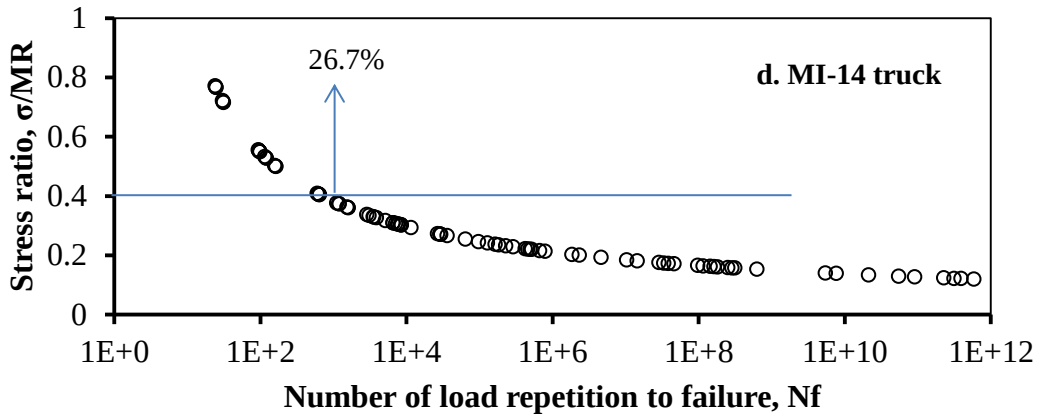

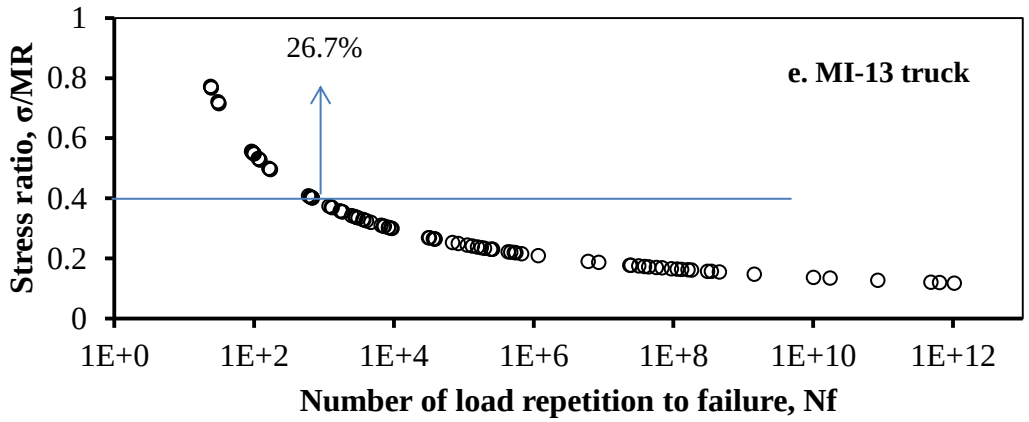

Figure 3.26: Fatigue damage analysis for standard (a) and Michigan (b-e) trucks on the 14-feet slab with asphalt shoulder under positive temperature (+30F) gradient. The stress ratio is calculated for the critical loading condition presented in Table 3.5.

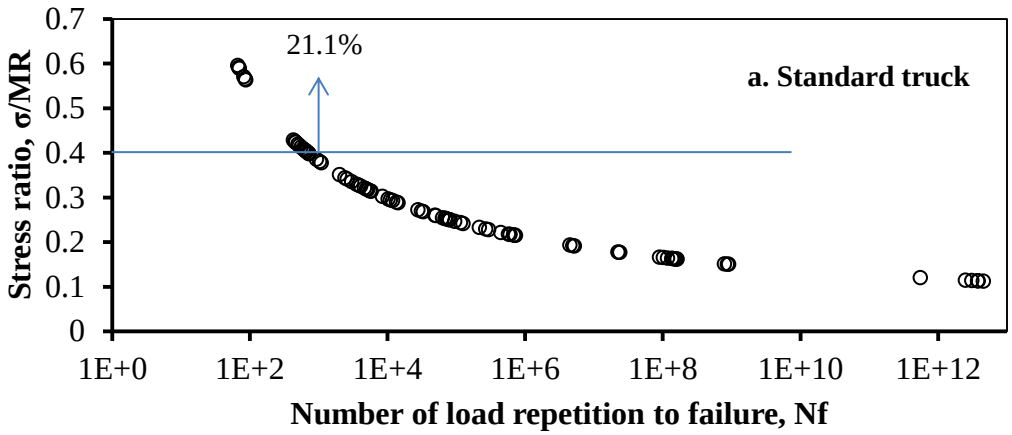
21.1%
a. Standard truck
Stress ratio, σ/MR
0.7
0.6
0.5
0.4
0.3
0.2
0.1
0
1E+0
1E+2
1E+4
1E+6
1E+8
1E+10
1E+12
Number of load repetition to failure, Nf

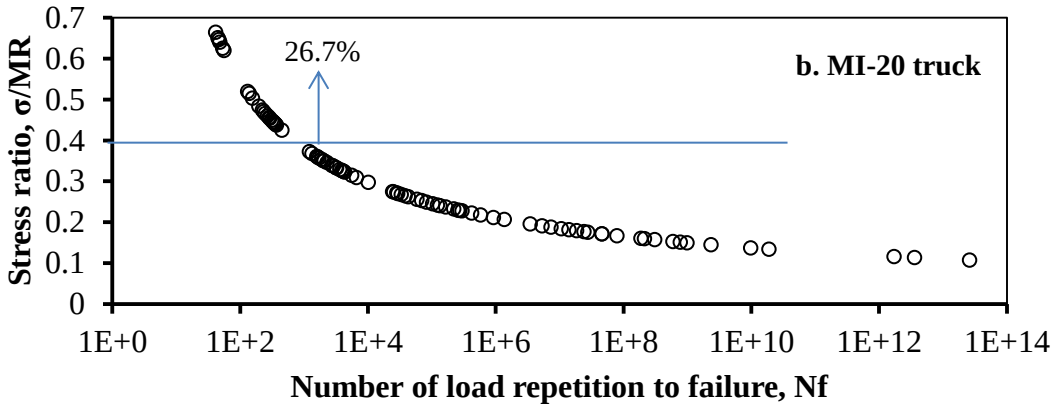
26.7%
b. MI-20 truck
Stress ratio, σ/MR
0.7
0.6
0.5
0.4
0.3
0.2
0.1
0
1E+0
1E+2
1E+4
1E+6
1E+8
1E+10
1E+12
1E+14
Number of load repetition to failure, Nf

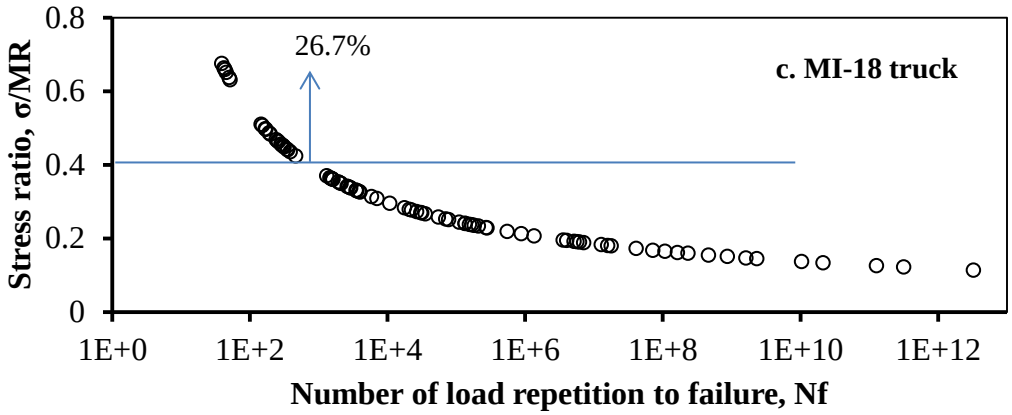
26.7%
c. MI-18 truck
Stress ratio, σ/MR
0.8
0.6
0.4
0.2
0
1E+0
1E+2
1E+4
1E+6
1E+8
1E+10
1E+12
Number of load repetition to failure, Nf

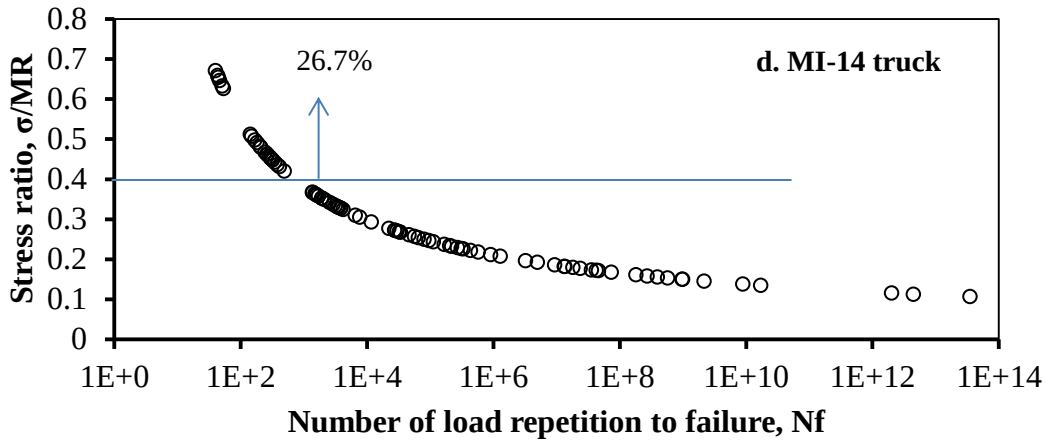

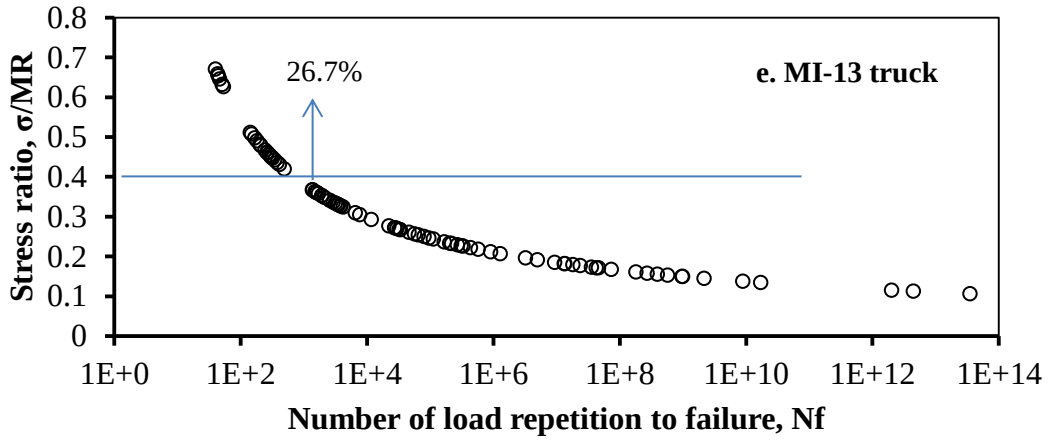

Figure 3.27: Fatigue damage analysis for standard (a) and Michigan (b-e) trucks on the 14-feet slab with asphalt shoulder under negative temperature (-30F) gradient. The stress ratio is calculated for the critical loading condition presented in Table 3.4.

Figure 3.28 shows the effect of temperature gradient on the number of repetitions to failure, N_f for various representative trucks on a 14 feet slab with asphalt shoulder. A lower N_f indicates a higher probability of fatigue damage. The values of N_f are calculated based on the stress ratios obtained for the critical loading conditions presented in Tables

3.4 and 3.5. The magnitude of N_f first increases and then decrease as the temperature gradient changes from -30F to +30F. The +30F provides the minimum value of N_f when compared with other temperature gradients. For the positive temperature gradients, the standard truck provides a lower value of N_f than the Michigan trucks. The opposite is true for the negative temperature gradients. So, the standard truck has a higher fatigue damage potential at positive temperature gradient and the Michigan trucks have a greater potential to fatigue damage at negative temperature gradient.

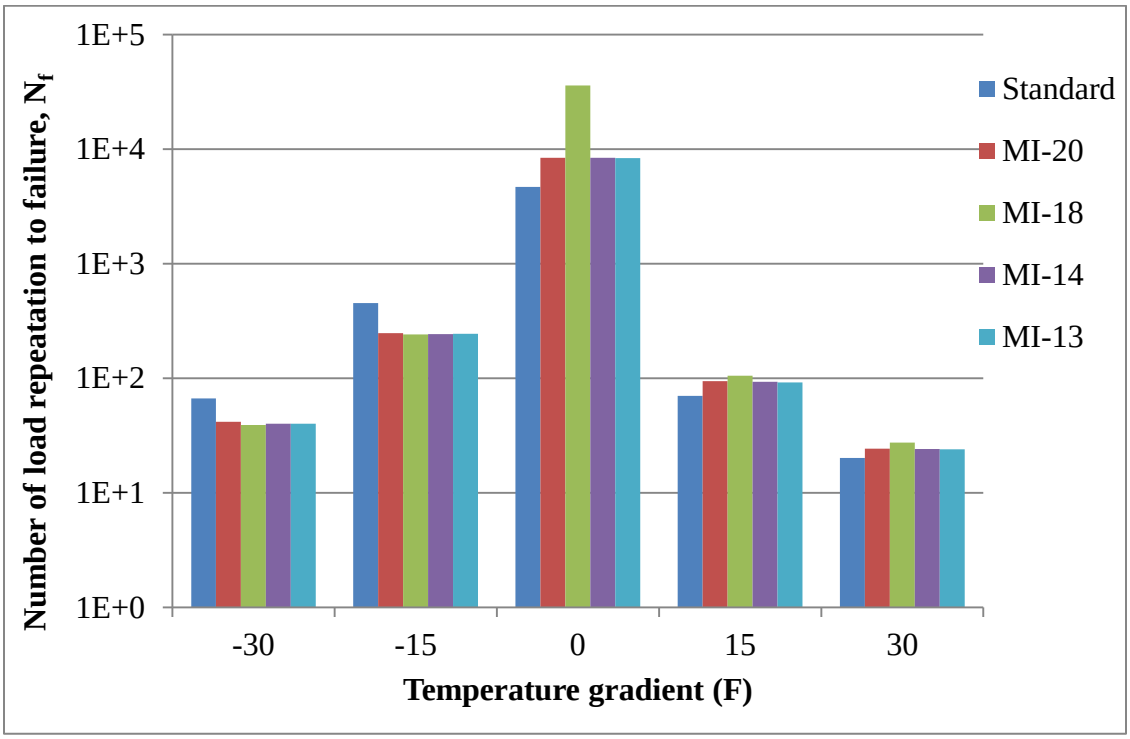

Figure 3.28: Effect of temperature gradient on the number of load repetitions to failure on a 14 feet slab with asphalt shoulder. A lower the number of load repetitions to failure yields a higher probability of damage.

Figure 3.29 shows effect of pavement thickness on the N_f for various representative trucks for the different slab thicknesses on a 14 feet slab with asphalt shoulder. The pavement stresses are selected for the temperature gradient of +30F, load transfer efficiency in transverse direction of 50%, modulus of subgrade reaction of 150 psi/in and coefficient of thermal expansion of 7.00E-06 in/in/^{0}F. Figure 3.29show that the values of N_f decrease with a reduction in the pavement thickness. So, a higher pavement thickness significantly improves pavement service life since it provides a larger number of load repetitions to failure. The increase of pavement thickness is effective in reducing the fatigue damage for all representative trucks. However, the standard 5-axle truck exhibited the lowest allowable number of load repetitions to failure, which means that the standard truck has the highest fatigue damage potential among the tested vehicles under +30F temperature difference.

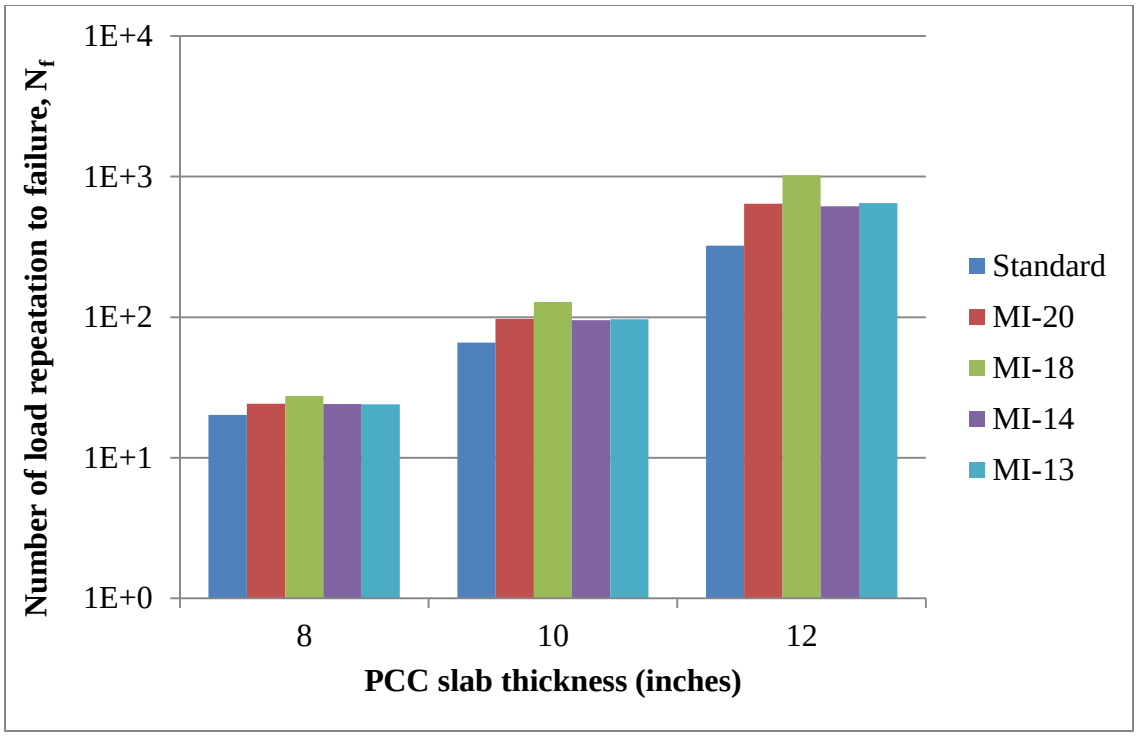

Figure 3.29: Effect of PCC slab thickness on the number of load repetitions to failure for different representative trucks on a 14 feet slab with asphalt shoulder. A lower number of load repetitions to failure yield greater fatigue damage.

Figure 3.30 shows the effect of load transfer efficiency on the number of repetitions to failure for various representative trucks on a 14 feet slab with asphalt shoulder. The pavement stresses under different trucks are selected for the temperature gradient of +30F, slab thickness of 10 inches, modulus of subgrade reaction of 150 psi/in and coefficient of thermal expansion of 7.00E-06 in/in/deg. F. The value of N_f decreases with a reduction in the different load transfer efficiency (LTE). However, for all the vehicles, the LTE of 50% provides the minimum value of N_f among all the LTE shown in Fig. 3.30.

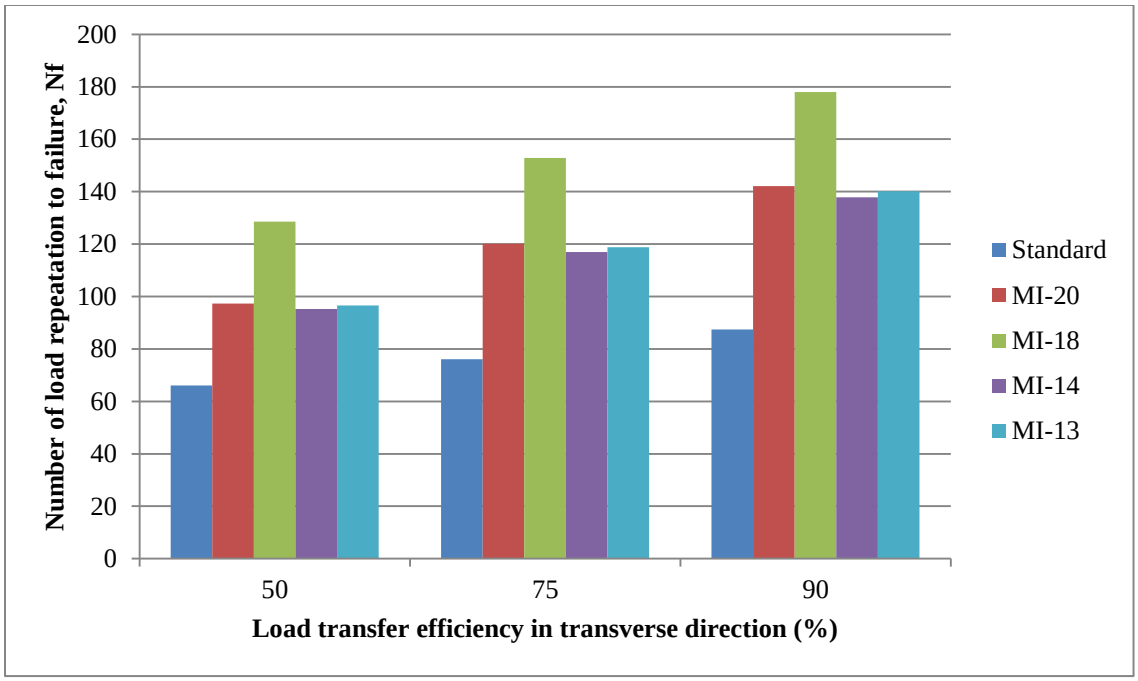

Figure 3.30: Effect of load transfer efficiency on the number of load repetition to failure on a 14 feet slab with asphalt shoulder. A lower value of N_f yields a greater fatigue damage.

3.3.2. Faulting damage analysis

As following the determination of the fatigue damage analysis from the previous step, rigid pavement faulting damage predictions for the standard 5-axle and 11-axle Michigan trucks were performed from critical response results of ISLAB2000 simulations considering all the various parameters related pavement thickness, joint system and subgrade conditions along with curling condition as described previously. For faulting damage analysis, the maximum differential deflections between the loaded slab and the unloaded slab were calculated as critical responses of faulting damage. These

deflection responses were utilized to estimate faulting damage in term of differential energy (DE).

In the MEPDG pavement design method, differential deflection across transverse joint represents critical response of faulting when repeated heavy axle loads come near transverse joints (critical loading condition of faulting) as shown in Fig. 3.31. Both positive and negative linear temperature gradients (ΔT: 0, ±10, ±15, ±30) were used in this section to predict MEPDG pavement damage model. For the corner deflection under the loaded slab the loading case scenario was selected as the wheel load at the left side of right transverse joint on the slab on interest. The energy difference in the elastic subgrade deformation under the maximum loaded slab and the unloaded slab was used for faulting damage equations of MEPDG described in Section 2.6.2 (see Eq. 2.21) were utilized in pavement damage predictions. The differential energies for all nodal points on slab of interest were compared with each other and the higher value was picked for the faulting damage analysis.

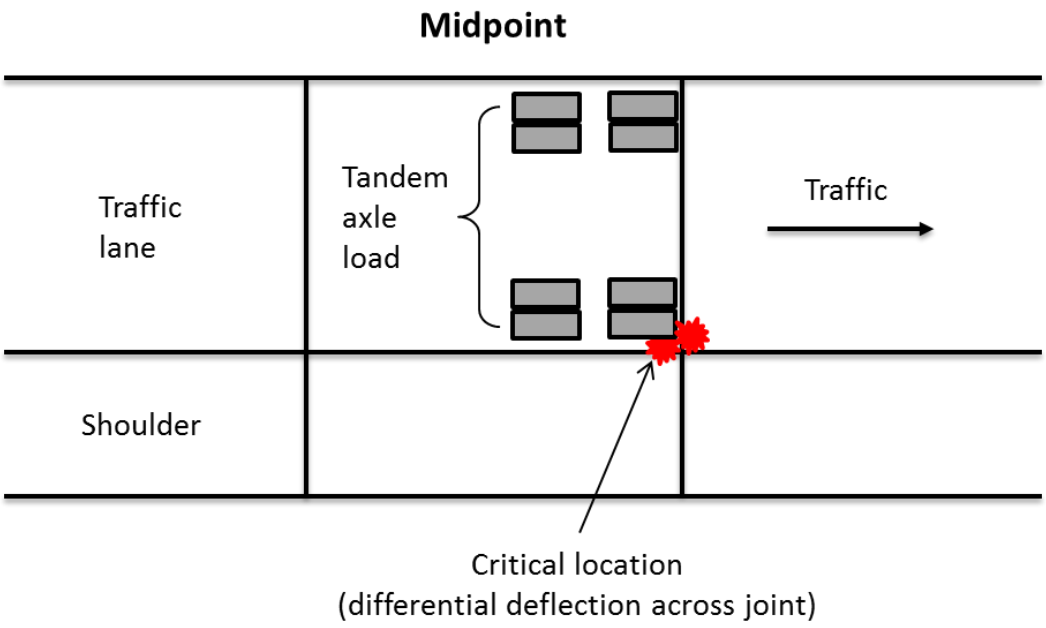

Figure 3.31: Critical load and structural response locations for JPCP joint faulting analysis.

The differential energy across the joint or crack is influenced by several factors, including heavy wheel loads and inadequate load transfer. Since the differential corner deflection depends on the free corner deflection and the load transfer efficiency (LTE), the presence of dowels is the most important design feature affecting joint faulting. However, faulting damage analyses results are plotted in separated figures to investigate the effect the slab thickness, temperature gradients and load transverse efficiency in transverse direction to the pavement performance. A greater differential energy indicates a higher potential for joint faulting. No faulting occurs without any differential deflection at the corner.

Figure 3.32 shows the effect of PCC slab thickness on the differential energy for the various representative trucks on a 14 feet slab with asphalt shoulder. The pavement stresses under different trucks are selected for the temperature gradient of +30F, load transfer efficiency in transverse direction of 50%, modulus of subgrade reaction of 150 psi/in and coefficient of thermal expansion of 7.00E-06 in/in/deg F. The differential energy decreases with an increase in the pavement thickness. In indicates that the pavement thickness of 8 inches has higher potential to pavement damage since it provides less differential energy to failure. The increase of pavement thickness is effective in reducing the pavement faulting damage for all representative trucks. Among all the trucks, the standard truck provides the highest DE for the 8 inches thickness and the lowest DE for the 10 and 12 inches thickness. Among the Michigan trucks, the differential energy for the MI-13 truck is the lowest. For the given loading conditions and pavement thickness of 8 inches, the standard truck has the highest faulting damage potential among the tested vehicles.

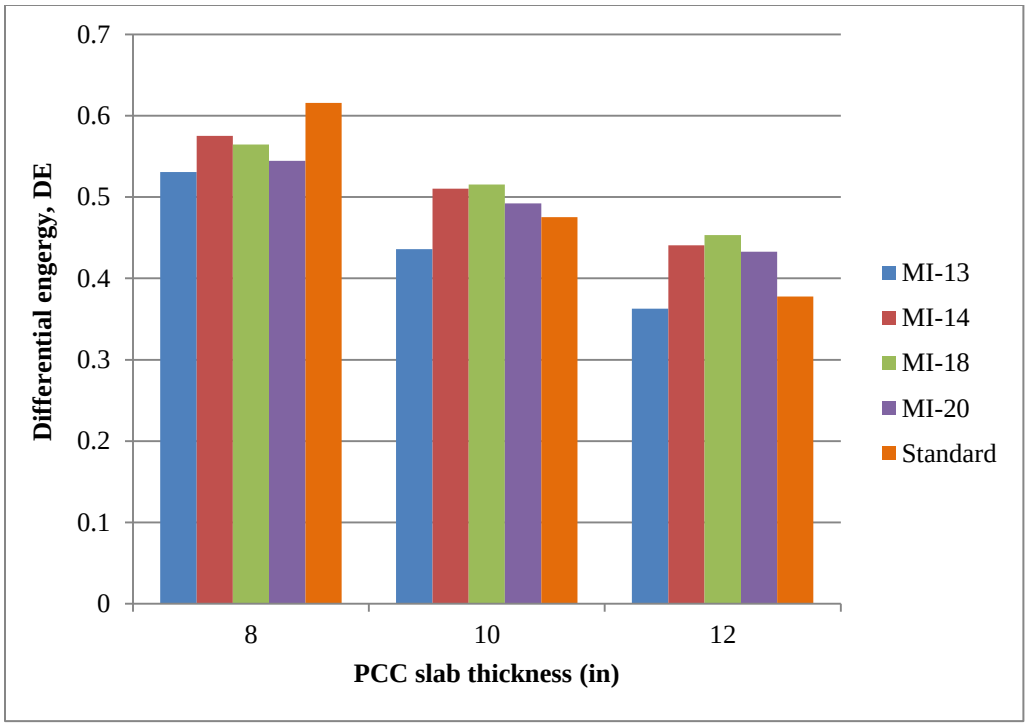

Figure 3.32: Effect of PCC slab thickness on the differential energy for the various representative trucks on a 14 feet slab with asphalt shoulder. A greater differential energy means a higher joint faulting.

Figure 3.33 shows a bar chart comparison of DE under various representative trucks to investigate the effect of load transfer efficiency in transverse direction to the faulting damage on a 14 feet slab with an asphalt shoulder. The pavement stresses under different trucks are selected for the temperature gradient of +30F, slab thickness of 8 inches, modulus of subgrade reaction of 150 psi/in and coefficient of thermal expansion of 7.00E-06 in/in/deg F. Figure 3.33 illustrates that a decrease in load transfer efficiency (LTE) gradually increases the differential energy. So for all the vehicles, the LTE of 50% yields the highest potential of faulting among all LTE tested. The effect of modulus of

subgrade reaction, k on the differential energy, DE is shown in Fig. 3.34. The pavement stresses under different trucks are selected for the temperature gradient of +30F, slab thickness of 8 inches, LTE of 50% and coefficient of thermal expansion of 7.00E-06 in/in/deg F. A higher modulus of subgrade reaction, k significantly decreases the DE, which indicate that a higher value of k increases the service life of pavement. In both the cases, the standard truck exhibits the highest amount of DE, which means that standard truck has the highest faulting damage potential among the tested vehicles.

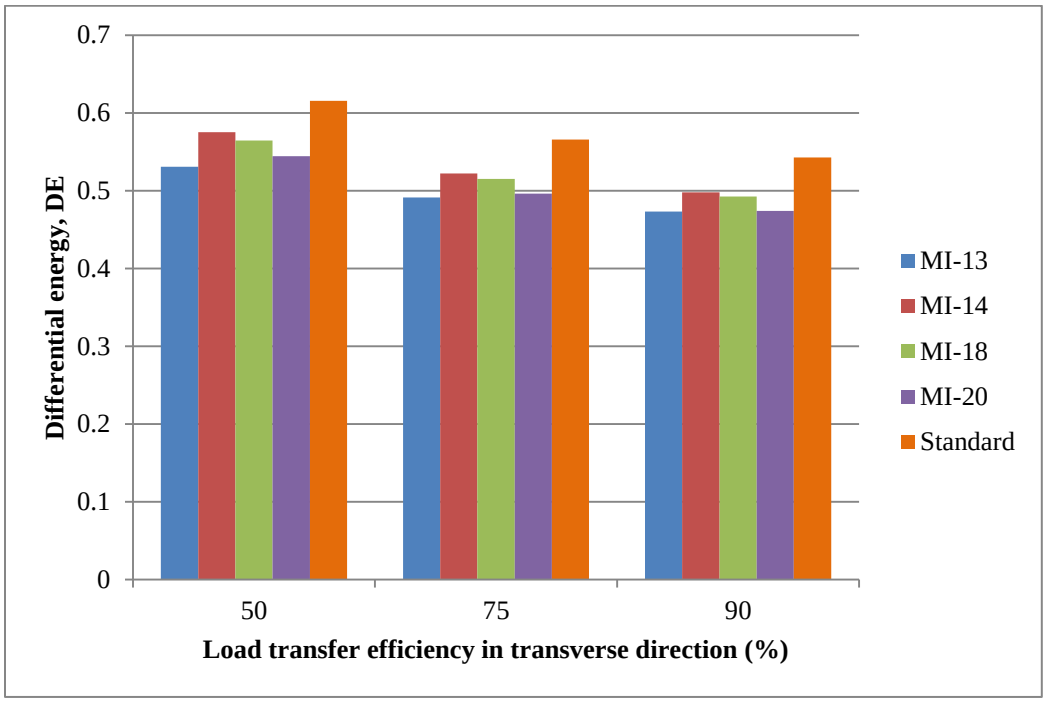

Figure 3.33: Effect of load transfer efficiency on the differential energy for various representative trucks on a 14 feet slab with asphalt shoulder. A greater differential energy means a higher joint faulting.

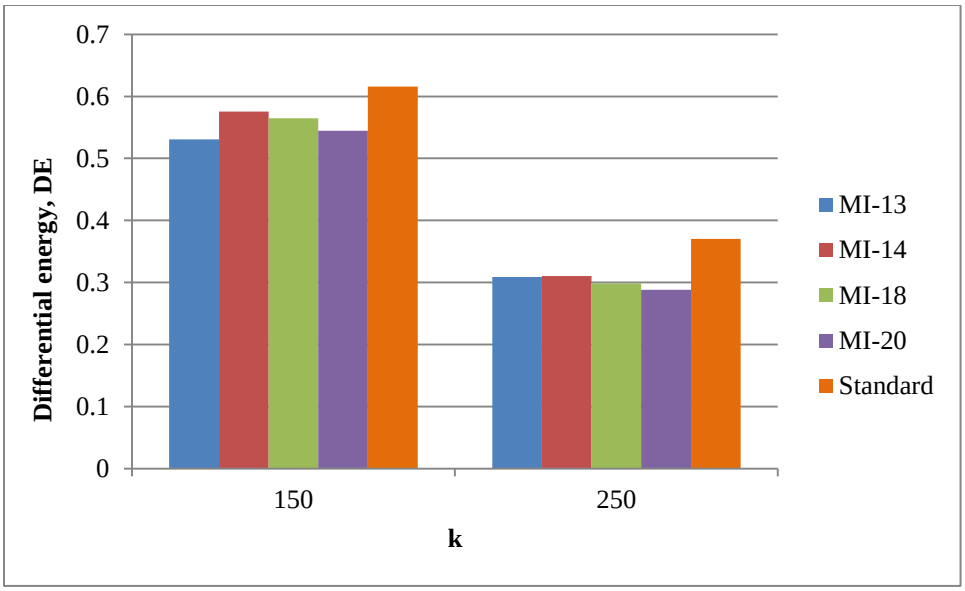

Figure 3.34: Effect of modulus of subgrade reaction on the differential energy for various representative trucks on a 14 feet slab with asphalt shoulder. A greater differential energy means a higher joint faulting.

3.4. Summary

The following findings could be made from the comparisons of top tensile stress between Michigan and standard truck.

- The tensile stress at the bottom of the slab is more critical than the tensile stress at the top of the slab under positive temperature difference (daytime) between the top and bottom of slab. The opposite is true for the negative temperature difference (nighttime).
- Transverse joint loading deserves greater consideration in critical stress analysis under negative temperature difference condition since it significantly affects the magnitude of upward slab curling.

- For all the vehicles, the maximum tensile stresses at the top and bottom surface of the slab appear between 84 and 96 inches from the left transverse joint of mid-slab.
- The positive temperature gradient (+30F) yields a greater maximum stress when compared with the negative temperature gradient (-30F)

The following findings could be drawn from the rigid pavement fatigue damage analysis with slab curling behavior of Michigan and standard trucks

- Based on the damage analysis results, the standard truck has higher fatigue damage risk on rigid pavements than the MI trucks at positive temperature gradient. The opposite is true for the negative temperature gradients. The Michigan trucks have a greater potential to fatigue damage at negative temperature gradient.
- Michigan trucks introduce damages to varying degrees on PCC pavement. Among Michigan trucks, MI-14 trucks have more damage potential.
- For Michigan trucks, as the temperature gradient increases, the fatigue damage increases. However, the change in N_f due to temperature gradient is not as significant for standard truck as the other trucks.
- By increasing the slab thickness, the number of load repetitions to failure could be improved significantly.
- For the same temperature gradient and slab thickness, as the load transfer efficiency in transverse direction increase, the number of load repetitions to failure also increases.

The following findings could be drawn from the rigid pavement faulting damage analysis with slab curling behavior of Michigan and standard trucks

- Based on the damage analysis results, the standard truck has higher faulting damage risk on rigid pavements than that of Michigan trucks.
- Michigan trucks introduce damages to varying degrees on PCC pavement. Among Michigan trucks, the MI-14 and MI-18 trucks have more faulting damage potential.
- By increasing the slab thickness, the differential energy significantly decreases.
- For the same temperature gradient and slab thickness, as the load transfer efficiency in transverse direction increase, the differential energy significantly decreases.
- For the same slab thickness, a higher modulus of subgrade reaction significantly decreases the differential energy.

CHAPTER 4

DAMAGE ANALYSES IN FLEXIBLE PAVEMENTS

4.1. Introduction

Just as with rigid pavements, flexible pavement structures are subject to distress formation from both external and environmental loadings. The structural response of the pavement system due to traffic loads is determined in this chapter based on the linear elastic flexible pavement response model. A set of input parameters which are typical for Michigan flexible pavement sections has been considered to conduct a mechanical loading analysis. These input parameters include the following:

- layer thicknesses
- material properties (adjusted for environmental and other effects, as necessary)
- elastic properties
- traffic condition
- load spectrum i.e., frequencies of vehicle types and weights within each vehicle type
- Tire contract pressure distributions and areas.

Using layered elastic analysis (LEA), critical pavement responses can be utilized to predict the likelihood of distress formation. The basic assumption of linear elastic analysis is that the pavement response (stress or strain) is linearly proportional to the

applied load. Finite element analysis (FEA) counts the non-linearity in the unbound materials in the flexible pavement system**.** Therefore, in this study FEA study has not been used for flexible pavement analysis because of the additional computational time needed for FEA. The critical pavement response variables used in these analyses include: (a) tensile horizontal strains at the bottom of the AC layer (for AC fatigue cracking) and (b) compressive vertical strains at the top of the subgrade (for subgrade rutting).

The MEPDG fatigue damage model(Eq. (2.13))and rutting model (Eq. (2.3)) for AC pavement can be used to calculate the fatigue and rutting damage based on critical strains, specific pavement conditions, and truck loadings. However, as the MEPDG equation for fatigue uses specific pavement temperatures to assess the number of loads until failure, the MEPDG equations have not been utilized for damage prediction in this chapter. For flexible pavement structures, the Jacob Uzan Layered Elastic Analysis (JULEA) multilayer elastic computer program (NCHRP 2004) is used to calculate the pavement responses needed for distress predictions for the cases in which all materials in the pavement structure can realistically be treated as linearly elastic. Four 11-axle Michigan trucks (MI-13, MI-14, MI-18 and MI-20) were selected in this analysis while the standard 5-axle semi-trailer was selected as a control vehicle.

A parametric study was performed by varying different variables in order to identify proper WinJULEA inputs for pavement response predictions close to realistic parameters. The following variables comprise the analysis:

- AC Properties
    - AC thickness (h_{AC}): 8, 10 and 12 inches
    - Elastic Modulus of AC: $200*10^3$ psi, $400*10^3$ psi, $600*10^3$ psi
    - Poisson's Ratio: 0.35 (AC), 0.4 (Base), 0.4 (Subbase), 0.45 (Subgrade)
    - Interface conditions between layers: Full slip (100,000)
- Base thickness (h_{base}): 6 inches
- Subbase thickness ($h_{subbase}$): 18 inches
- Elastic Modulus of Base: $20*10^3$ psi, $40*10^3$ psi
- Elastic Modulus of Subbase: $15*10^3$ psi
- Elastic Modulus of Subgrade: $12.5*10^3$ psi

Only one tire pressure, 120 psi, has been selected for the entire series of trucks analyzed to avoid analysis complexities. The influence line approach that was used with rigid pavements is not valid here since JULEA cannot simulate dynamic traffic loading condition. Moreover, LEA assumes that discontinuities in the AC layer do not exist so that position of the load with respect to the traffic lane is not addressed. Each pavement response variable is evaluated at the critical location within the pavement layer where the parameter is at its most extreme value. Three different locations, as shown in Fig. 4.1, were evaluated to determine the critical one. The three regions are: (a) between the left two wheels (two wheels at right give same result so only one side considered), (b) under the 2^{nd} left wheel, and (c) middle of axle.

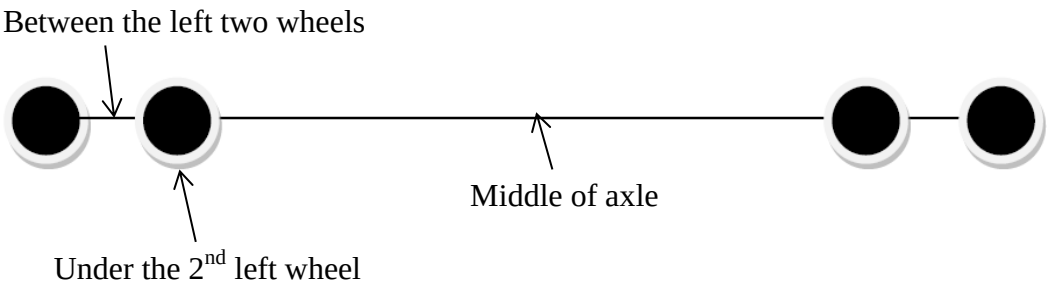

Figure 4.1: Schematic of a single axle.

4.2. Asphalt concrete fatigue damage analysis

The tensile strains developed in the different locations of axle due to traffic loading under the operating conditions mentioned above are discussed here. The tensile strain along the axle for the Standard and Michigan (MI-13, MI-14, MI-18 and MI-20) trucks are presented in Figs. 4.2 and 4.3. The AC thickness was considered as 8 inches. The elastic modulus of the AC layer and base were set to $400*10^3$ psi and $40*10^3$ psi respectively.

Figure 4.2 shows the horizontal tensile strains at the bottom of AC layer at different locations under the axle for a standard 5-axle truck. The magnitude of strains between the dual tires and under the 2nd wheel are almost the same, which are significantly larger than under the middle of axle. However, the similar characteristics also hold for the Michigan trucks. So, the tensile strain versus relative offset graphs for the Michigan trucks are redundant, which are not presented here.

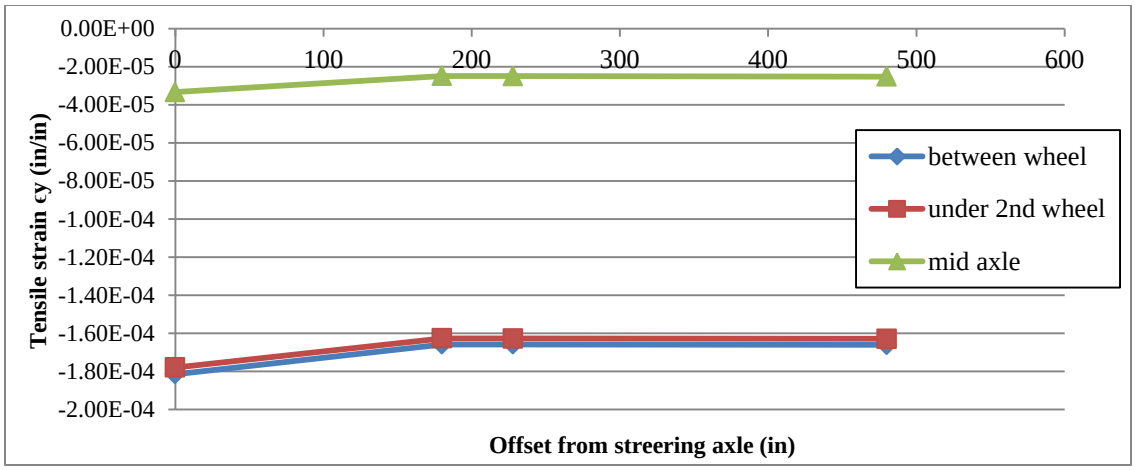

Figure 4.2: Pavement tensile strain responses produced by standard truck at different locations of axle.

Figure 4.3 shows a comparison of horizontal tensile strains at the bottom of AC layer at a location of between two dual tires for the 11-axle Michigan and standard 5-axle trucks. For the MI-20 and MI-18 trucks, the maximum tensile strain appears under both axles of a tandem axle. However, the MI-14 truck provides the maximum tensile strains under the 2nd and 3rd single axle. In case of MI-13 truck, the both axles of 1st tandem and 2nd tandem produce the maximum tensile strain response. Among the all the trucks, the standard truck provides the largest magnitude of tensile strain which is followed by the MI-14 truck. The MI-18 truck provides the least amount of strain. So, the standard truck has the highest potential for damage.

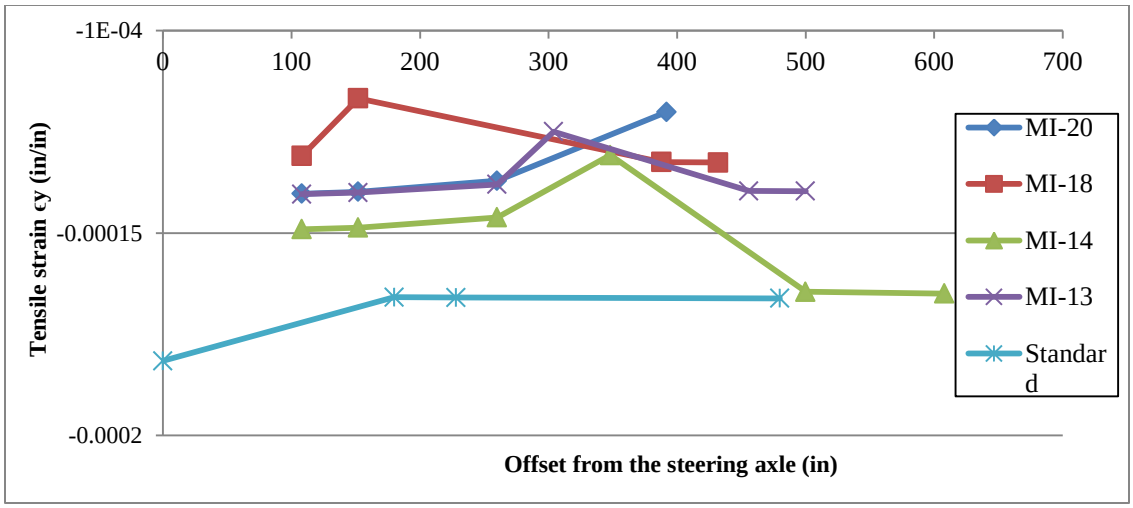

Figure 4.3: Pavement tensile strain responses produced by Michigan and standard truck between two wheels.

Bottom-up AC fatigue cracking is predicted in terms of allowable number of load repetitions, N_f, based on the Asphalt Institute and Shell design methods (see Section 2.5.2 (equation 2.12)) in this analysis. The allowable number of load repetitions for the maximum tensile strain was determined for each vehicle and then compared. The fatigue damage analyses results are plotted to investigate the effect the AC layer thickness, modulus of elasticity of AC and base layer to the flexible pavement performance.

Figure 4.4 shows the allowable number of load repetitions to failure, N_f for all the vehicles with different AC layer thickness. The maximum tensile strain for each vehicle, obtained from the Fig. 4.3, was considered for the calculation ofN_f. The elastic modulus of the AC layer and base were set to$400*10^3$ psi and $40*10^3$ psi respectively. Figure 4.4 shows that an increase in the pavement thickness significantly raises the N_f, which thereby improves the pavement service life. The MI-18 truck provides the highest value

of N_f because it develops the least amount of strain as shown in Fig. 4.3. The life expectancy of the flexible pavement under the action of loading by MI-18 is followed by the MI-20 and MI-14 trucks. However, the standard 5-axle truck exhibits the lowest allowable number of load repetitions to failure, which means that the standard truck has the highest fatigue damage potential among tested vehicles while MI-14 truck has the second highest risk.

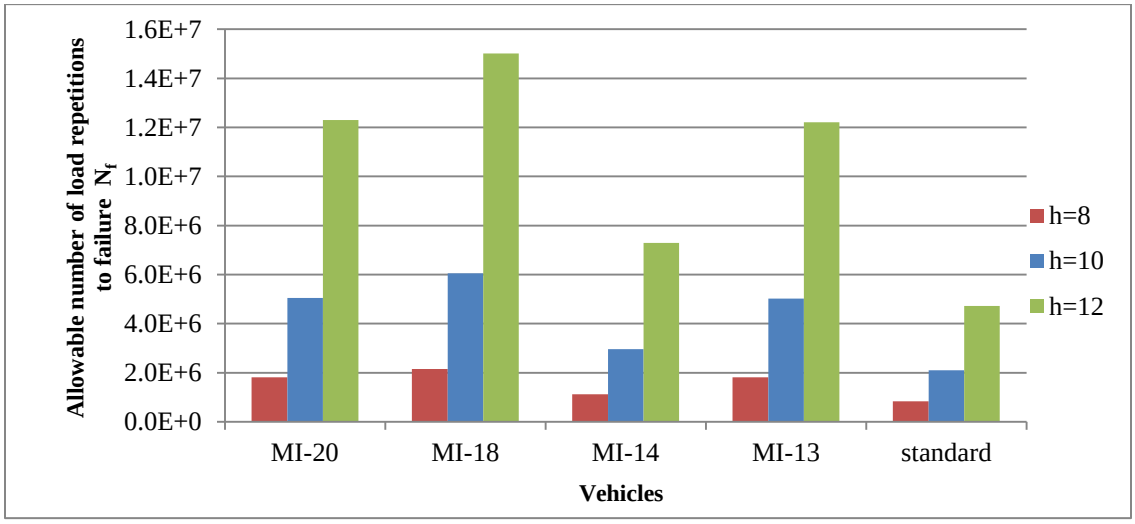

Figure 4.4: Fatigue damage analysis for different AC layer thickness.

The elastic modulus of AC layer is an important parameter related to fatigue distress of asphalt pavement. Figure 4.5 shows the allowable number of load repetitions for all vehicles with different modulus of elasticity of the AC layer considering the maximum tensile strain of each vehicle. The elastic modulus of base was set to $40*10^3$ psi (simulating a granular base) and the AC layer thickness was considered as 8 inches. For all the trucks, the number of load repetitions to failure significantly decreases with a

decrease in the elastic modulus of AC layer, which thereby significantly reduces the pavement service life with respect to fatigue cracking. However, standard truck exhibits the lowest allowable number of load repetitions to failure, which means that standard truck has the highest fatigue damage potential among tested vehicles.

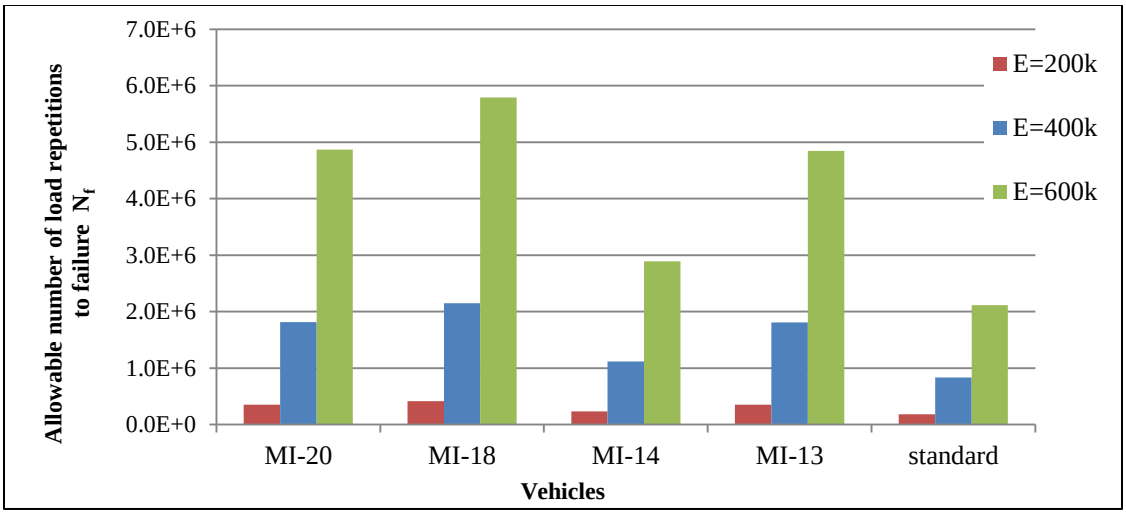

Figure 4.5: Fatigue damage analysis for different elastic modulus of AC layer.

The fatigue damage analysis was also investigated in terms of allowable number of load repetitions with different values of elastic modulus of base layer, which is shown in Fig. 4.6. The elastic modulus of AC was set to$400*10^3$ psi and the AC layer thickness were considered as 8 inch. Figure 4.6 shows that an increase in the elastic modulus of base layer improves the pavement service life by increasing the allowable number of load repetitions. However, the difference is not in a significant amount.

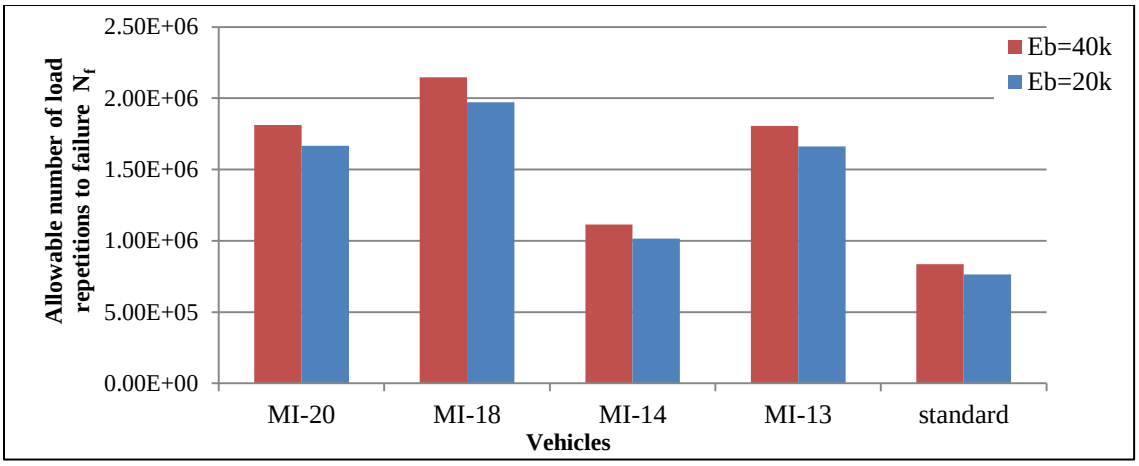

Figure 4.6: Fatigue damage analysis for different elastic modulus of base layer.

4.3. Subgrade rutting analysis

Significant vertical compressive strains have been shown to induce permanent deformations in the subgrade, leading to rutting in the wheel path of flexible pavement structures. The vertical compressive strain developed in a flexible pavement along the length of the truck for the standard 5-axle and Michigan (MI-13, MI-14, MI-18 and MI-20) 11-axle trucks are investigated here for the given operating conditions mentioned in Section 4.1. For this analysis, the AC thickness was considered as 8 inch. The elastic modulus of AC layer and base were set to $400*10^3$ psi and $40*10^3$ psi respectively.

Figure 4.7 shows the compressive vertical strains at the top of subgrade at different positions along the length of the standard 5-axle truck. The maximum compressive strain appears at the location of between two dual wheels as shown in Fig. 4.1. The locations under 2nd wheel also provide significantly higher compressive strain when compared with the location of between at mid-axle. The Michigan trucks also show the similar results which are not presented here. Since the location of between dual

wheels is the critical position, the subgrade rutting analyses are conducted based on the maximum vertical compressive strain developed on that location for all the vehicles. Moreover, the compressive strains on the top of the subgrade are almost the same regardless of single and tandem axles for standard truck which was not similar in the previous case of horizontal tensile strains in the AC layer (see Fig. 4.2).

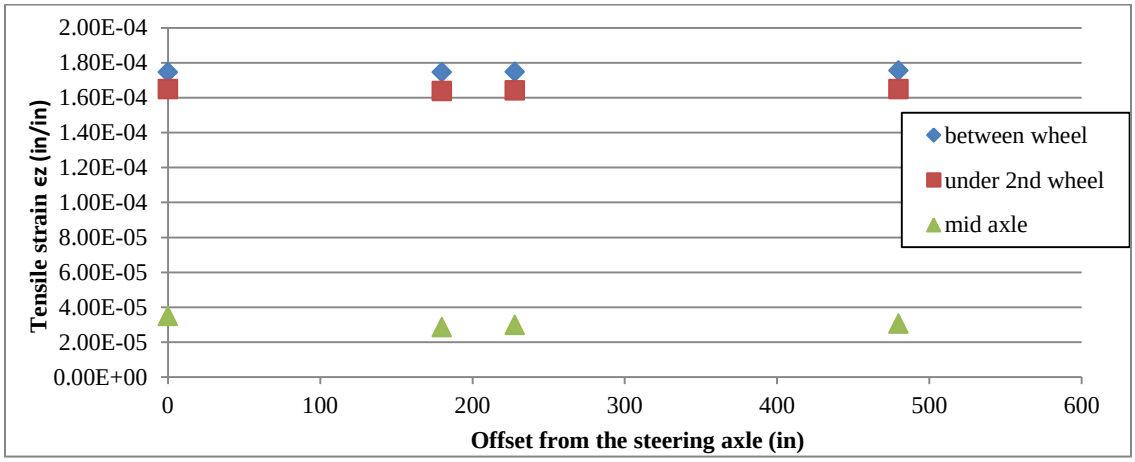

Figure 4.7: Pavement compressive strain responses produced by standard 5-axle truck at different locations of axle.

Figure 4.8 shows the compressive vertical strains at the top of the subgrade under different axles for the standard and Michigan (MI-20, MI-18, MI-14 and MI-13) trucks at the location of between the dual wheels. The maximum compressive vertical strain for the MI-20 and MI-18 trucks appears under both individual axles of the tandem. The MI-14 truck exhibits the maximum compressive strain under the 3rd axle of quad assembly while it is at the mid-axle of front tridem for the MI-13 truck. However, the axles responsible for the maximum compressive strains are not same as that of the maximum

tensile strains (Fig. 4.3).Figure 4.8 also shows that among all the trucks, the Standard truck provides the highest compressive vertical strain.

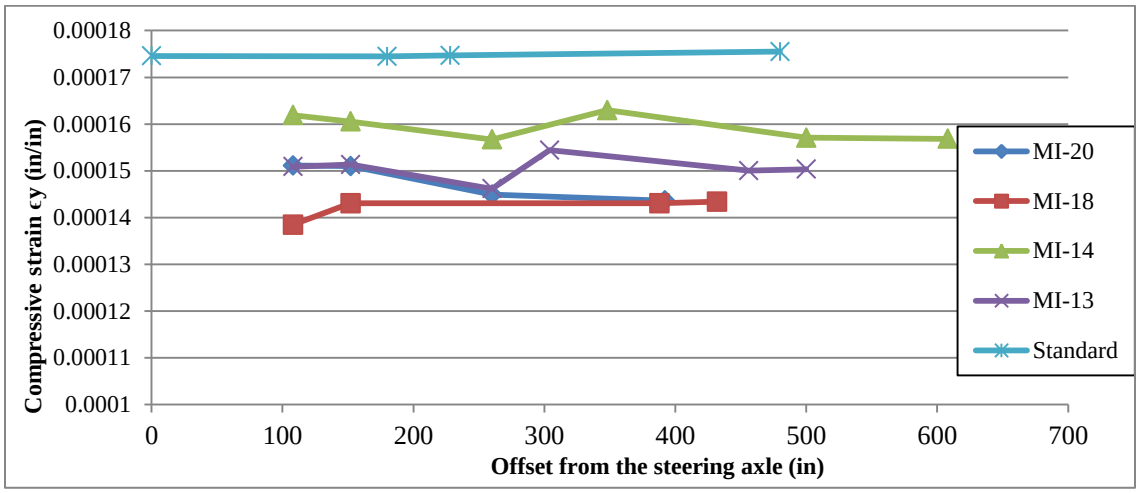

Figure 4.8: Pavement vertical compressive strain responses in the subgrade layer produced by Michigan and standard truck between two wheels.

The subgrade rutting is predicted in terms of allowable number of load repetitions, N_f, based on the Asphalt Institute and Shell design methods (see Section 2.5.1(equation 2.2)). The coefficients developed by both Asphalt Institute and U.K. Transport & Road Research Agencies are utilized for the calculation of N_f and compared (see Table 2.1). The N_f is calculated using the maximum vertical compressive strain obtained from Fig. 4.8 for each vehicle and then compared. The effect of the AC layer thickness and the modulus of elasticity of AC and base layer are considered here for the subgrade rutting analysis of a flexible pavement. No variation in rutting damage of the subgrade was found due to the change in subgrade modulus of elasticity; so effect of this

parameter is not shown here. The elastic modulus of AC layer and base were set to $400*10^3$ psi and $40*10^3$ psi, respectively.

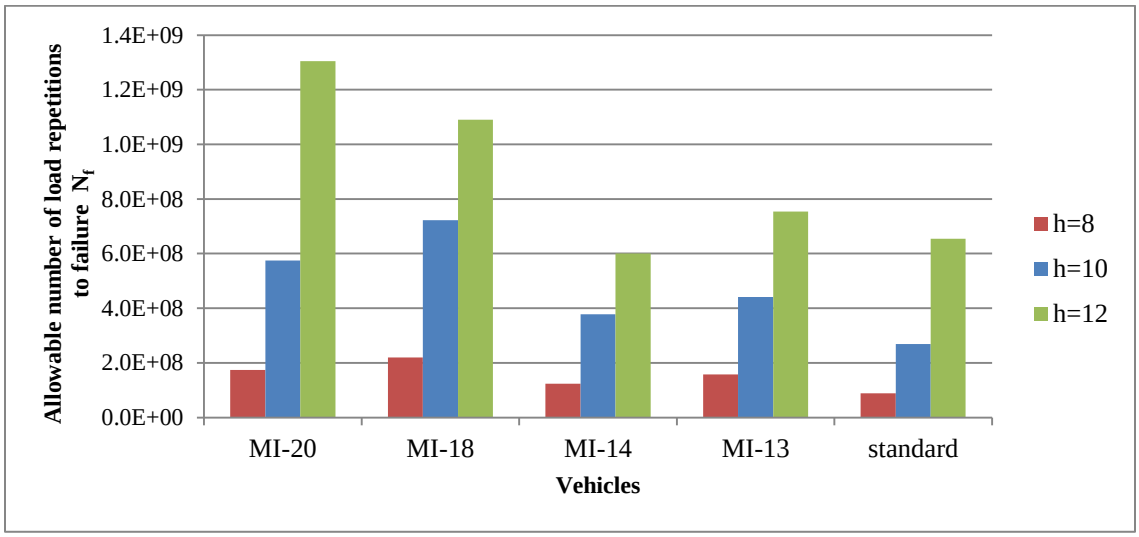

Figure 4.9: Subgrade rutting Analysis for different AC layer thickness using the coefficients developed by Asphalt Institute.

Figure 4.9 shows the effect of AC layer thickness on the N_f calculated using the coefficients developed by Asphalt Institute (Table 2.1) for all the standard and Michigan vehicles. For all the trucks, the N_f dramatically decreases with a decrease in the AC layer thickness. It indicates that the AC layer thickness of 8 inches provides significantly less pavement service life with respect to subgrade rutting. Among all the vehicles, for the 8 and 10 inches of AC layer thickness, the standard truck exhibits the lowest allowable number of load repetitions to failure and the MI-18 truck provides the highest value of N_f. However for the AC thickness of 12 inches, MI-14 truck yields the lowest and the MI-20 truck provide the highest values of N_f.

Figure 4.10 shows the effect of AC layer thickness on the N_f calculated using the coefficients developed by the U.K. Transport & Road Research Agency. The N_f calculated based on the U.K. Transport & Road Research Agency (Fig. 4.10) provides the similar trend for all the vehicles and AC layer thickness when compared with that calculated based on the Asphalt Institute (Fig. 4.9). However, the magnitude of N_f calculated based on the U.K. Transport &Road Research agency is significantly less than that calculated based on the Asphalt Institute (e.g., the N_f for the MI-20 truck based on the U.K. Transport & Road Research Agency is about 3 times lower than that calculated based on the Asphalt Institute).

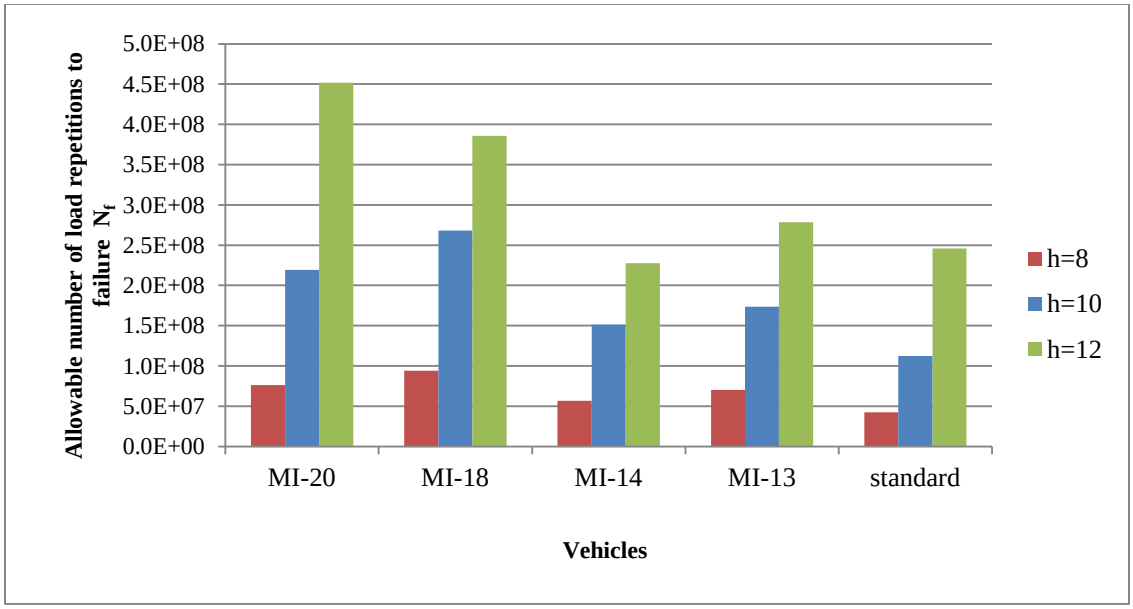

Figure 4.10: Subgrade rutting analysis for different AC layer thickness using the coefficients developed by U.K. Transport & Road Research Agency.

The effects of the AC layer elastic modulus on the N_f calculated based on the Asphalt Institute and U.K. Transport & Road Research Agency are shown in Fig. 4.11 and 4.12, respectively. The elastic modulus of base layer was set to$40*10^3$ psi and the AC layer thickness were considered as 8 inches. The elastic modulus of AC layer has a significant effect on the subgrade rutting of asphalt pavement. The value of N_f significantly decreases with a reduction in the elastic modulus of AC layer. It indicates that a higher elastic modulus yields a greater service life of pavement. Among all the vehicles, the MI-18 trucks provides the highest value of N_f and the Standard truck yields the least value of N_f for all the elastic modulus of pavement. So, the standard 5-axle truck has the highest potential of subgrade rutting.

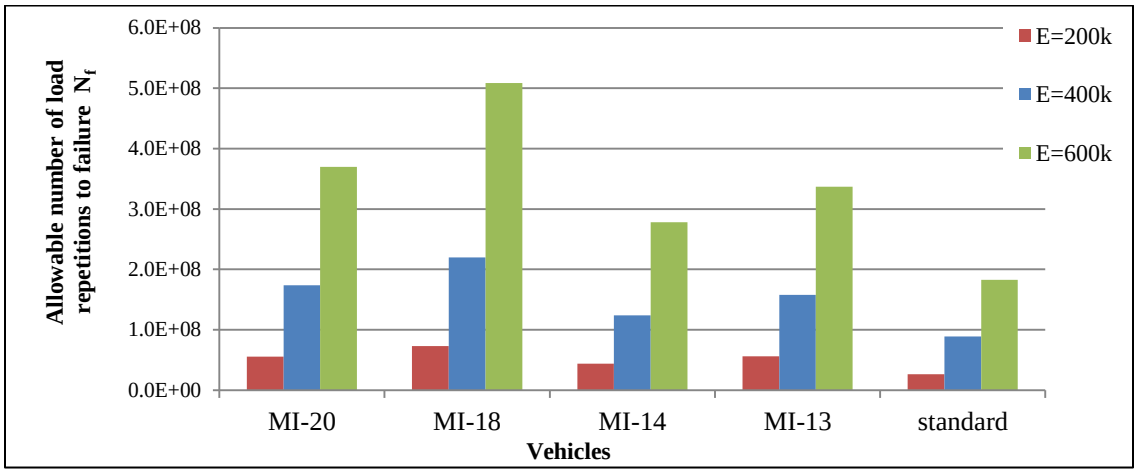

Figure 4.11: Subgrade rutting analysis for different elastic modulus of AC layer based on the coefficients developed by Asphalt Institute.

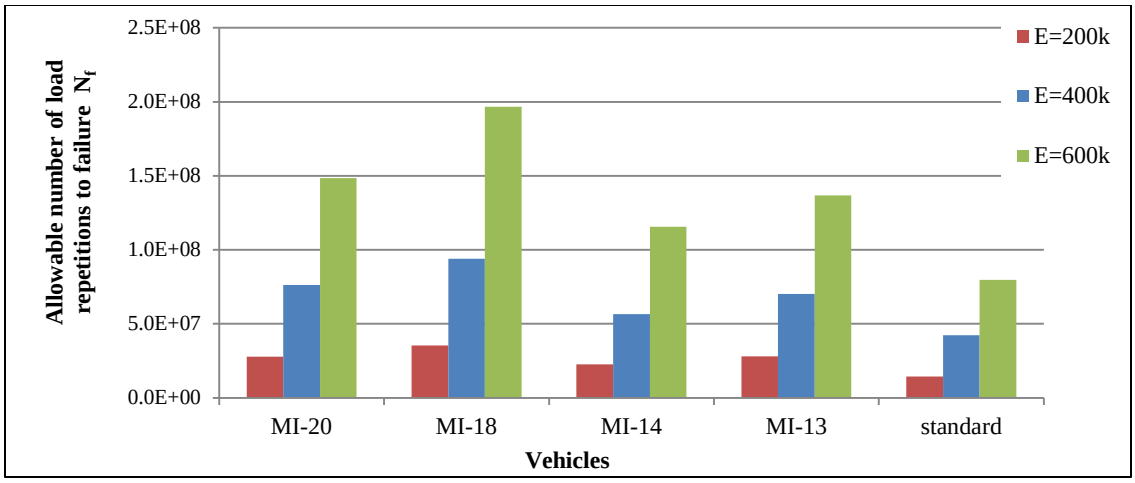

Figure 4.12: Subgrade rutting analysis for different elastic modulus of AC layer based on the coefficients developed by the U.K. Transport & Road Research Agency.

The effect of the elastic modulus of the base layer on the allowable number of load repetitions, N_f calculated based on the coefficients developed by the Asphalt Institute and the U.K. Transport & Road Research Agency are shown in Fig. 4.13 and 4.14 respectively. The elastic modulus of AC layer was set to$400*10^3$ psi and the AC layer thickness were considered as 8 inch. The value of N_f increases with a decrease in the elastic modulus of base layer. The variation of N_f for the different elastic modulus of base layer is not significant. However, the standard truck exhibits the lowest allowable number of load repetitions to failure as observed in the previous cases among all trucks. The magnitude of N_f calculated based on the Asphalt Institute is significantly larger than that calculated based on the U.K. Transport and Road Research Agency for all the vehicles and elastic modulus of base layers.

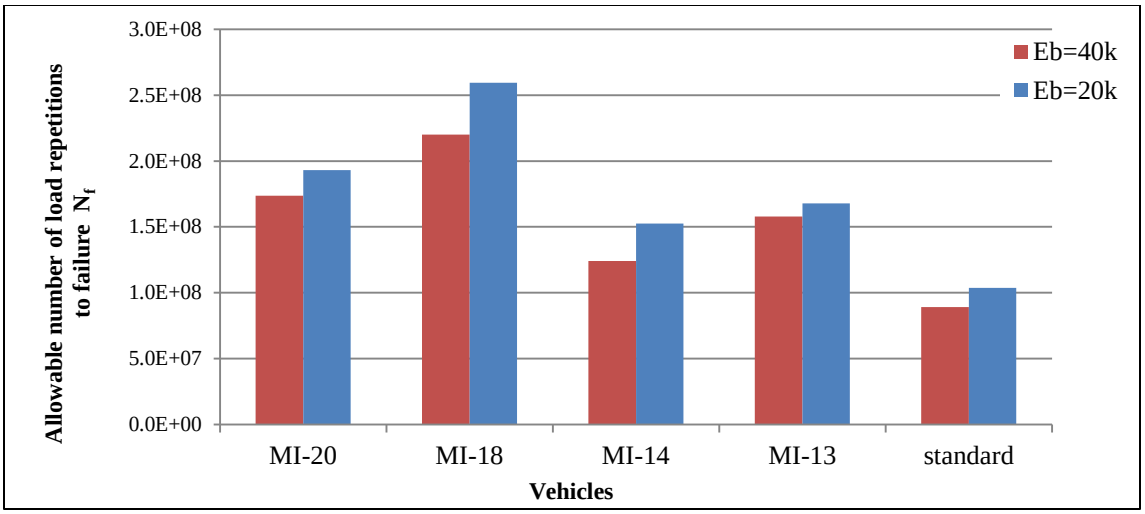

Figure 4.13: Subgrade rutting analysis for different elastic modulus of base layer based on the coefficients developed by Asphalt Institute.

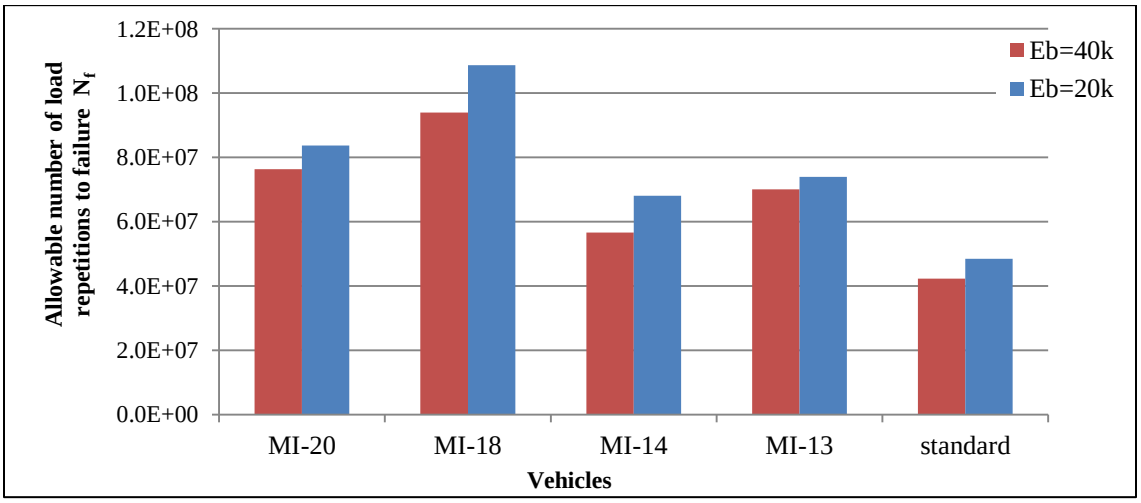

Figure 4.14: Subgrade rutting analysis for different elastic modulus of base layer based on the coefficients developed by the U.K. Transport and Road Research agency.

4.4. Summary

On the basis of results and discussion addressed above the following findings could be drawn from the flexible pavement (AC) fatigue damage analysis of Michigan and standard trucks

- The location of between dual wheels (left or right) produces the highest amount of horizontal tensile strains at the bottom for the AC layer when compared with other locations.
- The standard 5-axle truck produces the maximum tensile strain in the AC layer while the MI-18 trucks yields the least amount of tensile strain.
- As the number of axles increases, the heavy loads are distributed to larger areas and thus produce lower pavement damage.
- Based on the fatigue damage analysis results, the standard 5-axle truck has a higher risk of fatigue damage on flexible pavements than the four Michigan11-axle trucks analyzed. Among the Michigan trucks, the MI-14 truck has most fatigue damage potential.
- For all trucks, the number of load repetitions to failure decreases significantly with a reduction in the both slab thickness and elastic modulus of AC and base layers.

The following findings could be drawn from the flexible pavement subgrade rutting damage analysis of Michigan and standard trucks

- The location of between dual wheels (left or right) produce the highest amount of vertical compressive strains when compared with the other locations.

- The standard 5-axle truck produces the maximum compressive strain and the MI-18 truck yields the lowest compressive strain.
- For the MI-20 and MI-18 trucks, the maximum vertical compressive strain at the top of the subgrade was found to be produced under the same axle assembly (tandem). However, the axles responsible for the maximum vertical compressive strains in the subgrade in case of MI-14 and MI-13 were not found to be similar as tensile strains in the AC layer.
- Based on subgrade rutting analysis results, the standard 5-axle truck has higher risk of rutting damage on flexible pavements than the Michigan 11-axle trucks. Among Michigan trucks, the MI-14 trucks have most damage potential.
- For all the trucks analyzed, the number of load repetitions to failure increases with an increase in the slab thickness and elastic modulus of AC. However, the value of N_f decreases with an increase in the elastic modulus of base layer.
- The magnitude of N_f calculated based on the coefficients developed by the Asphalt Institute is significantly larger than that calculated based on the coefficients developed by the U.K. Transport and Road Research Agency.

CHAPTER 5

SUMMARY AND CONCLUSIONS OF THE THESIS

5.1. Introduction

The pavement responses under loading of multi-axles (11 axles) heavy Michigan trucks (MI-13, MI-14, MI-18 and MI-20) were analyzed for the various axle configuration and loading conditions, pavement properties, and temperature gradients. The results are compared with a standard 5-axle semi-trailer that is widely utilized across the nation. The damage potentials of rigid and flexible pavements are investigated under the given set of test conditions for both the Michigan and standard trucks. Two primary distresses: fatigue cracking (bottom-up or top-down transverse cracking) and faulting damage are analyzed in rigid pavement using the Mechanistic-Empirical Pavement Design Guide (MEPDG) method. The finite element analysis program ISLAB2000 is used to compute pavement responses (stress, strain or deflection). For the flexible pavement, the major load-related distresses: Permanent deformation (or rutting) and Alligator Fatigue Cracking (bottom-up) are analyzed based on the critical stress or strain values determined for each incremental load. The JULEA multilayer elastic computer program has been used to calculate the pavement responses for distress predictions.

5.2. Damage analysis in rigid pavement

The maximum stresses developed on the pavement under different loading condition are calculated using an influence line approach to determine the change of stresses caused by various load positions as the tire passes the slab. Based on the influence line analyses, for the standard truck, the compressive stress at the top of the slab is found to be significantly greater than the tensile stress while the temperature gradient between the top and bottom surface of slab is zero (Fig. 3.6). Like the standard truck, the Michigan trucks also provide higher compressive stress at the top of the slab under zero temperature gradient (Figs. 3.7-3.10). So for the standard and Michigan trucks, the bottom surface of pavement is crucial under the zero temperature gradient between top and bottom surface of pavement.

For the temperature gradient of +30F, the tensile stress at the top surface is negligible and the compressive stress at the top surface is significantly high (Figs. 3.12-3.16). So, the bottom of slab is crucial for the pavement design under the +30F temperature gradient. In addition, the standard truck provides a greater maximum tensile stress at the bottom surface of slab when compared with the Michigan trucks. Among all the trucks, the magnitude of maximum compressive stress for the MI-18 is the lowest. For all the vehicles, critical loading location as single or tandem axle at the mid-point of slab of interest has been found to produce higher pavement responses.

For the -30F temperature gradient, for all the standard and Michigan trucks, the tensile stress at the top surface of slab is significantly higher than that of compressive stress (Figs. 3.18-3.22). Under a negative temperature gradient, the top surface slab is

critical. The magnitude of maximum tensile stress at the top surface of mid-slab for the Michigan trucks has been found higher than that of standard truck. For all the Michigan trucks the magnitudes and the locations of the maximum tensile stresses are almost the same. For all the vehicles, critical loading location as single or tandem axle near the transverse joint of slab of interest has been found to produce higher pavement responses.

5.2.1. Effect of temperature gradient across the slab

For all the standard and Michigan trucks, the maximum tensile stress on the top surface increases with an increase in the negative temperature difference between the top and bottom surface of slab (Fig. 2.23). The opposite is true for the compressive stress, i.e. the maximum compressive stress increases with an increase in the positive temperature difference. The negative temperature gradient provides a maximum tensile stress on the top surface of slab while the positive temperature gradient yields a maximum tensile stress on the bottom surface of slab. The location of the maximum tensile stress for the standard trucks appears at the middle of mid-slab for both the +30F and -30F temperature gradients. For all the trucks, the positive +30F temperature gradient yields a greater magnitude of stress when compared with the -30F temperature gradient. It indicates that the +30F temperature gradient has a better potential for pavement damage.

5.2.2. Fatigue damage prediction in rigid pavement

For the +30F temperature difference, the standard truck shows the maximum pavement damage potential when compared with the Michigan trucks. For the standard truck, more than 33% of design cases provides stress ratio of 0.4 and more, whereas it is it is less than 27% for the Michigan trucks (Fig. 3.26). For the -30F temperature gradient, in comparison with standard truck, the Michigan trucks provide a higher percentile of stress ratios that have magnitude of 0.4 or greater (Fig. 3.27). The damage percentage for the standard truck under the negative temperature gradient is about 21%, which was more than 33% for the positive temperature gradient. However, the Michigan trucks give the almost same percentage of damage potential for both the positive and negative temperature gradients, which is about 27%. So, all the trucks have fatigue damage potential in some extent depending on the interaction of the factors including material properties and slab curling behavior.

The magnitude of load repetition to failure, N_f varies with temperature for all the standard and Michigan trucks. A lower N_f indicates a higher probability of fatigue damage. The magnitude of N_f first increases and then decrease as the temperature gradient changes from -30F to +30F. The +30F provides the minimum value of N_f when compared with other temperature gradients. For the positive temperature gradients, the Michigan trucks provide a greater value of N_f than the standard truck. The opposite is true for the negative temperature gradients. So, the standard truck has a higher fatigue damage potential at positive temperature gradient and the Michigan trucks have a greater potential to fatigue damage at negative temperature gradient.

The values of N_f decrease with a reduction in the pavement thickness. So, a higher pavement thickness significantly improves pavement service life since it provides a larger number of load repetitions to failure. There is no significant difference appears on the values of N_f for the different load transfer efficiency (LTE). However, for all the vehicles, the LTE of 50% provides the minimum N_f.

5.2.4. Faulting damage prediction in rigid pavement

The faulting damage is predicted based on the differential energy (DE) across the joint or crack. A higher DE yields a greater potential to faulting damage. The differential energy decreases with an increase in the pavement thickness. It indicates that the pavement thickness of 8 inches has higher potential to pavement damage since it provides high differential energy to failure (Fig. 3.32). Moreover, the standard truck gives the highest DE for the pavement thickness of 8 inches and a lower DE for the 10 and 12 inches thickness. Among the all the vehicles, the MI-13 truck yields the lowest magnitude of DE for all the pavement thickness. For the given loading conditions, the standard truck has the highest faulting damage potential for the 8 inches thick pavement and the Michigan trucks provide a greater faulting damage than the standard truck for the higher pavement thickness (10 and 12 inches). A decrease in load transfer efficiency (LTE) significantly increases the faulting damage since the differential energy increases by a decrease in the LTE (Fig. 3.33). However, a higher modulus of subgrade reaction, k significantly decreases the differential energy, which indicate that a higher value of k decreases the faulting damage of pavement (Fig. 3.34).

5.3. Damage analyses in flexible pavement

The damage analyses in flexible pavement are conducted based on the horizontal tensile and vertical compressive strains developed for maximum possible loading condition at the critical location pavement. The influence line approach is not utilized since the discontinuities in the AC layer due to traffic movement do not exist in the flexible pavements.

5.3.1. Fatigue damage prediction in flexible pavement

For the standard truck, the magnitude of strains between the dual tires and under the 2^{nd} wheel are almost the same, which are significantly larger than under the middle of axle (Fig. 4.2). However, the similar characteristics also hold for the Michigan trucks. For the MI-20 and MI-18 trucks, the maximum tensile strain appears under both axles of a tandem axle. However, the MI-14 truck provides the maximum tensile strains under the 2^{nd} and 3^{rd} single axle. In case of MI-13 truck, the both axles of 1^{st} tandem and 2^{nd} tandem produce the maximum tensile strain response. Among the all the trucks, the standard truck provides the largest magnitude of tensile strain which is followed by the MI-14 truck. The MI-18 truck provides the least amount of strain. So, the standard truck has the highest potential for damage.

An increase in the pavement thickness significantly raises the number of load repetition to failure (N_f) (Fig. 4.4). The MI-18 truck provides the highest value of N_f because it develops the least amount of strain (Fig. 4.3). The life expectancy of the flexible pavement under the action of loading by MI-18 is followed by the MI-20 and

MI-14 trucks. However, the standard 5-axle truck exhibits the lowest allowable number of load repetitions to failure, which means that the standard truck has the highest fatigue damage potential among tested vehicles while MI-14 truck has the second highest risk.

The elastic modulus of AC layer is an important parameter related to fatigue distress of asphalt pavement. For all the trucks, the value of N_f significantly decreases with a decrease in the elastic modulus of AC layer (Fig. 4.5). In addition, an increase in the elastic modulus of base layer improves the pavement service life by increasing the allowable number of load repetitions (Fig. 4.6). However, the difference is not in a significant amount.

5.3.2. Subgrade rutting prediction in flexible pavement

The vertical compressive strain developed in a flexible pavement along the length of the truck for the standard 5-axle and Michigan (MI-13, MI-14, MI-18 and MI-20) 11-axle trucks are investigated here for a set of operating conditions. The maximum compressive strain appears at the location of between two dual wheels (Fig. 4.7). The locations under 2nd wheel also provide significantly higher compressive strain when compared with the location of between at mid-axle. The Michigan trucks also show the similar results. Moreover, the compressive strains on the top of the subgrade are almost the same regardless of single and tandem axles for standard truck which is not similar to the case of horizontal tensile strains in the AC layer. The maximum compressive vertical strain for the MI-20 and MI-18 trucks appears under both individual axles of the tandem. The MI-14 truck exhibits the maximum compressive strain under the 3rd axle of quad

assembly while it is at the mid-axle of front tridem for the MI-13 truck. Among all the trucks, the standard truck provides the highest compressive vertical strain (Fig. 4.8).

The effects of AC layer thickness on the N_f are investigated based on the two models developed by Asphalt Institute and U.K. Transport & Road Research Agency. Both the models provide the similar trend for all the vehicles and AC layer thickness. However, U.K. Transport &Road Research Agency models gives significantly less value of N_f than that calculated based on the Asphalt Institute model (Figs. 4.9 and 4.10). For all the trucks, the N_f dramatically decreases with a decrease in the AC layer thickness. It indicates that the AC layer thickness of 8 inches provides significantly less pavement service life with respect to subgrade rutting. Among all the vehicles, for the 8 and 10 inches of AC layer thickness, the standard truck exhibits the lowest allowable number of load repetitions to failure and the MI-18 truck provides the highest value of N_f. However for the AC thickness of 12 inches, MI-14 truck yields the lowest and the MI-20 truck provide the highest values of N_f.

The elastic modulus of AC layer has a significant effect on the subgrade rutting of asphalt pavement. The value of N_f significantly decreases with a reduction in the elastic modulus of AC layer (Figs. 4.11 and 4.12). The elastic modulus of base layer provides an opposite phenomena, i.e. the N_f increases with a decrease in the elastic modulus of base layer (Figs. 4.13 and 4.14). The variation of N_f for the different elastic modulus of base layer is not significant. Among all the vehicles, the MI-18 trucks provides the highest value of N_f and the standard truck yields the least value of N_f for all the elastic modulus of pavement. So, the standard 5-axle truck has the highest potential of subgrade rutting.

In conclusion, all Michigan trucks introduce different levels of damage to PCC and AC pavements. The FE model ISLAB2000 and WinJULEA program are effective for predicting the rigid pavement responses under complicated heavy trucks with higher GVW. Seasonal change (temperature), vehicle loading/configurations, pavement thickness, slab joint system (load transfer) and modulus of subgrade support are all important factors that should be considered in rigid pavement design procedure. On the other hand, vehicle loading/configurations, pavement thickness, elastic modulus of AC and base layer are all important factors that should be considered in flexible pavement design procedure. At the end, the following recommendations could be made from this study:

- Heavy 11-axles trucks should be allowed to drive on Michigan pavement since individual axle weights are found to be more of the motivating force in pavement distress development when they are fully loaded instead of GVW.
- When applicable, dowel bars are recommended between pavement joints to minimize the fatigue and joint faulting damage to the pavement due to temperature curling coupled with heavy truck loading.
- Group of axles (up to 8 axles) are preferred for all trucks rather than single and tandem axles because those axles help to distribute the load and minimize pavement damage.
- The impact of heavy trucks on transportation infrastructure system should be studied before the design is finalized (gross weight, axle weight, tire pressure, axle spacing, wheel spacing, speed etc.).

- A rational method for damage prediction is needed that takes into account factors such as climate (differential drying shrinkage), geometric (joint spacing, shoulder type etc.).
- Heavy 11-axles trucks are preferred over 80,000 5-axles trucks in terms of safety and economic perspective based on the parameters included in this study (lesser roadway congestion, lesser crash exposure, lower costs for building and maintaining roads etcetera).

REFERENCES

AASHTO (1946). “Recommended Policy on Maximum Dimensions and Weights of Motor Vehicles to be operated over the Highways of the United States."Washington, D.C.

Acum, W. E. A. and L. Fox. “Computation of Load Stresses in a Three-Layer Elastic System”, Geotechnique.Vol.2, pp. 293-300, 1951.

ARA, Inc. (2007). Interim Mechanistic-Empirical Pavement Design Guide Manual of Practice.Final Draft.National Cooperative Highway Research Program Project 1-37A.

Benekohal, R.F., K.T. Hall, and H.W. Miller (1990). “Effect of Lane Widening on Lateral Distribution of Truck Wheels”, Transportation Research Record 1286, TRB, National Research Council, Washington, D.C., pp. 57-66.

Boussinesq, J., “Application des Potentiels a l'etude de l'equilibreet du Mouvement des Solids Elastiques.” Gatuthier-Villars, Paris, 1885.

Brill, R.D., “Field Verification of a 3D Finite Element Rigid Airport Pavement Model,” FederalAviation Administration DOT/FAA/AR-00/33, Washington D.C, July 2000.

Burmister DM (1945). The General Theory of Stresses andDisplacement in Layered Systems. J. Appl. Phys. 15: 89-94, 126-127, 296-302.

Burmister, D.M. The Theory of Stresses and Displacements in Layered Systems and Applications to the Design of Airport Runways. Highway Research Board, Vol. 23, 1943, pp. 126-144.

Byrum, C.R., and W. Hansen (1994). “Influence Function Approach to Analysis of Jointed Portland Cementr Concrete Pavement”, Transportation Research Record 1449, TRB, National Research Council, Washington, D.C., pp. 148-158.

Byrum, C.R. (2000). “Analysis by High Speed Profile of Jointed Concrete Pavement Slab Curvatures”, Transportation Research Record 1730, TRB, National Research Council, Washington, D.C., pp. 1-9.

Chatti, K. and H. S. Lee, “Evaluation of Strain and Energy Based Fatigue prediction Methods for Asphalt Pavement Subjected to Multiple Axle Loading” International Journal of Pavements, 2004, Vol. 3 No. 1& 2.

Chatti, K., and Lee, H. S. 2003. "Comparison of mechanistic fatigue prediction methods for asphalt pavements."Proc., Int. Conf. on Computational and Experimental Engineering and Sciences, Corfu, Greece.

Chatti, K., Manik, A., Salama, H., Haider, S. W., Brake, N., Mohtar, C. E. (2009). "Effect of Michigan Multi-axle Trucks on Pavement Distress," MDOT Final report, Volume I.

Chou, Y.T., Structural Analysis Computer Programs for Rigid Multicomponent Pavement Structures with Discontinuities- WESLIQID and WESLAYER; Report 1: Program Development and Numerical Presentations; Report 2: Manual for the WESLIQID Finite Element Program; Report 3: Manual for the WESLAYER Finite Element Program. Technical Report GL-81-6, U.S. Army Engineer Waterways Experiment Station, 1981.

Darestani, M. Y. (2007). Response of Concrete Pavements under moving vehicular loads and environmental effects, Queensland University of Technology.

Darter, M.I., K.T. Hall, and C. Kuo (1995). Support under Portland Cement Concrete Pavements. NCHRP Report 372. TRB, National Research Council.

Darter, M.I., L. Khazanovich, M.B. Snyder, S. Rao, and J. Hallin (2001). "Development and Calibration of a Mechanistic Design Procedure for Jointed Plain Concrete Pavements", Proceedings of the 7th International Conference on Concrete Pavements, Orlando, Florida, Vol. 1, pp. 113-131.

Davids, W.G., "Modeling of Rigid Pavements: Joint Shear Transfer Mechanisms and Finite Element Solution Strategies", Ph.D. dissertation, University of Washington, 1998.

ERES Consultants (1999).ISLAB2000 Finite Element Code for Rigid Pavement Analysis.Version 3.6, Champaign, Illinois.

Fekrat, A. Q. (2010). Calibration and Validation of EverFE2.24: A Finite Element Analysis Program for Jointed Plain Concrete Pavements, Ohio University.

Gillespie, T.D., Karamihas, S.M., Cebon, D., Sayers, M.W., Nasim, M.A., Hansen, W, and N. Ehsan. Effects of Heavy Vehicle Characteristics on Pavement Response and Performance, National Cooperative Highway Research Program Report 353, Transportation Research Board, National Research Council, Washington, DC, 1993.

Guo, E.H., G.F. Hayhoe, and D.R. Brill (2002). "Analysis of NAPTF Traffic Test Data for the First-Year Rigid Pavement Test Items", Proceedings of the 2002 Federal Aviation Administration Airport Technology Transfer Conference, Atlantic City, NJ.

Hajek, J. 1995. General Axle Load Equivalency Factors", Transportation Research Record No. 1482, Pavement Design and Analysis, 67-78.

Hajek, J. J. "General Axle Load Equivalency Factors." Transportation Research Record 1482.Transportation Research Board. Washington, D.C. 1990. pp. 67-78.

Hajek, J. J., and Agarwal, A. C. (1990). "Influence of axle group spacing on pavement damage." Transportation Research Record. 1286, Transportation Research Board, Washington, D.C., 138–149.

Hammons M.I. (1997). Development of an Analysis System for Discontinuities in Rigid Airfield Pavements.FAA, Technical Report GL-97-3.

Hammons, M. (1998) "Validation of Three-Dimensional Finite Element Modeling Technique for Jointed Concrete Pavements," 1998 Annual Meeting of the Transportation Research Board, Washington, DC, January.

Heath, A.C. and J.R. Roesler (2000a). "Combined Environmental and Traffic Loading in Rigid Pavement Analysis", University of California-Berkeley, Pavement Research Center, Richmond, California.

Heath, A.C., J.R. Roesler, and J.T. Harvey (2003) "Modeling Longitudinal, Corner and Transverse Cracking in Jointed Concrete Pavements", International Journal of Pavement Engineering, Vol. 4, No. 1, pp. 51-58.

Hiller, J. E. (2007).Development of Mechanistic-Empirical Principles for Jointed Plain Concrete Pavement Fatigue Design, University of Illinois - Urbana Champaign.

Hiller, J.E., and J.R. Roesler (2002) "Transverse Joint Analysis for Use in Mechanistic-Empirical Design of Rigid Pavements", Transportation Research Record 1809, TRB, National Research Council, Washington, D.C., pp. 42-51.

Huang, Y. (1993). Pavement Analysis and Design. Englewood Cliffs, NJ: Prentice-Hall, Inc. Highway and Transportation Officials, Washington, D.C., 1993.

Huang, Y. H., "Finite Element Analysis of Slabs on Elastic Solids", Transportation Engineering Journal, ASCE, 100(TE2): pp. 403-415, 1974.

ICC (1941)."Federal Regulation of the Sizes and Weights of Motor Vehicles."77th Congress, 1st Session, Interstate Commerce Commission, Washington, D.C.

Ilves, G. J., and Majidzadeh, K. (1991)."Re-evaluation of the methods for calculation of load equivalency and damage ratios."Rep. No.FHWA/OH-89/018.

Ioannides, A.M. (1984). Analysis of Slabs on Grade for a Variety of Loading and Support Conditions. Ph.D. Thesis. University of Illinois at Urbana-Champaign, Urbana, Illinois.

Jeong, J.H., and D.G. Zollinger (2005). "Environmental Effects on the Behavior of Jointed Plain Concrete Pavements", Journal of Transportation Engineering, Vol. 131, No. 2, pp 140-148.

Jiang, Y.J., and S.D. Tayabji (1998). "Mechanistic Evaluation of Test Data from Long-Term Pavement Performance Jointed Plain Concrete Pavement Test Sections", Transportation Research Record 1629, TRB, National Research Council, Washington, D.C., pp. 32-40.

Jones, A., "Tables of Stresses in Three-Layer Elastic Systems", Highway Research Board bulletin 342, pp. 176-214, 1962.

JULEA (Jacob Uzan Layered Elastic Analysis) developed by Dr. Jacob Uzan, Technion University, Israel.

Khazanovich, L. (1994). Structural Analysis of Multi-Layered Concrete Pavement Systems. Ph.D. Thesis. University of Illinois at Urbana-Champaign, Urbana, Illinois.

Khazanovich, L. and T. Yu (1998). ILSL2- A Finite Element Program for Analysis of Concrete

Korovesis, G. T. (1990). Analysis of Slabs-on-Grade Pavement Systems Subjected to Wheel and Temperature Loadings. Ph.D. Thesis. University of Illinois at Urbana-Champaign, Urbana, Illinois.

Kuo, C.M., K.T. Hall, and M.I. Darter, "Three-Dimensional Finite Element Model for Analysis of Concrete Pavement Support", Transportation Research Record 1505, National Research Council, Washington, D.C., , pp. 119-127, 1995.

Masad, E., R. Taha, and B. Muhuntban, "Finite-Element Analysis of Temperature Effets on Plain-Jointed Concrete Pavements", Journal of Transportation Engineering, ASCE, Vol. 122, No. 5, pp. 388-398, 1996.

Matthews, J. M., Monismith, C. L., and Craus, J, "Investigation of laboratory fatigue testing procedures for asphalt aggregate mixtures," Journal of Transportation Engineering, 119(4), 1993, pp.634-654.

McCracken, J. K. (2006). "Seasonal Analysis of the Response of Jointed Plain concrete pavements to FWD and Truck Loads," University of Pittsburgh.

MEPDG (2007), Mechanistic Empirical Pavement Design Guide, Version 1.003 Evaluation Copy), Developed for NCHRP 1-37A and NCHPR 1-40D, Developed by Applied Research Associates-Transportation and Arizona State University.

Michigan Department of Transportation (MDOT), "Michigan's Unique Truck-Weight Law", online version, May 2012, retrieved from the internet source:http://justfixtheroads.com/michigans-unique-truck-weight-law/

Miner, M.A. (1945). "Cumulative Damage in Fatigue", Transactions of the ASME, Vol. 67, pp. A159-A164.

NCHRP (2003), National Cooperative Highway Research Program, "Guide for Mechanistic-Empirical Design of New and Rehabilitated Pavement Structures."Final Report, Champaign, Illinois.

NCHRP (2004), National Cooperative Highway Research Program, "Guide for Mechanistic-Empirical Design of New and Rehabilitated Pavement Structures."NCHRP Project 1-37A Final Report, Washington, D.C. (2004).

NCHRP 2006, 'Mechanistic Empirical Pavement Design Guide', Transportation Research Board, Washington DC.

NCHRP Project 1-37A.Guide for Mechanistic-Empirical Design of New andRehabilitated Pavement Structures. Final Report, TRB, National Research Council, Washington, D.C., March 2004. http://trb.org/mepdg/guide.htm.

Newmark, N.M., "Influence Charts for Computation of Vertical Displacements in Elastic Foundations", University of Illinois Experiment Station Bulletin 367, 1947.

Pickett, G. and G. Ray, "Influence Charts for Rigid Pavements", Transactions, American Society of Civil Engineers (ASCE), Vol. 116, pp. 49-73, 1951.

Poblete, M., A. Garcia, J. David, P. Ceza, and R. Espinosa (1990)."Moisture Effects on the Behaviour of PCC Pavements", Proceedings of the 2nd International Workshop on the Theoretical Design of Concrete Pavements, Siquenza, Spain.

Poblete, M., R. Salsilli, R. Valenzuela, A. Bull, and P. Spratz (1988). "Field Evaluation of Thermal Deformations in Undoweled PCC Pavement Slabs", Transportation Research Record 1207, TRB, National Research Council, Washington, D.C., pp. 217-228.

Raad, L. and J. L. Figueroa, "Load Response of Transportation Support Systems", Transportation Engineering Journal.ASCE.Volume 106, No. TE1, Vol. 106, pp. 111-128, 1980.

Rao, C.B., E.J. Barenberg, M.B. Snyder, and S.K. Schmidt (2001). “Effects of Temperature and Moisture on the Response of Jointed Concrete Pavements”, Proceedings of the 7th International Conference on Concrete Pavements, Vol. 1, Orlando, FL, pp. 23-38.

Roesler, J. R. Fatigue of Concrete Beams and Slabs. Ph. D. Dissertation, University of Illinois, Urbana, IL, 1998.

Rufino, D. and J. Roesler, "Effect of Slab-Base Interaction on Measured Concrete PavementResponse," Journal of Transportation Engineering, 132(5), 425-433, May 2006.

Sadeghi, J. M. and Fathali, M. (2007).“Deterioration Analysis of Flexible Pavements under Overweight Vehicles,” Journal of Transportation Engineering.

Salsilli, R. A., E. J. Barenberg and M. I. Darter, “Calibrated Mechanistic Design Procedure to Prevent Transverse Cracking of Jointed Plain Concrete Pavements”, Proceedings of the fifth International Conference on Concrete Pavement Design and Rehabilitation, Purdue University. West LaFayette, IN, pp. 71-90, 1993.

Sanborn, J.L. and E.J. Yoder, “Stress and Displacements in an Elastic Mass under Semiellipsoidal Loads”, Proceedings, Second International Conference on the Structural Design of Asphalt Pavements, Ann Arbor, Michigan, 1967.

Sargand, S. M., &Abdalla, B. (2006). Truck/pavement/economic modeling and in-situ field test data analysis applications: Verification and validation of finite element models for rigid pavement using in-situ data – Selection of joint spacing. Ohio Research Institute for Transportation and the Invironment.

Schiffman, R.L., “General Solution of Stresses and Displacements in Layered Elastic Systems”, International Conference on the Structural Design of Asphalt Pavement, Proceedings, University of Michigan, Ann Arbor, Michigan, USA, 1962.

Sebaaly, P.E., and Tabatabaee, N. Effect of Tire Parameters on Pavement Damage and Load-Equivalency Factors. ASCE Journal of Transportation Engineering, Vol. 118, No. 6, 1992, pp 805-819.

T.D. Gillespie, S. K. (1993). Effect of Heavy-Vehicle Characteristics on Pavement Response and Performance. Washington, D.C.: Transportation Research Boared National Research Council.

Tabatabaie, A.M. and E.J. Barenberg, “Structural Analysis of Concrete Pavements”, Transportation Engineering Journal, ASCE, 106(TE5): pp. 832-849, 1980.

Tabatabaie, A.M., and E.J. Barenberg (1978). “Finite Element Analysis of Jointed of Cracked Concrete Pavements”, Transportation Research Record 671, TRB, National Research Council, Washington, D.C., pp. 11-18.

Tabatabaie-Raissi, A.M. (1977) “Structural analysis of concrete pavement joints”, Ph.D. Thesis, University of Illinois, Urbana, Champaign.

Tayabji, S.D. and Colley, B. E. (1986).Analysis of Jointed Concrete Pavments.U.S.Department of Transportation, Federal Highway Administration, Washington, D.C.

Thompson, M. R. (1987). “ILLI-PAVE Based Full-Depth Asphalt Concrete Pavement Design Procedure,” Proceedings, Sixth International Conference on Structural Design of Asphalt Pavements, Vol. 1, pp. 13-22.

Thompson, M.R. and E.J. Barenberg (1992).Calibrated Mechanistic Structural Analysis Procedure for Pavements - Phase 2, NCHRP Report 1-26, Transportation Research Board, National Research Council.

Thyagarajan, S. (2009).“Improvements to Strain Computation and Reliability Analysis of Flexible Pavements in the Mechanistic-Empirical Pavement Design,” Washington State University.

Tia, M., J.M. Armaghani, C-L Wu, S Lei, and K.L. Toye, “FEACONS III Computer Program for Analysis of Jointed Concrete Pavements”, Transportation Research Record No. 1136, Transportation Research Board, National Research Council, Washington DC, pp. 12-22, 1987.

TRIP, Key facts about Michigan’s surface transportation system and federal, 2015.

Uddin, W., R.M. Hackett, A. Joseph, Z. Pan, and A.B. Crowley, “Three-Dimensional Finite-Element Analysis of Jointed Concrete Pavement Having Discontinuities”, Transportation Research Record 1482, National Research Council, Washington, D.C., pp. 26-32, 1995.

Ullidtz, P., Modelling Flexible Pavement Response and Performance, Technical University of Denmark, PolytekniskForlag, 1987.

Van Cauwelaert, F. J., D. R. Alexander, T. D. White, and W. R. Baker, "Multilayer Elastic Program for Backcalculating Layer Moduli in Pavement Evaluation”, STP 1026.American Society for Testing and Materials, 1989.

Venkatramaiah, C. (2006). “Geotechnical Engineering,” NewAge International (P) Ltd Publishers, Delhi.

Wang, F (2005). “Mechanistic-Empirical Study of effects of Truck Tire Pressure on Asphalt Pavement Performance,” The University of Texas at Austin.

Wang, S. (2011). The effects of implements of husbandry farm equipment on rigid pavement performance, Iowa State University - Ames, Iowa.

Wang, S.K., M. Sargious and Y.K. Cheung, “Advanced Analysis of Rigid Pavements”, Transportation Engineering Journal, ASCE, 98(TE1): pp. 37-44, 1972.

Washington Department of Transportation (WSDOT), “WSDOT Pavement Guide Interactive”, online version, October 2003, retrieved from the internet source: http://training.ce.washington.edu/WSDOT/.

Westergaard HM (1926a). Stresses in Concrete Pavement Computed by Theoretical Analysis.Public Roads, Vol, 7, No. 2, pp. 25-35a.

Westergaard, H.M. (1927), “Analysis of Stresses in Concrete Pavements Due To Variations of Temperature”, Proceedings, Highway Research Board, Vol. 6, National Research Council, Washington D.C., pp. 201-217.

Westergaard, H.M., “Analysis of Stresses in Concrete Pavement Due to Variations of Temperature,” Proceedings, Highway Research Board, Vol. 6, pp. 201-215, 1926b.

William, G. W. (2003). “Effect of Temperature Variations on Premature Cracking of Dowel Jointed Concrete Pavements,”West Virginia University.

Yu, H. T., Khazanovich L, Darter M I. 2004, Consideration of JPCP curling and warping in the 2002 design guide. CD-ROM, Presented at 83rd Annual Transportation Research Board Meeting, Transportation Research Board, Washington, D C, 2004.

Yu, H.T., and L. Khazanovich (2001). “Effects of Construction Curling on Concrete Pavement Behavior”, Proceedings of the 7th International Conference on Concrete Pavements, Orlando, Florida, Vol. 1, pp. 55-68.

Yu, H.T., L. Khazanovich, M.I. Darter, and A. Ardani (1998), “Analysis of Concrete Pavement Responses to Temperature and Wheel Loads Measured from Instrumented Slabs”, Transportation Research Record 1639, TRB, National Research Council, Washington, D.C., pp. 94-101.

Zaghloul, S.M., T.D. White, and T. Kuczek, “Evaluation of Heavy Load Damage Effect on Concrete Pavements Using Three-Dimensional, Nonlinear Dynamic Analysis”, Transportation Research Record 1449, National Research Council, Washington, D.C., pp. 123-133, 1994.

APPENDIX A

Summary fatigue damage analyses results in rigid pavement for a 14 ft. slab with an asphalt shoulder

Table A: Fatigue damage analysis results in rigid pavements for a 14ft slab with an asphalt shoulder.

E	α	K	ΔT	LTE	h	Standard	MI-20	MI-18	MI-14	MI-13
psi	in/in/deg F	pci	^{o}F	%	in.	N_f				
5.E+06	7.E-06	150	-30	50	8	15962.3	4201.81	18591.9	11492.7	7320.3
5.E+06	7.E-06	150	-30	50	10	3266644	556234	2.2E+07	4613426	1E+06
5.E+06	7.E-06	150	-30	50	12	2.7E+09	6.5E+08	5.8E+11	2.1E+10	1E+09
5.E+06	7.E-06	150	-15	50	8	19731	163879	2142591	288910	257684
5.E+06	7.E-06	150	-15	50	10	2152329	3.8E+08	2.3E+11	2.9E+08	4E+08
5.E+06	7.E-06	150	-15	50	12	5.4E+08	1E+12	2.6E+19	5.9E+11	1E+12
5.E+06	7.E-06	150	0	50	8	1896.27	3638.76	19011.6	3590.83	3605.7
5.E+06	7.E-06	150	0	50	10	38571.5	245940	4422474	229244	244479
5.E+06	7.E-06	150	0	50	12	1350617	5.5E+07	3.8E+09	4.6E+07	6E+07
5.E+06	7.E-06	150	15	50	8	75.2356	117.943	147.556	115.286	115.43
5.E+06	7.E-06	150	15	50	10	465.259	1206.8	2011.79	1115.83	1184.7
5.E+06	7.E-06	150	15	50	12	5537.97	31989.9	78739.1	26640.1	32498
5.E+06	7.E-06	150	30	50	8	23.3038	30.8307	36.7843	30.3518	30.436
5.E+06	7.E-06	150	30	50	10	92.0381	164.009	234.212	157.607	163.88
5.E+06	7.E-06	150	30	50	12	592.103	1655.74	2975.58	1528.92	1708
5.E+06	7.E-06	250	-30	50	8	23389.5	2143.29	5611.27	5141.52	3726.6
5.E+06	7.E-06	250	-30	50	10	7302856	114021	1609165	787911	259044
5.E+06	7.E-06	250	-30	50	12	1.2E+10	2.5E+07	2.7E+09	6.3E+08	7E+07
5.E+06	7.E-06	250	-15	50	8	82246.2	44855.6	104336	63997.4	69717
5.E+06	7.E-06	250	-15	50	10	2.4E+07	1.2E+07	2.2E+08	3.8E+07	2E+07
5.E+06	7.E-06	250	-15	50	12	2.3E+10	3.7E+10	1.8E+13	3.9E+11	8E+10
5.E+06	7.E-06	250	0	50	8	4684.38	8424.25	36115	8400.6	8390.1
5.E+06	7.E-06	250	0	50	10	200840	686632	1.2E+07	665073	675574
5.E+06	7.E-06	250	0	50	12	9560604	1.8E+08	1.6E+10	1.6E+08	2E+08
5.E+06	7.E-06	250	15	50	8	70.4139	94.3109	105.401	93.4264	92.366
5.E+06	7.E-06	250	15	50	10	336.759	622.956	887.954	600.479	605.71
5.E+06	7.E-06	250	15	50	12	2746.32	8518.61	16226.7	7787.57	8382.1

5.E+06	7.E-06	250	30	50	8	20.1719	24.3186	27.5361	24.1114	24.004
5.E+06	7.E-06	250	30	50	10	66.0692	97.3314	128.502	95.2676	96.577
5.E+06	7.E-06	250	30	50	12	323.727	642.611	1022.79	616.309	649.64
5.E+06	7.E-06	150	-30	75	8	9343.85	2795.07	20859.6	7575.52	4721.9
5.E+06	7.E-06	150	-30	75	10	1221273	281287	2.9E+07	2315912	557385
5.E+06	7.E-06	150	-30	75	12	5.3E+08	2.3E+08	1.1E+12	7.7E+09	5E+08
5.E+06	7.E-06	150	-15	75	8	11648.2	73281	2434291	128679	112247
5.E+06	7.E-06	150	-15	75	10	857166	9.6E+07	3.5E+11	1.8E+08	2E+08
5.E+06	7.E-06	150	-15	75	12	1.3E+08	6.5E+11	8.2E+19	3.1E+11	6E+11
5.E+06	7.E-06	150	0	75	8	1392.73	3099.72	18639.3	3084.59	3104.2
5.E+06	7.E-06	150	0	75	10	25872.4	199230	3976477	183193	198824
5.E+06	7.E-06	150	0	75	12	662782	4.2E+07	2.9E+09	3.3E+07	4E+07
5.E+06	7.E-06	150	15	75	8	71.1507	122.986	147.178	119.592	119.95
5.E+06	7.E-06	150	15	75	10	402.915	1299.91	1947.25	1181.22	1276.8
5.E+06	7.E-06	150	15	75	12	4149.58	35678.2	71495	28600.4	36846
5.E+06	7.E-06	150	30	75	8	22.6615	31.6126	36.6731	30.9931	31.085
5.E+06	7.E-06	150	30	75	10	84.8995	170.094	228.681	161.938	170.04
5.E+06	7.E-06	150	30	75	12	502.315	1733.1	2794.17	1574.68	1809.5
5.E+06	7.E-06	250	-30	75	8	14998.2	1623.8	6096.31	3867.09	2769.9
5.E+06	7.E-06	250	-30	75	10	3119521	72180.6	1955305	493366	157076
5.E+06	7.E-06	250	-30	75	12	2.9E+09	1.3E+07	4E+09	3.1E+08	3E+07
5.E+06	7.E-06	250	-15	75	8	46353.3	24846.4	112380	36158.3	38886
5.E+06	7.E-06	250	-15	75	10	8333348	4428539	2.7E+08	1.4E+07	9E+06
5.E+06	7.E-06	250	-15	75	12	4.4E+09	8.4E+09	2.9E+13	9.1E+10	2E+10
5.E+06	7.E-06	250	0	75	8	3479.49	7125.69	35876.4	7102.49	7097.7
5.E+06	7.E-06	250	0	75	10	123914	536657	1.2E+07	516665	527948
5.E+06	7.E-06	250	0	75	12	5092219	1.3E+08	1.4E+10	1.2E+08	1E+08
5.E+06	7.E-06	250	15	75	8	68.7681	97.1798	105.979	96.05	94.734
5.E+06	7.E-06	250	15	75	10	311.936	658.599	881.279	629.237	636.59
5.E+06	7.E-06	250	15	75	12	2314.37	9253.21	15556.7	8288.79	9108.3
5.E+06	7.E-06	250	30	75	8	19.9775	24.7837	27.5852	24.5123	24.354
5.E+06	7.E-06	250	30	75	10	63.3895	100.125	127.36	97.4446	99.02
5.E+06	7.E-06	250	30	75	12	294.778	665.855	992.028	632.479	674.91
5.E+06	7.E-06	150	-30	90	8	7513.87	2448.85	21879.8	6590.75	4075.9
5.E+06	7.E-06	150	-30	90	10	818430	226606	3.3E+07	1836990	434329
5.E+06	7.E-06	150	-30	90	12	2.8E+08	1.6E+08	1.3E+12	5.4E+09	3E+08
5.E+06	7.E-06	150	-15	90	8	9270.21	55447.3	2579458	97440.9	83935
5.E+06	7.E-06	150	-15	90	10	578852	5.9E+07	4.2E+11	1.4E+08	9E+07
5.E+06	7.E-06	150	-15	90	12	7.4E+07	4.6E+11	1.3E+20	2.3E+11	5E+11

5.E+06	7.E-06	150	0	90	8	1210.59	2921.38	18354.7	2873.93	2896.2
5.E+06	7.E-06	150	0	90	10	21883.6	179387	3757946	164305	179620
5.E+06	7.E-06	150	0	90	12	499136	3.6E+07	2.5E+09	2.9E+07	4E+07
5.E+06	7.E-06	150	15	90	8	69.4436	125.017	147.035	121.345	121.85
5.E+06	7.E-06	150	15	90	10	379.915	1336.43	1921.64	1207.14	1315.1
5.E+06	7.E-06	150	15	90	12	3699.44	37074.1	68697.6	29341.4	38665
5.E+06	7.E-06	150	30	90	8	22.4326	31.9688	36.673	31.2875	31.375
5.E+06	7.E-06	150	30	90	10	82.4323	172.883	227.057	163.941	172.78
5.E+06	7.E-06	150	30	90	12	472.766	1768.31	2735.16	1595.72	1854.6
5.E+06	7.E-06	250	-30	90	8	12514.4	1487.58	6306.6	3526.09	2511.2
5.E+06	7.E-06	250	-30	90	10	2213210	62246.1	2117057	423163	133119
5.E+06	7.E-06	250	-30	90	12	1.6E+09	1E+07	4.6E+09	2.5E+08	2E+07
5.E+06	7.E-06	250	-15	90	8	36491.6	20302	116261	29469.7	31401
5.E+06	7.E-06	250	-15	90	10	5405313	3206781	2.9E+08	1E+07	6E+06
5.E+06	7.E-06	250	-15	90	12	2.2E+09	5.1E+09	3.5E+13	5.5E+10	1E+10
5.E+06	7.E-06	250	0	90	8	3030.83	6600.2	35572	6578.29	6577.8
5.E+06	7.E-06	250	0	90	10	97297.6	477431	1.1E+07	458896	470390
5.E+06	7.E-06	250	0	90	12	3914597	1.1E+08	1.3E+10	9.8E+07	1E+08
5.E+06	7.E-06	250	15	90	8	68.0416	98.4069	106.28	97.1782	95.773
5.E+06	7.E-06	250	15	90	10	302.442	673.797	879.715	641.612	650
5.E+06	7.E-06	250	15	90	12	2164.05	9562.34	15323.8	8501.18	9422.4
5.E+06	7.E-06	250	30	90	8	19.9155	25.0018	27.6284	24.6999	24.514
5.E+06	7.E-06	250	30	90	10	62.4862	101.47	127.141	98.4939	100.14
5.E+06	7.E-06	250	30	90	12	285.14	677.34	983.235	640.522	686.56

APPENDIX B

Summary of faulting damage analyses results in rigid pavement for a 14 ft. slab with an asphalt shoulder

Table B: Faulting damage analysis results in rigid pavement for a 14 ft. slab with an asphalt shoulder.

E psi	α in/in/deg F	K pci	ΔT °F	LTE %	h in.	Standard	MI-20	MI-18	MI-14	MI-13
						DE				
150	5.E+06	7.E-06	-30	50	8	0.31425	0.021317	0.01127	0.01957	0.057988
150	5.E+06	7.E-06	-30	50	10	0.2192	0.024102	-0.01391	-0.022	-0.03594
150	5.E+06	7.E-06	-30	50	12	0.123916	0.07342	0.034168	0.023057	0.013789
150	5.E+06	7.E-06	-15	50	8	0.064861	0.086668	0.053038	0.057842	0.017191
150	5.E+06	7.E-06	-15	50	10	0.040743	0.105049	0.071034	0.069043	0.038302
150	5.E+06	7.E-06	-15	50	12	0.023163	0.117378	0.082993	0.07636	0.053584
150	5.E+06	7.E-06	0	50	8	0.135722	0.16574	0.134149	0.143339	0.117104
150	5.E+06	7.E-06	0	50	10	0.103193	0.158206	0.128368	0.128841	0.089866
150	5.E+06	7.E-06	0	50	12	0.086002	0.156311	0.127366	0.121622	0.089203
150	5.E+06	7.E-06	15	50	8	0.339442	0.308952	0.312358	0.318769	0.290577
150	5.E+06	7.E-06	15	50	10	0.26451	0.273946	0.283965	0.281878	0.235508
150	5.E+06	7.E-06	15	50	12	0.214166	0.244234	0.255973	0.248403	0.198889
150	5.E+06	7.E-06	30	50	8	0.615498	0.544511	0.564659	0.575268	0.530645
150	5.E+06	7.E-06	30	50	10	0.475208	0.492222	0.515411	0.510407	0.435887
150	5.E+06	7.E-06	30	50	12	0.377618	0.432717	0.453349	0.440453	0.36273
250	5.E+06	7.E-06	-30	50	8	0.395866	-0.17338	-0.17573	-0.15657	-0.17803
250	5.E+06	7.E-06	-30	50	10	0.233375	-0.07816	-0.08997	-0.08968	-0.09402
250	5.E+06	7.E-06	-30	50	12	0.138911	-0.02648	-0.03995	-0.04309	-0.04517
250	5.E+06	7.E-06	-15	50	8	0.056056	0.006449	-0.00583	-0.00409	-0.01726
250	5.E+06	7.E-06	-15	50	10	0.040041	0.02325	0.010507	0.010173	-0.00131
250	5.E+06	7.E-06	-15	50	12	0.02593	0.03378	0.020536	0.018705	0.009787
250	5.E+06	7.E-06	0	50	8	0.063882	0.06569	0.0556	0.059452	0.055953
250	5.E+06	7.E-06	0	50	10	0.047373	0.061395	0.049915	0.052502	0.040935
250	5.E+06	7.E-06	0	50	12	0.038512	0.05983	0.048774	0.048784	0.033687
250	5.E+06	7.E-06	15	50	8	0.186911	0.148179	0.147118	0.153778	0.154797
250	5.E+06	7.E-06	15	50	10	0.149235	0.137869	0.141352	0.143502	0.129049
250	5.E+06	7.E-06	15	50	12	0.121797	0.12607	0.131147	0.130081	0.109593

250	5.E+06	7.E-06	30	50	8	0.370195	0.288281	0.298416	0.310114	0.308878
250	5.E+06	7.E-06	30	50	10	0.293602	0.278523	0.291563	0.293001	0.263481
250	5.E+06	7.E-06	30	50	12	0.234894	0.251556	0.26352	0.259484	0.222
150	5.E+06	7.E-06	-30	75	8	0.377443	-0.06985	-0.10444	-0.10902	-0.12701
150	5.E+06	7.E-06	-30	75	10	0.208954	0.022595	-0.01616	-0.02418	-0.03763
150	5.E+06	7.E-06	-30	75	12	0.117012	0.071137	0.031012	0.020037	0.011185
150	5.E+06	7.E-06	-15	75	8	0.060961	0.085706	0.050608	0.054529	0.015922
150	5.E+06	7.E-06	-15	75	10	0.037807	0.103362	0.067656	0.064806	0.036237
150	5.E+06	7.E-06	-15	75	12	0.021072	0.114825	0.078864	0.071323	0.050641
150	5.E+06	7.E-06	0	75	8	0.118385	0.158874	0.128858	0.137018	0.102983
150	5.E+06	7.E-06	0	75	10	0.09286	0.150628	0.122412	0.12176	0.082549
150	5.E+06	7.E-06	0	75	12	0.079078	0.14974	0.120903	0.113981	0.084797
150	5.E+06	7.E-06	15	75	8	0.30595	0.273782	0.278784	0.282215	0.264246
150	5.E+06	7.E-06	15	75	10	0.244525	0.244648	0.258737	0.251833	0.218359
150	5.E+06	7.E-06	15	75	12	0.201021	0.219724	0.235843	0.223025	0.186987
150	5.E+06	7.E-06	30	75	8	0.565638	0.496142	0.515225	0.52206	0.491492
150	5.E+06	7.E-06	30	75	10	0.446426	0.450172	0.478485	0.466105	0.410384
150	5.E+06	7.E-06	30	75	12	0.359044	0.402636	0.424152	0.403409	0.343986
250	5.E+06	7.E-06	-30	75	8	0.383754	-0.17357	-0.17543	-0.15718	-0.17734
250	5.E+06	7.E-06	-30	75	10	0.225248	-0.07853	-0.09037	-0.08996	-0.0942
250	5.E+06	7.E-06	-30	75	12	0.133377	-0.02706	-0.04068	-0.04364	-0.04568
250	5.E+06	7.E-06	-15	75	8	0.053392	0.006262	-0.00619	-0.00458	-0.01755
250	5.E+06	7.E-06	-15	75	10	0.037853	0.022902	0.009832	0.009408	-0.00169
250	5.E+06	7.E-06	-15	75	12	0.024274	0.033199	0.019524	0.017618	0.009104
250	5.E+06	7.E-06	0	75	8	0.054346	0.06335	0.051494	0.057338	0.0482
250	5.E+06	7.E-06	0	75	10	0.04174	0.058803	0.047901	0.050097	0.036312
250	5.E+06	7.E-06	0	75	12	0.034781	0.057017	0.046542	0.046134	0.031751
250	5.E+06	7.E-06	15	75	8	0.16544	0.131177	0.129148	0.135805	0.138705
250	5.E+06	7.E-06	15	75	10	0.136332	0.123731	0.127815	0.128559	0.118726
250	5.E+06	7.E-06	15	75	12	0.113372	0.113653	0.120419	0.117251	0.102261
250	5.E+06	7.E-06	30	75	8	0.336594	0.264328	0.2703	0.282487	0.28377
250	5.E+06	7.E-06	30	75	10	0.274323	0.257011	0.270447	0.269297	0.247458
250	5.E+06	7.E-06	30	75	12	0.22268	0.232254	0.246919	0.239216	0.210593
150	5.E+06	7.E-06	-30	90	8	0.372309	-0.07046	-0.10532	-0.10968	-0.12745
150	5.E+06	7.E-06	-30	90	10	0.205615	0.021717	-0.01732	-0.02532	-0.03852
150	5.E+06	7.E-06	-30	90	12	0.114726	0.069948	0.029635	0.018595	0.009951
150	5.E+06	7.E-06	-15	90	8	0.059632	0.08526	0.049189	0.052648	0.015023
150	5.E+06	7.E-06	-15	90	10	0.036806	0.10253	0.065929	0.062795	0.035084
150	5.E+06	7.E-06	-15	90	12	0.020348	0.113719	0.076938	0.069158	0.049178

150	5.E+06	7.E-06	0	90	8	0.110903	0.156947	0.12593	0.133645	0.096662
150	5.E+06	7.E-06	0	90	10	0.088492	0.150065	0.119469	0.118355	0.080624
150	5.E+06	7.E-06	0	90	12	0.076263	0.149738	0.117941	0.110566	0.082599
150	5.E+06	7.E-06	15	90	8	0.290949	0.257359	0.263391	0.26543	0.252166
150	5.E+06	7.E-06	15	90	10	0.23578	0.235841	0.247472	0.238629	0.210601
150	5.E+06	7.E-06	15	90	12	0.195528	0.224201	0.227132	0.212315	0.181352
150	5.E+06	7.E-06	30	90	8	0.542709	0.473947	0.492382	0.497785	0.473129
150	5.E+06	7.E-06	30	90	10	0.433551	0.444436	0.461938	0.446758	0.398682
150	5.E+06	7.E-06	30	90	12	0.351142	0.40946	0.411545	0.387818	0.335757
250	5.E+06	7.E-06	-30	90	8	0.379673	-0.17371	-0.17525	-0.15726	-0.17699
250	5.E+06	7.E-06	-30	90	10	0.222542	-0.07875	-0.09058	-0.08997	-0.09429
250	5.E+06	7.E-06	-30	90	12	0.131555	-0.02737	-0.04102	-0.04392	-0.04592
250	5.E+06	7.E-06	-15	90	8	0.052489	0.00613	-0.00647	-0.00494	-0.01776
250	5.E+06	7.E-06	-15	90	10	0.037106	0.022651	0.009405	0.008938	-0.00195
250	5.E+06	7.E-06	-15	90	12	0.023718	0.03285	0.019006	0.017051	0.00872
250	5.E+06	7.E-06	0	90	8	0.050248	0.062779	0.050429	0.056108	0.04477
250	5.E+06	7.E-06	0	90	10	0.039311	0.058157	0.046814	0.04885	0.034236
250	5.E+06	7.E-06	0	90	12	0.03321	0.056832	0.045448	0.044869	0.031022
250	5.E+06	7.E-06	15	90	8	0.155768	0.123206	0.120858	0.127394	0.13135
250	5.E+06	7.E-06	15	90	10	0.130496	0.117208	0.121613	0.121765	0.113958
250	5.E+06	7.E-06	15	90	12	0.109651	0.110624	0.115615	0.111628	0.098925
250	5.E+06	7.E-06	30	90	8	0.32108	0.253141	0.25715	0.269623	0.271972
250	5.E+06	7.E-06	30	90	10	0.265392	0.247362	0.260738	0.258619	0.239919
250	5.E+06	7.E-06	30	90	12	0.2172	0.233619	0.239516	0.230434	0.205369

APPENDIX C

Summary of fatigue damage analyses results in flexible AC pavement

Table C: Fatigue damage analysis results in flexible AC pavement.

EAC ^{o}F	Ebase in.	hAC in.	Standard	MI-20	MI-18	MI-14	MI-13
			N_f				
4.00E+05	4.00E+04	8	8.35E+05	1.81E+06	2.15E+06	1114477	1.81E+06
2.00E+05	4.00E+04	8	179561.1	350835.4	412883.4	234741.7	349925.4
6.00E+05	4.00E+04	8	2115239	4867394	5793251	2891349	4848629
4.00E+05	4.00E+04	10	2095828	5048309	6049932	2958121	5025134
2.00E+05	4.00E+04	10	427287.6	935347.7	1110029	574051	932305.2
6.00E+05	4.00E+04	10	5431914	13720906	16608763	8102995	13638825
4.00E+05	4.00E+04	12	4714384	12301414	15010472	7289491	12211185
2.00E+05	4.00E+04	12	936632.8	2256509	2703370	1315008	2245124
6.00E+05	4.00E+04	12	12369419	33506950	41771358	21019131	33183086
4.00E+05	2.00E+04	8	762904.4	1666145	1972444	1016093	1660958

APPENDIX D

Summary of subgrade rutting analyses results in flexible AC pavement

Table D: Subgrade rutting analysis results in flexible AC pavement.

EAC ^{o}F	Ebase in.	hAC in.	Standard	MI-20	MI-18	MI-14	MI-13	Standard	MI-20	MI-18	MI-14	MI-13
			N_f (Asphalt Institute)					N_f (U.K. Transport & Road Research)				
4.E+05	4.E+04	8	91166378	1.74E+08	2.2E+08	1.47E+08	1.8E+08	43172630	76285110	93941740	65874183	78518249
2.E+05	4.E+04	8	26433585	55265655	72917870	41849342	57712560	14481766	27759872	35450797	21720337	28841491
6.E+05	4.E+04	8	1.94E+08	3.7E+08	5.1E+08	3.32E+08	3.81E+08	84244159	1.48E+08	1.97E+08	1.35E+08	1.52E+08
4.E+05	4.E+04	10	3.05E+08	5.75E+08	8.08E+08	5.4E+08	5.99E+08	1.25E+08	2.19E+08	2.96E+08	2.08E+08	2.27E+08
2.E+05	4.E+04	10	79483621	1.51E+08	1.99E+08	1.28E+08	1.52E+08	38252699	67354444	85935837	58423006	67645192
6.E+05	4.E+04	10	7.35E+08	1.13E+09	1.42E+09	1.4E+09	1.22E+09	2.72E+08	3.98E+08	4.87E+08	4.81E+08	4.24E+08
4.E+05	4.E+04	12	9.13E+08	1.32E+09	1.88E+09	1.83E+09	1.36E+09	3.3E+08	4.58E+08	6.23E+08	6.09E+08	4.69E+08
2.E+05	4.E+04	12	2E+08	3.89E+08	5.22E+08	3.5E+08	4.11E+08	86423645	1.55E+08	2.01E+08	1.41E+08	1.63E+08
6.E+05	4.E+04	12	2.33E+09	2.75E+09	3.7E+09	5.06E+09	2.72E+09	7.52E+08	8.72E+08	1.13E+09	1.49E+09	8.64E+08
4.E+05	2.E+04	8	1.05E+08	1.95E+08	2.6E+08	1.69E+08	1.92E+08	49083724	84266740	1.09E+08	74285064	83413970